Generation and Analysis of Harsh Wave Environments

vorgelegt von
Diplom-Technomathematikerin
Janou Hennig
aus Berlin

von der Fakultät V – Verkehrs- und Maschinensysteme
der Technischen Universität Berlin
zur Erlangung des akademischen Grades

Doktorin der Naturwissenschaften
– Dr. rer. nat. –

genehmigte Dissertation

Promotionsausschuss:

Vorsitzender:	Prof. Dr.-Ing. Wolfgang Nitsche
Berichter:	Prof. Dr.-Ing. Günther F. Clauss
Berichter:	Prof. Dr.-Ing. Stefan Krüger

Tag der wissenschaftlichen Aussprache: 01. April 2005

Berlin 2005
D 83

Abstract

In this work, a *modified non-linear theory* for modelling wave propagation is presented. The hybrid model combines linear wave theory with Stokes Third Order wave theory to consider non-linear wave characteristics such as an increase of wave celerity and crest-trough asymmetry with wave steepness. The new approach is fast and precise and applicable in day-to-day use for experimental investigations. The method can be adapted easily for new requirements as the implementation of different wave theories as well as empirical terms is possible.

Compared to numerical wave tanks, the method is capable of upstream transformation of wave trains and is therefore ideally suited for generating wave board control signals. The potential of the reproducible procedure is demonstrated by generating different kinds of tailored deterministic wave sequences at both Technical University Berlin and Hamburg Ship Model Basin. The following wave sequences are generated in the model basin and applied to the investigation of non-linear wave-structure interaction:

- Transient wave packets
- Sea states with deterministically embedded steep wave sequences
- Regular waves with a superimposed *Three Sisters* wave
- Observed wave records (*New Year Wave*)

Deterministic wave sequences are applied to model tests for investigating the wave-ship interaction at extreme sea conditions. The transformation to arbitrary – stationary or moving – positions or models allows for a precise relation of cause and effect. With this technique, wave scenarios can be analyzed from the point of view of a sailing ship. As an exact and reproducible encounter of ship and wave in the model basin is realized, mechanisms of large rolling and capsizing can be examined deterministically. Both extreme and resonance phenomena possibly leading to ship accidents are investigated:

- Parametric roll
- Loss of stability at the wave crest
- Impact excitation in combination with the above

Based on these developments, methodologies for the quantitative assessment of capsizing risk are validated by direct comparison of time series from numerical and experimental simulations – providing a basis for the improvement of current intact stability criteria. In conclusion, ships are designed with improved seakeeping characteristics and an increased safety with respect to the danger of extreme roll angles and capsizing.

Zusammenfassung

In der vorliegenden Arbeit wird eine *modifizierte nichtlineare Theorie* zur versuchstechnischen Generierung und Analyse extremer Seegangsbedingungen hergeleitet. Das hybride Verfahren basiert auf linearer Wellentheorie nach Airy, ergänzt durch nichtlineare Stokes-Wellentheorie dritter Ordnung. Die Anwendung linearer Wellentheorie erlaubt die Implementierung einer schnellen iterativen Methode und deren praktische Anwendung für Modellversuche.

Eine Hauptanwendung des Verfahrens liegt in der Generierung maßgeschneiderter deterministischer Wellenzüge im Versuchskanal. Für die Untersuchung nichtlinearer Wechselwirkungen zwischen Welle und Struktur wird hierfür ein Zielort definiert, an dem der Wellenzug eine vorgegebene Form aufweisen bzw. definierten Parametern genügen soll. Eine so vorgegebene Zeitreihe wird mithilfe der modifizierten nichtlinearen Theorie auf die Position des Wellenerzeugers umgerechnet. Aus dem am Wellenblatt vorliegenden Wellenzug werden durch Multiplikation mit verschiedenen Übertragungsfunktionen entsprechende Steuersignale für den Wellenerzeuger berechnet.

Mit dem hergeleiteten Verfahren können verschiedenste Arten deterministischer Wellensequenzen generiert werden:

- transiente Wellenpakete und Riesenwellen
- realistische Seegänge mit gezielt eingelagerten gefährlichen Wellensequenzen
- sogenannte *Three Sisters* – eine Wellensequenz mit drei hohen Wellenbergen – in regulären Wellen
- maßstabsgetreue Realisierung von in der Natur gemessenen Wellensequenzen im Versuchskanal (*New Year Wave*)

Diese Seegangsszenarien finden Anwendung bei vollständig automatisierten

deterministischen Kenterversuchen zur Untersuchung von Roll- und Kentermechanismen von Schiffen. Dabei werden parametrisch erregtes Rollen, Resonanz, Stabilitätsverlust auf dem Wellenberg sowie die Anregung durch Riesenwellen untersucht. Um diese Mechanismen zu erschließen, wird ein stationär gemessener Wellenzug in das bewegte Bezugssystem des fahrenden Schiffes überführt.

Transformationen deterministischer Wellensequenzen werden weiterhin zur Validierung von numerischen Bewegungssimulationsverfahren verwandt, wie sie auf Werften zur Bewertung von Schiffsentwurf und -betrieb eingesetzt werden. Hierbei können erstmals Zeitreihen aus Modellversuchen und numerischen Simulationen in allen sechs Freiheitsgraden direkt quantitativ verglichen werden. Durch validierte und verbesserte Bewertungsmethoden wird ein Beitrag zur effizienten Bewertung der Schiffssicherheit geleistet.

Acknowledgement

This thesis was written in the framework of my research activity at the Ocean Engineering Section of Technical University Berlin. I wish to express my gratitude to the many people who gave me support and encouragement in the making of the thesis.

I would like to thank my promoter and supervisor Prof. Dr.-Ing. G. F. Clauss who gave me the inspiration and freedom, rendering this thesis possible. Thank you for the good and challenging cooperation in years. Also many thanks to my second promoter Prof. Dr.-Ing. S. Krüger from Technical University Hamburg-Harburg, who immediately agreed upon taking over this function. I thank him for the interest in my work and for all the fruitful talks about concepts in ship safety during shared research projects. Prof. Dr.-Ing. W. Nitsche as invaluable chairman of the doctoral committee I express my gratitude.

Special thanks go to my colleagues of the Ocean Engineering Section for the good fun we had at work, cheering me up with laughter and coffee together in good times and bad. Thank you also for helping to reduce my work load. Namely, I would like to thank my colleague Dipl.-Ing. Christian Schmittner who planned, discussed, and worked with me since our student time. Special thanks go to Dr.-Ing. Walter Kühnlein (now at Hamburg Ship Model Basin) who awoke my interest in model testing and who infected me with his passion for wave generation. Both Christian and Walter helped improving this work significantly by reading and discussing earlier versions. I thank Mr. Jürgen Heeg for many useful tips on signal processing – and the excellent software development through many years of good team work. Many thanks go to Ms. Kornelia Tietze for her ambitious and professional support and good mood. Invaluable contributions come from my colleagues cand. Ing. Sebastian Weickgenannt and Dipl.-Ing. Marc Elsholz. Thank you very much!

I have to thank the colleagues, many of whom have become good friends, for a cooperation for years, with detailed discussions and engaged research work:

I had the good luck to meet and talk to impressive personalities and capacities in different fields. Thus, I appreciate the vivid cooperation with Dipl.-Ing. Heike Cramer, Flensburg Shipyard – without her, many parts of this thesis would not have been written. I thank my colleagues from the Hamburg Ship Model Basin, Dipl.-Ing. Kay-Enno Brink, Dipl.-Ing. Arndt Schumacher and Steve Gehrisch, for the professional and sincere cooperation which led to the experimental results of this thesis. I also thank Dipl.-Oz. Konny Reichert, OceanWaveS, for the fruitful cooperation and the inspiring talks.

The funding of two research projects on capsizing by the Federal Ministry of Research and Education (BMBF) is deeply acknowledged. The extensive test program in the framework of *SinSee* and *Roll-S* allowed for the investigation and validation of the presented methods.

I appreciate the committed support by Prof. Dr.-Ing. Wolf and Prof. Dr. Grigorieff who paved my way to study Ocean Engineering regardless of some obvious difficulties. This finally resulted in this thesis.

I would like to thank the countless experienced colleagues who sincerely discussed my ideas with me. Without their keen support and encouragement and the permanent atmosphere of scientific curiosity I met at conferences and institutions, my work would not have been successful.

Last but not least, I thank my family and friends for always believing in me, giving me the power to meet the challenges of the working life. My parents Brigitte and Klaus always stood behind me – and are most guilty for my insatiable inquisitiveness. I thank my brothers Aljoscha and Janosch for sharing the important events in my life with me. Thank you, Christian, for your love and patience also through unsettling times!

Contents

List of Figures

List of Tables

Chapter 1

Introduction

1.1 Ocean waves and ship stability

Wind driven ocean waves can cause large roll motions or even capsizing of a ship posing a significant threat to crew and passengers, ship and cargo. Thus, encountering a rogue wave such as shown in Fig. 1.1 might be one of the most horrible visions for a ship master. Such rogue waves have often been considered as seafarer's tales before their increasing number was reported and investigated by research projects: Reports on individual extreme waves in deep water mention either single high waves or several successive high waves, extreme crest and wave height as well as unusual group patterns. By mariners, they are often described as white or green wall of water approaching the ship at high speed. Unsolved questions include the underlying mechanism of extreme waves, under which conditions they appear, and how frequently they occur (Grue (2002)).

Extreme wave conditions in a storm arise from the most unfavorable, spontaneous interaction of waves within the related severe sea spectrum. Also opposing currents such as the notorious Agulhas Current off southeast Africa meeting storm swells from farther south or particular bottom topographies are reasons for the generation of rogue waves. Rogue waves are inconsistent with standard statistical distributions and they occur more often than predicted by classical approaches.

A general definition of a rogue wave group can be given in terms of the significant wave height H_s: The wave (group) is called rogue if both its maximum wave height is more than twice the significant wave height and the

Figure 1.1: Rogue wave estimated at $H_{max} = 20$ m moving toward ship in the Gulf Stream off Charleston, South Carolina, with light winds of 15 knots (picture taken from http://www.mpc.ncep.noaa.gov/).

sea state is severe,

$$\begin{aligned} H_{max} &> 2H_s, \\ H_s &> 10 \text{ m}. \end{aligned} \tag{1.1}$$

This definition will be used throughout the thesis.

There is a probability of 40 % of exceeding this value in a storm (Faulkner (2003)). Thus, different authors propose different definitions: Faulkner (2000) presents extreme wave conditions and proposes the definition $H_{max} > 2.4H_s$ for abnormal wave height. From probability analysis of rogue wave data recorded from 1994 to 1998 at North Alwyn, Wolfram et al. (2000) suggest $H_{max} > 2.3H_s$. From their wave analysis they also found that most rogue waves occur as sequences consisting of three subsequent wave crests (*Three Sisters*) which have the characteristic pattern of wave heights $H_s - 2H_s - H_s$. The rogue waves were generally 50 % steeper than the significant steepness. Exceptional waves have also been reported in hurricane *Camille* (Guedes Soares et al. (2004a)) and from the Sea of Japan off Yura harbor (Mori et al. (2000)).

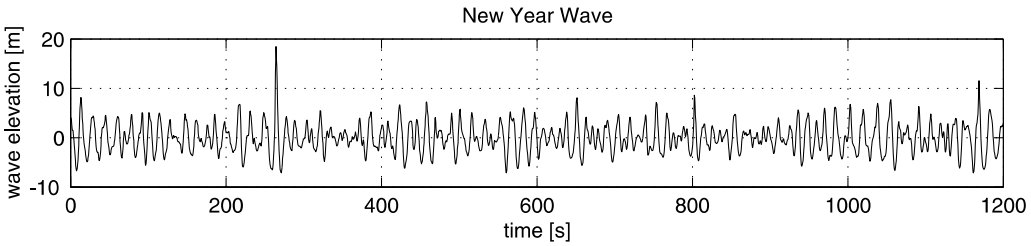

Figure 1.2: *New Year Wave* registered on January 1, 1995, at the Draupner jacket platform in the North Sea – $H_s = 11.92$ m, $H_{max} = 25.63$ m $= 2.15 H_s$; $\zeta_c = 18.5$ m $= 0.72 H_{max}$, $d = 70$ m.

One of the best documented rogue wave events is reported from the Draupner jacket gas platform in the Norwegian Ekofisk field in the North Sea (Haver (2000), Haver and Anderson (2000)), measured by a downward pointing radar. The platform was hit by the giant wave with a wave height of 25.6 m (see Fig. 1.2) that caused severe damage to equipment on deck. Related to the significant wave height of 11.92 m the maximum wave height rises to $H_{max} = 2.15 H_s$ (zero-upcrossing) with a crest of $\zeta_c = 0.72 H_{max} = 18.5$ m and a preceding trough of only 7.5 m (at a water depth of 70 m). This so-called *New Year Wave* will be referred to later on.

There are also other impressive rogue wave reports such as from the *Schiehallion* FPSO moored in the North Atlantic. In November 1998, its bow plating was pushed in by 0.25 m due to an extremely steep wave at 20 m above mean water level (Buchner and Voogts (2004), Toffoli et al. (2003)). In the autumn of 1995, the ship master of the *Queen Elizabeth 2* saw a "white wall of water for a couple of minutes" during a severe storm off Newfoundland.

All these observations document the physical existence of rogue waves and denote a potential risk for ships and offshore structures. Thus, it seems to be appropriate to draw attention to the investigation of extreme waves — even more since the ocean environment seems to get harsher: Microseismological registrations of pounding waves show a significant increase of large waves in the northeast Atlantic Ocean. Microseisms – i. e. ground movements with periods of 4-16 s – which are induced by ocean waves and coastal surf, disclose a significant increase of wave height in the Norwegian sea over the past 20 years in parallel with increased surface air temperature and storminess (Grevemeyer et al. (2000)).

With regard to ship accidents it can be stated that within the last decade, more than hundred large tankers and container ships have been lost in severe weather conditions, some of them due to the interaction with dangerous wave

groups causing large roll angles (Faulkner (2000), Kjeldsen (2000)). Particular wave groups, e. g. the so-called *Three Sisters*, the *Seventh Wave*, "white walls of water" or "holes in the sea" are suspected to be one main reason for unexpectedly sudden capsizes. Faulkner and Buckley (1997) describe a number of episodes with massive damage to ships due to rogue wave impacts. Thus, the German cruise liner *Bremen* encountered a rogue wave during a storm in the South Atlantic which smashed a bridge window with subsequent flooding of the bridge and a total shutdown of all engines (Schulz (2001)). Fortunately, the engines could be restarted, and the ship made it safely to the next harbour. A similar incident happened to the cruise liner *Voyager* during a winter storm in the Mediterranean just recently. These incidents illustrate the fatal risk of freak waves and document the importance to draw attention to their genesis and effect on marine structures. In the eighties a Norwegian study on severe wave conditions was motivated by the loss of vessels up to 76 m in the Norwegian waters due to capsizing in deep water plunging breakers – so-called freak waves (Kjeldsen (1983)). As a consequence a new design philosophy considering single waves in addition to the traditional design sea states is developed. Kjeldsen concludes: "After all we must provide for the worst."

But not only rogue waves with extreme wave height, steepness and groupiness are suspicious to cause damage to ships. France et al. (2001) analyze a case of auto parametrically excited rolling motion – shortened to "parametric roll" throughout the thesis – where a post-Panamax container ship has lost one third of its cargo due to roll angles up to 40° in a severe storm ($H_s = 14.6$ m, $T_P = 14.7$ s). Another third of the cargo was found in various stages of damage. As this example demonstrates, all wave parameters like propagation velocity, direction and wave length together with ship speed, course and load conditions are important factors for the instantaneous safety of the ship. Accidents also happen due to disadvantageous seakeeping characteristics and could be avoided by safer ship design and operation (see chapter 6). The risk of ship accidents can be reduced by weather routing as the wave environment encountered by a routed ship is generally less severe (Olsen et al. (2004)). However, the conditions found by a ship during its lifetime can be still rough enough. Thus, the detailed knowledge of the processes leading to large roll angles and capsizing is an important goal.

Wave excitation denotes the beginning of a complex cause-reaction chain which results in the particular ship motions. The wave-structure interaction has to be investigated carefully in order to understand the underlying hydrodynamic processes. Especially in ship design numerical simulation tools have improved significantly and are already considered routinely within the

design process but are still under development and require further experimental confirmation. Thus, experimental investigations for the evaluation of ship motion behaviour are indispensable, both for the validation of numerical motion simulation tools and also for basic insights into the underlying mechanism.

1.2 Deterministic investigation of intact stability

For standard seakeeping tests the seaway is represented by spectral parameters such as peak period and significant wave height and realized in the model basin. The expected wave climate a marine structure is going to experience during its lifetime can be looked up from scatter diagrams by global wave climate archives (e. g. Hogben (2001)). However, for the analysis of large roll motions and capsizing as a cause-reaction chain both wave generation and test procedure have to be deterministic.

As a first step in the deterministic test procedure dangerous situations have to be defined and realized in the model basin. The wave – both rogue waves or other wave sequences respectively – is defined by its target location in the model basin, wave frequency range, height and groupiness characteristics.

In order to get the desired target wave train at the target position, the wave sequence has to be related to appropriate control signals of the wave maker. Thus, the wave train has to be transformed upstream to the position of the wave maker. Since high and steep waves have to be considered, a nonlinear method is required which allows for transforming the given surface elevation to an arbitrary location. The method has to be fast and precise to be applicable and appropriate for experiments.

As a second step the wave train encountered by the ship model has to be analyzed. Thus, the wave train has to be transformed to the moving reference frame of the cruising ship — given either the wave board motion and/or undisturbed stationary measurements of the wave train since measurements in a model tank cannot provide the wave train at the actual position of the sailing model.

This means that a transformation method is required which is capable to transform a wave train both upstream (wave generation) and downstream (analysis in the moving reference frame). The test procedure has to allow for the exact correlation of wave excitation with resultant ship motion.

Both by generation of deterministic wave sequences and the deterministic capsizing test procedure, the process of large rolling and capsizing can be analyzed as a cause-reaction chain. Dangerous situations can be simulated realistically and deterministically. This also allows the direct comparison of measured and simulated time series, and consequently the validation of numerical motion simulation tools applied to safer ship design and operation.

1.3 Structure of the thesis

In order to implement a technique for upstream and downstream transformation of wave trains, aspects of linear and non-linear wave theories and methods to model non-linear wave propagation are discussed and summarized in chapter 2.

In chapter 3, a *modified non-linear theory* is introduced which is able to transform a given wave train — as surface elevation time series — upstream (for wave generation) and downstream (for wave analysis in the moving reference frame) iteratively. The approach is based on "fast" linear wave theory since short and high wave groups evolve from long and low wave groups. Consequently, rogue waves have a "linear (describable) past". The non-linear characteristics are implemented using Stokes Third Order wave theory. Although both models – linear and Third Order – cannot be used exclusively the underlying characteristics can be adopted for an easy-to-handle non-linear iterative procedure.

In chapter 4, examples for deterministic wave sequences are given. Both standard model seas and special wave sequences are realized. Converging waves are used for the experimental generation of extreme waves within a storm sea. The process of wave generation at a given target position in the model tank based on the *modified non-linear theory* is explained. Several types of wave transformations (upstream and downstream as well as the calculation of the wave train in the moving reference frame) based on the modified approach are presented.

Chapter 5 focuses on the experimental investigation of large roll motions of a ship due to unfavorable environmental conditions. A computer controlled capsizing test procedure is introduced and results for different types of deterministic wave sequences are given. The test procedure along with the non-linear transformation gives the exact time-space correlation of wave excitation and ship motion, and an arbitrary wave registration can be transformed into the moving reference frame of a cruising ship.

In chapter 6, the results of the entire procedure are used for the validation of a modern numerical motion simulation tool such as used during the design process at shipyards. As a new concept, the direct comparison of time series from numerical simulations and capsizing tests based on deterministic wave sequences is presented. Results from the validation and their implication for safer ship design and operation are discussed.

Chapter 7 summarizes the findings of the thesis and gives a perspective for future developments and applications.

1.4 General remarks

Throughout the thesis mainly two different model basins are referred to:

- Towing tank at the Hamburg Ship Model Basin (HSVA) – tank dimensions: length 300 m, width 18 m, water depth 5.6 m, double flap wave maker ($\omega = 0.5 \ldots 15$ rad/s)
- Wave tank at Technical University Berlin (TUB) – tank dimensions: length 80 m, width 4 m, water depth 1.5 m, piston type wave maker ($\omega = 0.5 \ldots 12$ rad/s)

All surface elevation measurements presented in this thesis are either performed by ultrasonic wave probes or by gauges of the surface-piercing resistive type comprising pairs of stainless steel rods, placed parallel with the wave crests.

The term "registration" is only used if the time series has been measured. Otherwise simply "time series" is used. Furthermore, the terms "linear" and "non-linear" abbreviate "linear describable" and "non-linear describable", respectively.

"Technical University Berlin" is abbreviated "TUB". "HSVA" is the Hamburg Ship Model Basin.

Chapter 2

Mathematical Description of Ocean Waves

In this chapter, mathematical basics for modelling wind driven ocean waves are given. In particular, Stokes First and Third Order wave theories are summarized as the advantages of linear and non-linear wave theory will be combined in the next chapter to derive the *modified non-linear theory* for modelling wave propagation in terms of the surface elevation.

Also other wave models are mentioned to give a brief review on what is available in the face of wave generation and analysis for experimental investigations, i. e. upstream and downstream transformation of surface elevation time series.

2.1 Basic equations of the water wave problem

The waves to be considered are caused by wind over the free water surface. Wave length and height increase with duration and fetch of the wind system which can be described by different mathematical models (Sobey (2002), Fontaine (2001)). For the mathematical description of ocean waves, an already perturbed free surface is assumed. The wave generation process is re-modelled by a wave maker (see chapter 4).

The perturbed ocean surface is a boundary of the domain Ω (Fig. 2.1) which is also bounded by the sea bottom and open and infinite in all other directions. Uni-directional, long-crested, non-breaking waves are considered. An ideal –

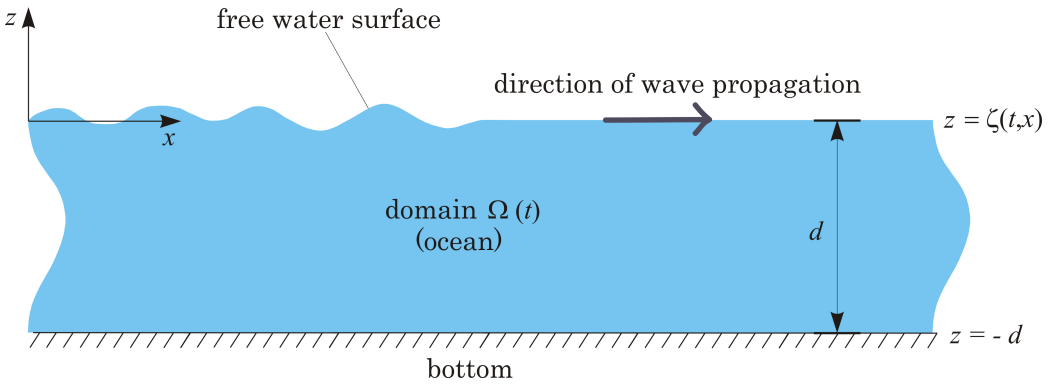

Figure 2.1: Domain for the water wave problem.

i. e. incompressible and inviscid – fluid (water) is assumed. Surface tension is neglected. These are the assumptions to derive the following equations.

2.1.1 Laplace equation

Consider a finite volume of fluid V which is of arbitrary size and shape but fixed and wholly contained within the fluid. According to the law of conservation of mass, the only way that the mass m of the volume V can change is by mass transport across its boundaries (e. g. Truckenbrodt (1968)). In general, mass m must be in accord with the equation

$$\frac{dm}{dt} = -\int_A \vec{n} \cdot \rho \vec{v} dA, \tag{2.1}$$

where $\vec{n}$ is the outward unit normal to the surface A of V. However, the definition of fluid density ρ gives

$$\frac{dm}{dt} = \frac{d}{dt}\int_V \rho dV = \int_V \frac{\partial \rho}{\partial t} dV, \tag{2.2}$$

since V is fixed. Inserting this in Eq. 2.1,

$$-\int_A \vec{n} \cdot \rho \vec{v} dA = \int_V \frac{\partial \rho}{\partial t} dV, \tag{2.3}$$

and transforming the surface integral by the divergence theorem, this yields

$$\int_V \left(\frac{\partial \rho}{\partial t} + \nabla(\rho \vec{v}) \right) dV = 0. \tag{2.4}$$

Since V is arbitrary, the only way that Eq. 2.4 can be satisfied in general is that the integrand vanishes, consequently

$$\frac{\partial \rho}{\partial t} + \nabla(\rho \vec{v}) = 0, \tag{2.5}$$

which is one form of the equation of continuity. With constant density ρ, this gives:

$$\nabla \vec{v} = 0. \tag{2.6}$$

Since the flow is assumed being irrotational and inviscid, rotation of the velocity field vanishes,

$$\nabla \times \vec{v}(t) = 0, \quad \text{if} \quad \nabla \times \vec{v}(t=0) = 0, \tag{2.7}$$

and a velocity potential $\Phi : \mathbb{R}^3 \to \mathbb{R}$, $\nabla\Phi = \vec{v}$, can be introduced with

$$\nabla \times (\nabla \Phi) = 0. \tag{2.8}$$

Inserting Φ in the equation of continuity yields the Laplace equation for the domain Ω:

$$\triangle \Phi = \nabla(\nabla \Phi) = 0 \quad \text{in} \quad \Omega(t). \tag{2.9}$$

2.1.2 Kinematic free surface boundary condition

The free surface – which is the dividing rule between air and water – is defined implicitly by

$$S(x, z, t) := \zeta(x, t) - z = 0. \tag{2.10}$$

It is deformed with time and does not allow penetration of water particles. Thus, the total derivative of S vanishes:

$$\frac{DS}{Dt} = S_t + uS_x + wS_z = \zeta_t + u\zeta_x - w = 0. \tag{2.11}$$

Inserting the velocity potential Φ, this gives the kinematic boundary condition for the problem:

$$\zeta_t + \Phi_x \zeta_x - \Phi_z = 0 \quad \text{on} \quad z = \zeta(x, t). \tag{2.12}$$

2.1.3 Dynamic free surface boundary condition

The Bernoulli equation applies on the free surface:

$$\rho\Phi_t + \frac{\rho}{2}|\vec{v}^2| + p + \rho g z = p_0 \quad \text{on} \quad z = \zeta(x,t). \tag{2.13}$$

Since the density of air is much less than the density of water, pressure variations due to air movements introduced by disturbances of the surface can be neglected. Thus, the pressure in the Bernoulli equation is assumed being the atmospheric pressure, $p = p_0$. Inserting the velocity potential, Eq. 2.13 becomes

$$\Phi_t + \frac{1}{2}(\Phi_x^2 + \Phi_z^2) + g\zeta = 0 \quad \text{on} \quad z = \zeta(x,t). \tag{2.14}$$

2.1.4 Bottom boundary condition

At the rigid sea bottom (constant water depth), normal velocities vanish:

$$w = \Phi_z = 0 \quad \text{on} \quad z = -d. \tag{2.15}$$

2.2 Solvability of the water wave problem

The considered water wave problem summarizes as:

$$\begin{aligned}
\triangle\Phi &= 0 \quad \text{in} \quad \Omega(t) && (2.16)\\
\zeta_t + \Phi_x\zeta_x - \Phi_z &= 0 \quad \text{on} \quad z = \zeta(x,t) && (2.17)\\
\Phi_t + \frac{1}{2}(\Phi_x^2 + \Phi_z^2) + g\zeta &= 0 \quad \text{on} \quad z = \zeta(x,t) && (2.18)\\
\Phi_z &= 0 \quad \text{on} \quad z = -d && (2.19)
\end{aligned}$$

To obtain a complete two-dimensional Cauchy problem, initial conditions for the solutions Φ and ζ have to be formulated:

$$\begin{aligned}
\Phi(t=0,x,z) &= \Phi_I(x,z) && (2.20)\\
\zeta(t=0,x) &= \zeta_I(x) && (2.21)
\end{aligned}$$

Thus, propositions on solvability exist: According to Kano and Nishida (1979) and Nishida (1986), the Cauchy problem has a sound formulation. Nevertheless, a closed solution cannot be obtained due to the coupling of potential Φ and unknown boundary ζ. However, different approaches provide adequate approximations as discussed in the following sections.

2.3 Perturbation wave theory

According to Levi-Civita (1925), a perturbation approach is adequate and solvability for small amplitudes can be proven since the problem has an asymptotic series for small parameters. In Stokes wave theory, the wave steepness $\varepsilon := \zeta_a k$ with ζ_a wave amplitude, k wave number, is assumed being "sufficiently small". The solutions of the Cauchy problem, Φ and ζ, are developed as perturbation series around ε,

$$\Phi = \Phi_\varepsilon = \sum_{m=0}^{\infty} \Phi_m \varepsilon^m, \tag{2.22}$$

$$\zeta = \zeta_\varepsilon = \sum_{m=0}^{\infty} \zeta_m \varepsilon^m, \tag{2.23}$$

and inserted in Eqs. 2.16-2.19.

By comparison of coefficients follows for the Laplace equation 2.16 and the bottom boundary condition 2.19:

$$\begin{aligned} \triangle\Phi_m &= 0, \quad m = 0, 1, 2, \ldots, && (2.24)\\ \Phi_{m,z} &= 0, \quad m = 0, 1, 2, \ldots. && (2.25) \end{aligned}$$

The kinematic free surface boundary condition 2.17 becomes

$$\begin{aligned} \zeta_{0,t} &= 0, && (2.26)\\ \Phi_{1,x}\zeta_{0,x} + \zeta_{1,t} &= \Phi_{1,z}, \\ \Phi_{2,x}\zeta_{0,x} + \zeta_{2,t} &= \Phi_{2,z} - \Phi_{1,x}\zeta_{1,x} - \zeta_1(\Phi_{1,xz}\zeta_{0,x} - \Phi_{1,zz}), \\ &\ldots \quad . \end{aligned}$$

Same approach applies for the dynamic boundary condition 2.18:

$$\begin{aligned} \zeta_0 &= 0, && (2.27)\\ g\zeta_1 + \Phi_{1,t} &= 0, \\ g\zeta_2 + \Phi_{2,t} + \frac{1}{2}\left(\Phi_{1,x}^2 + \Phi_{1,z}^2\right) + \zeta_1 + \Phi_{1,tz} &= 0, \\ &\ldots \quad . \end{aligned}$$

With $\zeta_0 = 0$ in 2.27, the kinematic boundary condition becomes:

$$\begin{aligned} \zeta_{1,t} &= \Phi_{1,z}, && (2.28)\\ \zeta_{2,t} &= \Phi_{2,z} - \Phi_{1,x}(\zeta_{1,x} - \Phi_{1,zz}), \\ &\ldots \quad , \\ \zeta_{n,t} &= \Phi_{n,z} + G_{n-1}, \end{aligned}$$

where G_{n-1} is a term depending on Φ_m and ζ_m with $m \leq n-1$.

Accordingly, for the dynamic boundary condition follows

$$\begin{aligned} g\zeta_1 + \Phi_{1,t} &= 0, \\ g\zeta_2 + \Phi_{2,t} + \frac{1}{2}\left(\Phi_{1,x}^2 + \Phi_{1,z}^2\right) + \zeta_1 + \Phi_{1,tz} &= 0, \\ &\cdots , \\ g\zeta_n + \Phi_{n,t} &= F_{n-1}, \end{aligned} \tag{2.29}$$

with F_{n-1} depending on Φ_m and ζ_m, $m \leq n-1$.

The solutions Φ_m and ζ_m are calculated successively from the corresponding Φ_{m-1} and ζ_{m-1}. Depending on the order of considered terms, different wave theories are obtained. Up to first order, the surface boundary conditions are valid on $z = \zeta_0 = 0$.

2.3.1 Linear wave theory (Airy)

Linear wave theory according to Airy refers to perturbation up to first order, $\Phi = \varepsilon\Phi_1$ and $\zeta = \varepsilon\zeta_1$. The surface boundary conditions have to be satisfied at $z = 0$. Thus, the following strongly simplified system within a fixed domain is obtained:

$$\triangle\Phi = 0 \quad \text{in} \quad \Omega = \{(x,z)|x \in \mathbb{R}; -d < z < 0\}, \tag{2.30}$$

$$\zeta_t - \Phi_z = 0 \quad \text{on} \quad z = 0, \tag{2.31}$$

$$g\zeta + \Phi_t = 0 \quad \text{on} \quad z = 0, \tag{2.32}$$

$$\Phi_z = 0 \quad \text{on} \quad z = -d, \tag{2.33}$$

$$\Phi(0,x,z) = \Phi_I(x,z), \tag{2.34}$$

$$\zeta(0,x) = \zeta_I(x). \tag{2.35}$$

Alternatively, the linearized free surface boundary conditions 2.31 and 2.32 can be summarized as Cauchy-Poisson condition:

$$\Phi_{tt} + g\Phi_z = 0 \quad \text{on} \quad z = 0. \tag{2.36}$$

The solutions of this problem are assumed being time harmonic and obtained by separation of variables. They have the following form (e. g. Wehausen and Laitone (1960)):

$$\Phi(t,x,z) = \frac{\zeta_a g}{\omega(k)} \frac{\cosh k(z+d)}{\cosh(kd)} \sin(kx - \omega(k)t). \tag{2.37}$$

The corresponding surface elevation is:

$$\zeta(t,x) = \zeta_a \cos(kx - \omega(k)t), \tag{2.38}$$

where the frequency $\omega(k)$ is determined by the dispersion relation:

$$\omega^2(k) = kg \tanh(kd). \tag{2.39}$$

Usually, Airy wave theory is adequate for wave steepness $\zeta_a k < 0.05\pi$.

Table 2.1 summarizes the results of linear wave theory. The index 0 refers to deep water. The following simplifications are assumed:

- Deep water ($\frac{d}{L} \geq 0.5$):

$$\cosh k(z+d) \approx \sinh k(z+d) \approx \frac{1}{2} e^{kz} e^{kd}, \tag{2.40}$$

$$\cosh kd \approx \sinh kd \approx \frac{1}{2} e^{kd}. \tag{2.41}$$

- Shallow water ($\frac{d}{L} \leq 0.04$):

$$\cosh k(z+d) \approx \cosh kd \approx 1, \tag{2.42}$$

$$\sinh k(z+d) \approx k(z+d), \tag{2.43}$$

$$\sinh kd \approx kd. \tag{2.44}$$

2.3.2 Stokes Third Order wave theory

Series expansion of velocity potential and wave elevation up to third order leads to Stokes Third Order solutions (e. g. Kinsman (1965)). Third Order is considered here because the propagation velocity is crucial for the iteration method proposed in chapter 3. On the other hand, Stokes Second Order wave theory does not reflect an increase of propagation speed due to wave steepness.

Third Order wave theory also reflects other properties of steep surface waves (see chapter 3) such as an increase of crest-trough asymmetry as well as a velocity profile between wave crest and mean sea level of exponential shape such as confirmed by particle image velocimetry (PIV) (Grue (2002)).

$\boxed{\text{Phase}}$ $\theta = kx - \omega t$	Deep water	Intermediate depth	Shallow water
Relative water depth $\frac{d}{L}$	$\frac{d}{L} \geq 0.5$	$0.04 < \frac{d}{L} < 0.5$	$\frac{d}{L} \leq 0.04$
Velocity potential Φ	$\frac{\zeta_a g}{\omega} e^{kz} \sin\theta$	$\frac{\zeta_a g}{\omega} \frac{\cosh k(z+d)}{\cosh kd} \sin\theta$	$\frac{\zeta_a g}{\omega} \sin\theta$
Surface elevation ζ	$\zeta_a \cos\theta$	$\zeta_a \cos\theta$	$\zeta_a \cos\theta$
Dynamic pressure $p_{dyn} = -\rho\frac{\partial\Phi}{\partial t}$	$\rho g \zeta_a e^{kz} \cos\theta$	$\rho g \zeta_a \frac{\cosh k(z+d)}{\cosh kd} \cos\theta$	$\rho g \zeta_a \cos\theta$
Water particle velocities			
- horizontal $u = \frac{\partial\Phi}{\partial x}$	$\zeta_a \omega e^{kz} \cos\theta$	$\zeta_a \omega \frac{\cosh k(z+d)}{\sinh kd} \cos\theta$	$\zeta_a \omega \frac{1}{kd} \cos\theta$
- vertical $w = \frac{\partial\Phi}{\partial z}$	$\zeta_a \omega e^{kz} \sin\theta$	$\zeta_a \omega \frac{\sinh k(z+d)}{\sinh kd} \sin\theta$	$\zeta_a \omega (1 + \frac{z}{d}) \sin\theta$
Water particle accelerations			
- horizontal $\dot{u} = \frac{\partial u}{\partial t}$	$\zeta_a \omega^2 e^{kz} \sin\theta$	$\zeta_a \omega^2 \frac{\cosh k(z+d)}{\sinh kd} \sin\theta$	$\zeta_a \omega^2 \frac{1}{kd} \sin\theta$
- vertical $\dot{w} = \frac{\partial w}{\partial t}$	$-\zeta_a \omega^2 e^{kz} \cos\theta$	$-\zeta_a \omega^2 \frac{\sinh k(z+d)}{\sinh kd} \cos\theta$	$-\zeta_a \omega^2 (1 + \frac{z}{d}) \cos\theta$
Wave celerity $c = \frac{\omega}{k} = \frac{L}{T}$	$c_0 = \sqrt{\frac{g}{k_0}} = \frac{g}{\omega}$	$c = \sqrt{\frac{g}{k} \tanh kd}$	$c = \sqrt{gd}$
Group velocity $c_{gr} = \frac{d\omega}{dk}$	$c_{gr} = \frac{c_0}{2} = \frac{g}{2\omega}$	$c_{gr} = \frac{c}{2}\left[1 + \frac{2kd}{\sinh 2kd}\right]$	$c_{gr} = c = \sqrt{gd}$
Circular frequency $\omega = \frac{2\pi}{T}$	$\omega = \sqrt{k_0 g}$	$\omega = \sqrt{kg \tanh kd}$	$\omega = k\sqrt{gd}$
Wave length $L = \frac{2\pi}{k}$	$L_0 = \frac{g}{2\pi} T^2$	$kd \tanh kd = \frac{\omega^2}{g} d$	$L = T\sqrt{gd}$
Wave number $k = \frac{2\pi}{L}$	$k_0 = \frac{\omega^2}{g}$		$k = \frac{\omega}{\sqrt{gd}}$
Water particle displacements			
- horizontal ξ	$-\zeta_a e^{kz} \sin\theta$	$-\zeta_a \frac{\cosh k(z+d)}{\sinh kd} \sin\theta$	$-\zeta_a \frac{1}{kd} \sin\theta$
- vertical η	$\zeta_a e^{kz} \cos\theta$	$\zeta_a \frac{\sinh k(z+d)}{\sinh kd} \cos\theta$	$\zeta_a (1 + \frac{z}{d}) \cos\theta$
Particle trajectories	Circular orbits	Elliptical orbits	Elliptical orbits

Table 2.1: Results of linear wave theory (Airy).

The results of Stokes Third Order wave theory according to Skjelbreia (1959) are listed below. Table 2.2 summarizes the deep water simplifications. Stokes wave theories of higher order are commonly applied to "not too shallow" water, $d/L > 0.15$. The wave steepness is limited to $\zeta_a k = 0.44$.

Velocity potential:

$$\begin{aligned}\Phi &= \zeta_a \frac{\omega}{k} \frac{\cosh k(z+\eta+d)}{\sinh kd} \sin\theta + \frac{3}{8}\zeta_a^2 \omega \frac{\cosh 2k(z+\eta+d)}{\sinh^4 kd} \sin 2\theta \\ &+ \frac{1}{64}\zeta_a^3 k\omega \cosh 3k(z+\eta+d) \frac{11-2\cosh 2kd}{\sinh^7 kd} \sin 3\theta, \qquad (2.45) \\ \theta &= kx - \omega t\end{aligned}$$

Wave height:

$$H = \zeta_{\theta=0^\circ} - \zeta_{\theta=180^\circ} = 2\zeta_a + \frac{3}{4}\zeta_a^3 k^2 \cdot \frac{1}{8} \frac{8\cosh^6 kd + 1}{\sinh^6 kd} \qquad (2.46)$$

Surface elevation:

$$\zeta = \zeta_a \cos\theta + \frac{1}{2}\zeta_a^2 k \frac{\cosh kd(\cosh 2kd + 2)}{2\sinh^3 kd} \cos 2\theta + \frac{3}{8}\zeta_a^3 k^2 \cdot \frac{1}{8} \frac{8\cosh^6 kd + 1}{\sinh^6 kd} \cos 3\theta \qquad (2.47)$$

Dynamic pressure:

$$p_{dyn} = -\rho \left(\frac{\partial \Phi}{\partial t} + \frac{1}{2}(u^2 + w^2) \right) \qquad (2.48)$$

Water particle velocities

- horizontal:

$$\begin{aligned}u = \frac{\partial \Phi}{\partial x} &= \zeta_a \omega \frac{\cosh k(z+\eta+d)}{\sinh kd} \cos\theta + \frac{3}{4}\zeta_a^2 \omega k \frac{\cosh 2k(z+\eta+d)}{\sinh^4 kd} \cos 2\theta \\ &+ \frac{3}{64}\zeta_a^3 \omega k^2 \cosh 3k(z+\eta+d) \frac{11-2\cosh 2kd}{\sinh^7 kd} \cos 3\theta \qquad (2.49)\end{aligned}$$

- vertical:

$$\begin{aligned}w = \frac{\partial \Phi}{\partial z} &= \zeta_a \omega \frac{\sinh k(z+\eta+d)}{\sinh kd} \sin\theta + \frac{3}{4}\zeta_a^2 \omega k \frac{\sinh 2k(z+\eta+d)}{\sinh^4 kd} \sin 2\theta \\ &+ \frac{3}{64}\zeta_a^3 \omega k^2 \sinh 3k(z+\eta+d) \frac{11-2\cosh 2kd}{\sinh^7 kd} \sin 3\theta \qquad (2.50)\end{aligned}$$

Water particle accelerations

- horizontal:

$$\dot{u} = \frac{\partial u}{\partial t} + \frac{1}{2}\frac{\partial}{\partial x}(u^2 + w^2) \tag{2.51}$$

- vertical:

$$\dot{w} = \frac{\partial w}{\partial t} + \frac{1}{2}\frac{\partial}{\partial (z + \eta + d)}(u^2 + w^2) \tag{2.52}$$

Wave celerity:

$$c = \frac{\omega}{k} = \sqrt{\frac{g}{k}\tanh kd\left(1 + (\zeta_a k)^2 \frac{\cosh 4kd + 8}{8\sinh^4 kd}\right)} \tag{2.53}$$

Circular frequency:

$$\omega = \sqrt{kg\tanh kd\left(1 + (\zeta_a k)^2 \frac{\cosh 4kd + 8}{8\sinh^4 kd}\right)} \tag{2.54}$$

Particle displacements as referred to the mean particle position

- horizontal:

$$\begin{aligned}
\xi = & - \frac{1}{k}[F_1(1 - \frac{1}{8}F_1^2)\cosh k(z+d) + \frac{1}{8}F_1(3F_1^3 + 10F_2)\cosh 3k(z+d)]\sin\theta' \\
& - \frac{2}{k}[-\frac{1}{2}F_1^2 + F_2\cosh 2k(z+d)]\sin 2\theta' \\
& - \frac{3}{k}[\frac{1}{4}F_1(F_1^2 - 5F_2)\cosh k(z+d) + F_3\cosh 3k(z+d)]\sin 3\theta' \\
& + \frac{ct}{2}F_1^2[\cosh 2k(z+d) - F_1\cosh k(z+d)\cosh 2k(z+d)\cos\theta']
\end{aligned} \tag{2.55}$$

- vertical:

$$\begin{aligned}
\eta = & \frac{1}{k}[F_1(1 - \frac{3}{8}F_1^2)\sinh k(z+d) + \frac{1}{8}F_1(F_1^2 + 6F_2)\sinh 3k(z+d)]\cos\theta' \\
& + \frac{2}{k}F_2\sinh 2k(z+d)\cos 2\theta' \\
& + \frac{3}{k}[-\frac{3}{4}F_1F_2\sinh k(z+d) + F_3\sinh 3k(z+d)]\cos 3\theta' \\
& - \frac{ct}{2}F_1^3\sinh k(z+d)\cosh 2k(z+d)\sin\theta'
\end{aligned} \tag{2.56}$$

with

$$\theta' = kx' - \omega t, \tag{2.57}$$

x' horizontal position of particle in its mean position, and

$$\begin{aligned} F_1 &= \zeta_a k \frac{1}{\sinh kd}, \\ F_2 &= \frac{3}{4}(\zeta_a k)^2 \frac{1}{\sinh^4 kd}, \\ F_3 &= \frac{3}{64}(\zeta_a k)^3 \frac{11 - 2\cosh 2kd}{\sinh^7 kd}. \end{aligned} \tag{2.58}$$

The equation for the determination of wave height H from wave "amplitude" ζ_a,

$$H = \zeta_{\theta=0^\circ} - \zeta_{\theta=180^\circ} = 2\zeta_a + \frac{3}{4}\zeta_a^3 k^2, \tag{2.59}$$

can be useful for the analysis of steep regular waves in a model basin — as an example given the wave height $H = 0.4$ m and wave length $L = 5$ m. Thus, the wave number is given by $k \approx 1.26$ 1/m and the wave steepness is $H/L = 0.08$. Eq. 2.59 is solved with respect to ζ_a by application of the Cardan formulae:

$$\zeta_a = \sqrt[3]{\frac{H}{2} + \sqrt{\frac{H^2}{4}\left(\frac{8}{9}\frac{1}{k^2}\right)^3}} + \sqrt[3]{\frac{H}{2} - \sqrt{\frac{H^2}{4}\left(\frac{8}{9}\frac{1}{k^2}\right)^3}}. \tag{2.60}$$

Insertion of k and H as above gives $\zeta_a \approx 0.23$ m. In contrast, $\zeta_a = H/2$(=0.2 m) is only valid for strictly harmonic (or very small) waves.

2.4 Other wave models

2.4.1 Solitary and cnoidal waves

As small parameter for the series expansion, also the relative water depth $2\zeta_a/d$ can be used. The wave steepness $\zeta_a k$ and the relative water depth are summarized by the Ursell parameter,

$$U_R = \frac{8\pi^2 \zeta_a}{k^2 d^3}, \tag{2.61}$$

which is used to define the validity limits of different wave theories (Clauss et al. (1988)).

$\boxed{\text{Phase}}$	$\theta = kx - \omega t$	Deep water
Relative water depth	$\frac{d}{L}$	$\frac{d}{L} \geq 0.5$
Velocity potential	Φ	$\zeta_a \frac{\omega}{k} e^{k(z+\eta)} \sin\theta$
Surface elevation	ζ	$\zeta_a \cos\theta + \frac{1}{2}\zeta_a^2 k \cos 2\theta + \frac{3}{8}\zeta_a^3 k^2 \cos 3\theta$
Wave height	H	$2\zeta_a + \frac{3}{4}\zeta_a^3 k^2$
Dynamic pressure	p_{dyn}	$-\rho(\frac{\partial\Phi}{\partial t} + \frac{1}{2}(u^2 + w^2))$
Water particle velocities		
- horizontal	$u = \frac{\partial\Phi}{\partial x}$	$\zeta_a \omega e^{k(z+\eta)} \cos\theta$
- vertical	$w = \frac{\partial\Phi}{\partial z}$	$\zeta_a \omega e^{k(z+\eta)} \sin\theta$
Water particle accelerations		
- horizontal	$\dot{u} = \frac{\partial u}{\partial t}$	$\zeta_a \omega^2 e^{k(z+\eta)} \sin\theta$
- vertical	$\dot{w} = \frac{\partial w}{\partial t}$	$-\zeta_a \omega^2 e^{k(z+\eta)} \cos\theta$
Wave celerity	$c = \frac{\omega}{k} = \frac{L}{T}$	$\sqrt{\frac{g}{k}(1 + (\zeta_a k)^2)}$
Group celerity	$c_{gr} = \frac{d\omega}{dk}$	$\frac{c}{2} + \frac{g}{\omega}(\zeta_a k)^2$
Circular frequency	$\omega = \frac{2\pi}{T}$	$\sqrt{kg(1 + (\zeta_a k)^2)}$
Wave length	L	$\frac{T^2 g}{2\pi}(1 + (\zeta_a k)^2)$
Water particle displacements		
- horizontal	ξ	$-\zeta_a \left[e^{kz} + \frac{3}{2}(\zeta_a k)^2 e^{3kz}\right] \sin\theta' + ct \left[(\zeta_a k)^2 e^{2kz} - \zeta_a k e^{3kz} \cos\theta'\right]$
- vertical	η	$\zeta_a \left[e^{kz} + \frac{1}{2}(\zeta_a k)^2 e^{3kz}\right] \cos\theta' + ct(\zeta_a k)^3 e^{3kz} \sin\theta'$
		$\theta' = kx' - \omega t$, x' horizontal position of particle in its mean position

Table 2.2: Results of Stokes Third Order wave theory for deep water.

Dispersive long waves are characterized by an Ursell parameter of $U_R > 26$ which means that they are relatively long compared to the water depth. Therefore, they are also referred to as shallow water waves. If they propagate at constant speed without change of form they are called permanent waves where non-linearity tends to steepen the crest while dispersion counteracts this trend. For permanent waves these two effects have to be in perfect balance. Dispersive long waves of permanent form are described by the Boussinesq equation which gives two cases, cnoidal and solitary waves (Crapper (1984)).

Cnoidal waves are periodic permanent waves and can also be derived by series expansion which gives the shallow water wave theory. A solitary wave has a single hump height above the undisturbed depth d which diminishes to zero at infinity. This type of wave has been first described by John Scott Russell in 1834. The surface elevation is given as

$$\begin{aligned} \zeta &= a\mathrm{sech}^2\left(\sqrt{\frac{3a}{4d^3}}(x-ct)\right), \\ c &= c_I\left(1+\frac{a}{2d}\right). \end{aligned} \tag{2.62}$$

The solitary wave progresses without change of form with speed c which is greater than the undisturbed wave speed $c_I = \sqrt{gd}$. Solitary waves can be easily generated in a long tank by almost any kind of impulse. Well-known examples for shallow water waves are Tsunamis.

2.4.2 Sea states

The presented Stokes wave theories describe the rather academic case of regular waves. However, the classical approach to model the apparently chaotic wave field of a natural seaway in a model basin is based on linear wave theory, i. e. the superposition of a number of independent harmonic waves with amplitude ζ_{aj} and random phase φ_j:

$$\zeta(t) = \sum_{j=1}^{n} \zeta_{aj}\cos(\omega_j t - \varphi_j). \tag{2.63}$$

Each component wave contributes an amount of energy to the seaway proportional to its squared wave amplitude (Clauss et al. (1992)) according to the chosen spectrum.

A more realistic sea state can be simulated by pairwise interaction of linear components of the wave spectrum through a perturbation expansion of the

governing equations. This leads to second or higher order bound waves (see chapter 3). But long waves can carry small high frequency waves far from the first order boundary $z = 0$ where the linear equations are not valid. For this case, it is more appropriate to expand the free surface boundary conditions at the long wave surface rather than at the undisturbed surface. It is known as the phase modulation solution. In this solution, the exponential function depends not only on z but also on the phase of the long wave. To expand this idea to nearly equal frequencies in the energy containing part of the spectrum, Zhang et al. (1999) have developed the hybrid wave model. They divide the spectrum into several ranges, typically two long wave and two short wave ranges. Interactions of waves in the same or neighboring bands are calculated using the conventional solution. The interaction of waves in band separated by at least one other band are calculated using the phase modulation solution (Forristal (2001)).

The ocean environment of a deterministic wave sequence considered throughout this thesis, is represented by single moded wave spectra. Since the ships investigated in chapter 5 and 6 are built for North Sea routes, the JONSWAP spectrum is applied which has been derived by Hasselmann et al. (1973) from field measurements.

The JONSWAP energy density spectrum is defined as (Clauss and Riekert (1996)):

$$S(\omega) = \frac{\alpha g^2}{\omega^5} e^{-\frac{5}{4}\left[\frac{\omega_P}{\omega}\right]^4} \gamma^B, \tag{2.64}$$

with

$$\begin{aligned}
\alpha &= 0.3395 \left(\frac{H_s \omega_P^2}{g}\right)^{2.036} [1 - 0.298 \ln \gamma], \qquad (2.65)\\
B &= e^{\frac{-(\omega-\omega_P)^2}{2\sigma^2\omega_P^2}},\\
\sigma &= \begin{cases} 0.07 & \text{for} \quad \omega \leq \omega_P \\ 0.09 & \text{for} \quad \omega > \omega_P \end{cases},\\
\omega_P &= \frac{2\pi}{T_P}.
\end{aligned}$$

It is considered to be a suitable description of a broadbanded ocean spectrum in a fetch-limited sea such as the North Sea. If the peak enhancement factor is given as $\gamma = 1$ the Pierson-Moskowitz spectrum (Pierson and Moskowitz (1964)) is obtained which is also known as ITTC spectrum (ITTC (2002)). H_s and T_P have to be chosen according to the planned operating location.

However, many research groups worry about the restrictions which are due to this spectrum:

- Since static response was the predominant design criterion for offshore structures when the spectrum was developed, the spectral model is mainly focused on reproducing accurately the energy contents in the vicinity of the main spectral peak, whereas other frequency bands are rather neglected.

- Among the chosen spectral shapes, particularly the ω^{-5} decay of the tail of the spectrum ("high frequency tail") is based on linear wave description with regard to wind wave generation. Furthermore, validation by buoy measurements neglects the fact that buoys erase the non-linear parts of the surface elevation signal.

- The JONSWAP project proposed a modification of the Pierson-Moskowitz spectrum suited for the North Sea. Thus, the generalization to other regions has to be validated before application.

The validity of the various spectral models is subject to many investigations, such as Olagnon (2001) – including suggestion of alternative spectral models – or Battjes et al. (1987) – with respect to a better fit of a ω^{-4} high frequency tail. Hogben (2001) summarizes values of T_P for given values of H_s depending on the general sea condition – classified as Open Ocean, Long Seas, Limited Fetch, and Steep Seas. All these considerations play a minor role for the investigations in this work as it is rather concerned with deterministic processes related to wave sequences of limited duration.

2.4.3 Design waves

A commonly used method for the prediction of linear or non-linear wave induced loads on ships and offshore structures due to an exceptionally high wave – e. g. a 100-years wave – is the so-called design wave approach based on a suitable model. In general, the chosen model is either non-linear and regular (Stokes Third Order wave theory for $d/L > 0.15$, stream function theory (Dean (1974)) for more shallow water) or linear and random with empirical stretching models for the kinematics (vertical extrapolation of particle velocities above mean water level, e. g. Wheeler stretching). Woltering (1996) shows that stretching can be replaced by consequent Lagrangian evaluation of Stokes wave theories.

Classical approaches tend to underestimate the wave height and response of the most probable design wave. A more sophisticated approach is the *NewWave* Theory as introduced by Tromans et al. (1991). The *NewWave* is

the model of an extreme wave with the most probable shape in a linear random Gaussian model for a sea state. Thus, the shape is the auto-correlation function of the chosen spectrum as the average shape of a large crest tends to the scaled auto-correlation function of the surface. The height of the extreme crest is usually chosen arbitrarily, different heights correspond to different levels of likelihood in the random sea state (Taylor and Clifford (1999)). An important feature of the model is that it links an averaged local extreme event to the global properties of the sea state since the auto-correlation function is the Fourier transform of the underlying power spectrum.

The *NewWave* is the design event of choice for fixed platforms as it gives the most probable shape of the extreme event, thus the highest velocities and forces.

2.4.4 Creamer transform

Creamer et al. (1989) proposed a transformation of a linear wave surface which gives a very accurate representation of the non-linear bound wave structure as shown by Taylor et al. (1999). The Creamer transform is given by

$$\zeta_k = \frac{1}{|k|} \int \exp(-ikx)\{\exp(ik\zeta_H) - 1\}dx, \tag{2.66}$$

where ζ_H is the horizontal fluid particle displacement at $z = 0$, calculated from linear theory by taking the Hilbert transform of the linear surface elevation, which gives a phase shift of 90°. The integration over the whole periodic domain gives the complex amplitude of the non-linear component at wave number k (Forristal (2001)).

Creamer et al. (1989) give a mathematical justification for the transform, and the asymmetry between crests and troughs is reproduced quite exactly. The Creamer transform can be used to distinguish resonant and non-resonant wave-wave interactions (Taylor and Clifford (1999)). It is also possible to strip away the local non-resonant bound wave structure to receive the corresponding linear, free wave spectrum. Local space-to-time and time-to-space transformations can be performed by the Creamer transform. However, slow cumulative interactions between components cannot be covered by this model.

Also, the transform is shown to reproduce very accurately the modulation of short waves by longer waves. Thus, the linear input is simply the linear superposition of short wave packet and long carrier wave. Once a linear estimate of the shape of the free surface is specified as an initial condition,

the Creamer transform can be used to estimate both the equivalent non-linear surface and the local wave kinematics. This implies that an important use for the Creamer transform may be in providing a compatible pair of surface elevation and velocity potential values at all points on the free surface for starting non-linear numerical simulations, if there is no requirement to model a wave paddle.

2.4.5 Numerical Wave Tanks

Many commercial and non-commercial solvers exist which are also referred to as Numerical Wave Tanks. Most of them model a wave maker as a certain boundary and calculate the corresponding wave propagation applying a potential theory approach or solving the RANS (Reynolds Averaged Navier-Stokes) equations. Another aspect is how the domain is discretized (FEM, VOF, structured or unstructured mesh), see e. g. Clauss and Steinhagen (1999), Steinhagen (2001), Clauss et al. (2004b). Grue (2002) as well as Clamond and Grue (2001) present a method essentially based on a fast converging iterative solution procedure of the Laplace equation. It is applied to the formation of steep waves. Forristal (2001) gives a review of several Numerical Wave Tanks. Numerical Wave Tanks are an interesting prerequisite to pre-simulate test conditions before the execution of the physical model test as shown by Bonnefoy (2004).

2.5 Discussion of existing wave models

The wave models mentioned here serve as examples without any claim to be complete, but they already document that a large variety for different types of applications exists. One of the key factors for the generation and transformation of deterministic wave sequences is the knowledge of how the wave propagates. This characteristic depends sensitively on the wave theory chosen for modelling the wave train.

The standard wave models used in ocean engineering are based on either Stokes wave theory – thus non-linear but regular – or linear wave theory with empirical stretching models for the kinematics – thus irregular but linear. The design wave models presented here are used for the statistical evaluation of designs by a representative (deterministic) design wave and are not able to model upstream and downstream wave propagation deterministically.

Numerical Wave Tanks are generally not capable to transform a given wave

train upstream to the position of the wave generator. In order to generate a predetermined wave sequence at a target location the numerical wave tank has to be combined with optimization routines (Clauss and Steinhagen (2000)). As this process is highly time consuming the use for day to day experimental investigations is limited to the generation of particular scenarios.

None of the presented models is capable to perform both upstream and downstream transformations of arbitrary – in particular non-regular – given wave trains within a reasonable time frame. As a consequence, a hybrid method considering non-linear wave propagation is presented in the following chapter to meet the requirements of wave transformation for experimental purposes.

To illustrate the demand for such a hybrid method in comparison with available models, Fig. 2.2 shows a simulation of the *New Year Wave*. The wave is modelled in the TUB wave tank at scale 1:81 using the *modified non-linear theory* as will be introduced in chapter 3. Both the *modified non-linear theory* and the Numerical Wave Tank based on potential theory/ FEM (Steinhagen (2001)) predict the non-linear evolution of the wave train and the wave-wave interaction well. The Numerical Wave Tank calculates the potential field at each time step, thus also velocity, acceleration and pressure fields are known. In contrast to the Numerical Wave Tank, the *modified non-linear theory* is able to provide control signals both for generating deterministic wave trains in a model tank and as an input for the moving wall boundary of the Numerical Wave Tank.

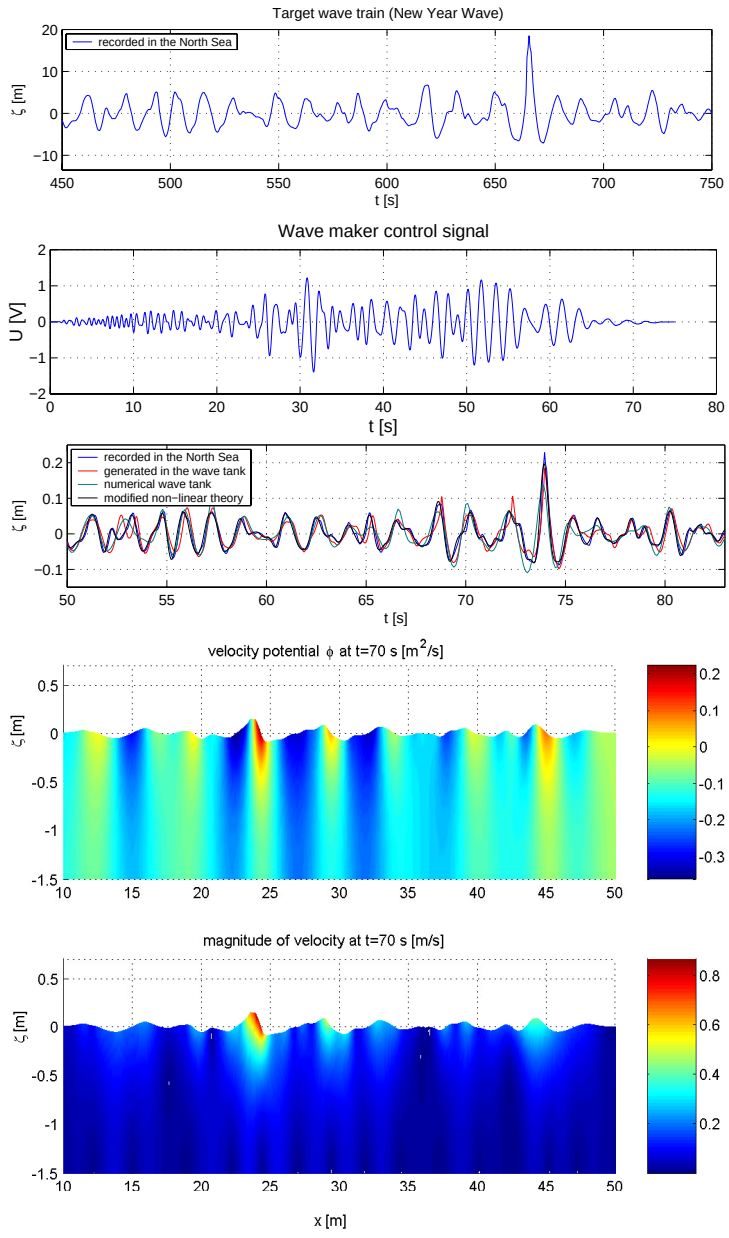

Figure 2.2: Generation and analysis of the New Year Wave: Applying the *modified non-linear theory* the target wave train (top) is transformed upstream to the position of the wave maker. The resultant control signal is shown in the second graph. Both the *modified non-linear theory* and the Numerical Wave Tank based on potential theory are able to calculate the downstream wave train at the target position — the Numerical Tank only from the wave board motion which is provided by the modified theory. The corresponding wave field characteristics are provided by the Numerical Wave Tank (scale 1:81).

Chapter 3

Modified Non-linear Theory for Modelling Wave Propagation Iteratively

If a wave train is given as time series at a defined location, it might be interesting to known how the same wave train appears at another location. Therefore, a method to describe wave propagation is required. Figure 3.1 shows two registrations of a small wave packet in the towing tank of HSVA, measured at the positions $x = 5.47$ m and $x = 38.23$ m. Applying linear wave theory, the first registration is transformed to the location of the second probe and compared to the registration. The good agreement is evident and reasonable since the wave packet is small in height and linear theory is appropriate.

For steeper wave trains – i. e. ratio of wave height to wave length is greater than 0.05 – application of linear wave theory is not adequate since the following non-linear phenomena which are observed in model tests and mathematical models cannot be modelled by Airy wave theory:

- Dispersion depending on wave steepness: Propagation velocity increases with wave steepness which is equivalent to an increase of wave length compared to a linear wave of same frequency. Fig. 3.2 shows the phase velocity increase vs "amplitude" of a Stokes Third Order wave.
- Lagrangian mass transport and Eulerian wave induced (reverse) current can be observed in wave tanks and deduced from wave theories: It might happen that surface water apparently flows in direction of wave propagation though a flow meter installed in deeper water indicates a

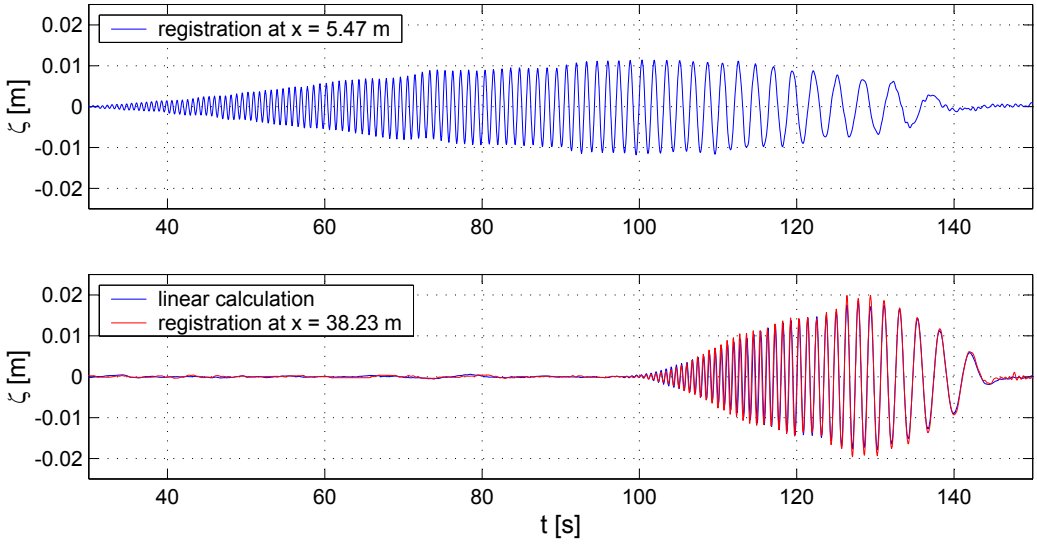

Figure 3.1: Registration of a transient wave packet by a wave probe at $x = 5.47$ m (top), linear transformation to the position $x = 38.23$ m and comparison to the measured wave train at that position. The very good agreement confirms that linear calculation is adequate in this case.

velocity in opposite direction (which is also an explanation for sediment transport). This effect can be directly related to the increase of propagation speed due to wave steepness — from wave theories follows that the wave gets longer if it is superimposed with a current u: L=(c+u)T.

- Non-harmonic shape: Crest-trough ζ_c/H, crest-front (front slope) ζ_c/L and vertical shape asymmetry L'/L increase with steepness (L and L' are the two horizontal sections of the wave crest divided by a perpendicular from the crest maximum to mean water level). The asymmetry parameters can be defined in time domain accordingly. Fig. 3.3 gives an example for a measured focusing wave which shows a vertical asymmetry close to the concentration point.

- Wave-wave interaction (in the application sense of Stokes type perturbation expansions)

  - Resonant interaction: bound waves
  - Wave height increases with steepness (see Fig. 3.4) – in particular as the wave focuses it becomes narrower and up to 30 % higher than linear theory would predict which is due to second and third order terms. For uni-directional waves, this extra elevation in-

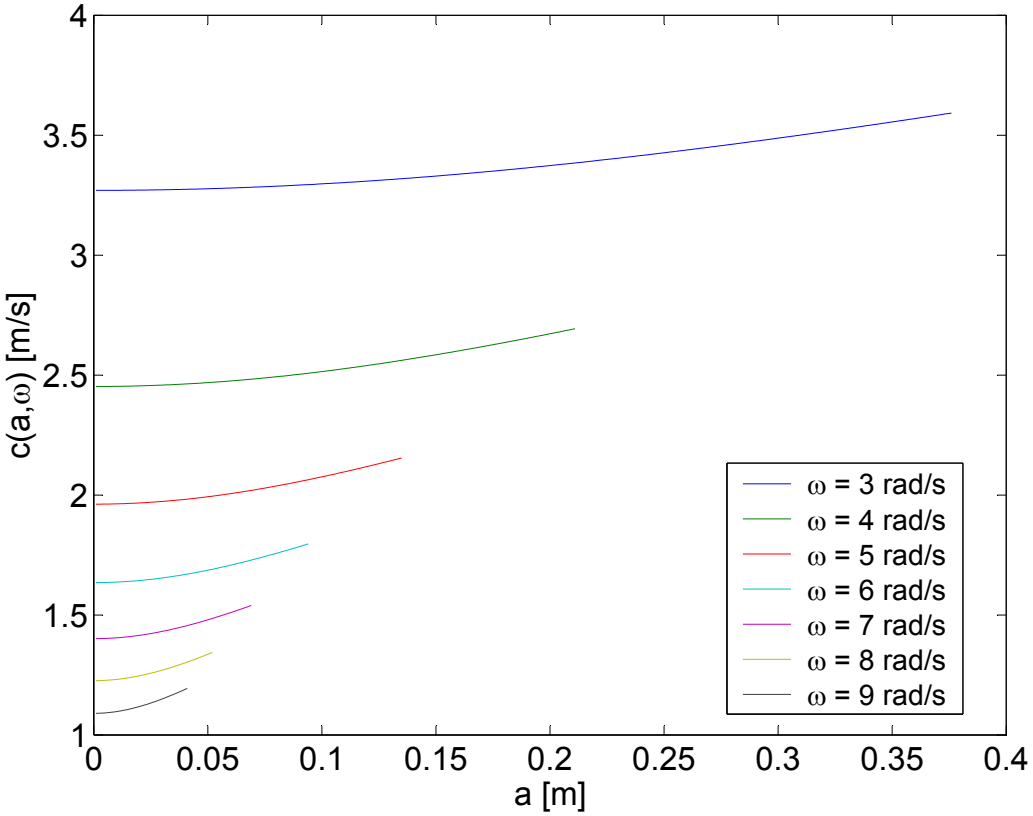

Figure 3.2: Wave celerity as a function of wave "amplitude" according to Stokes Third Order wave theory. The higher the frequency the steeper the wave and the more pronounced is the effect of phase speed increasing with wave amplitude.

creases with the input amplitude of the group and decreases with bandwidth.

- Non-resonant interaction: energy passes over from one frequency or wave number to another which is the reason for Benjamin-Feir instabilities (Benjamin and Feir (1967))
- Asymmetrical focussing and de-focussing of a wave group: Assuming a focus point – the so-called concentration point – a linearly describable wave group has the same – mirror-inverted – shape at a given distance $\triangle x$ to that point as it has at the distance $-\triangle x$. This is not the case for steep waves.

As shown in the previous chapter, there is a wide range of methods for design and computer simulation of steep wave events. However, a theory is required

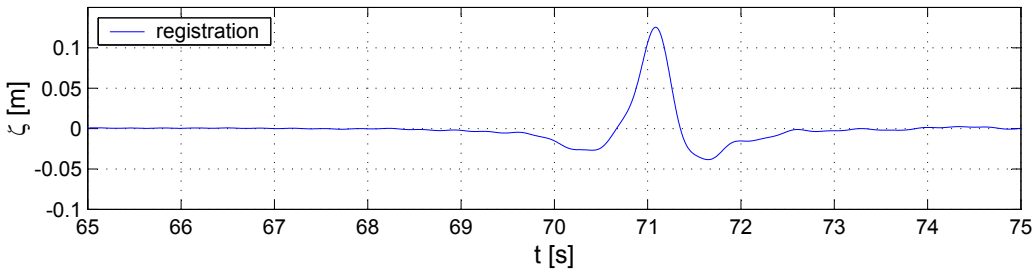

Figure 3.3: Registration of a transient wave packet with pronounced vertical asymmetry due to wave steepness ($ak_s = 0.44$).

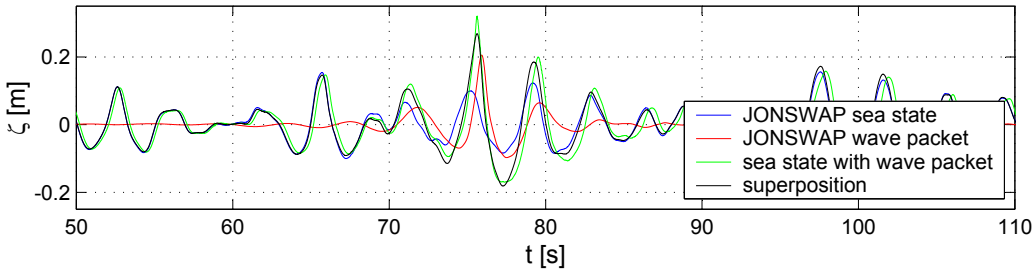

Figure 3.4: Comparison of measured water elevations of superimposed wave groups (water depth $d = 1.5$ m): The wave maker control signals of an irregular wave sequence and a single high wave group are superimposed. Both signals are measured separately and as result of the superimposed control signals. The result is compared to the superposition of the individual registrations ("superposition" in the legend). Non-linear wave-wave interaction becomes evident as the maximum crest height is larger than the sum of both local crest heights.

which is both

- fast enough to realize wave generation and analysis for experimental applications within a reasonable time frame and
- able to model the non-linear wave characteristics.

Therefore, the approach presented in this chapter uses

- fast linear wave theory as a backbone and
- Stokes Third Order wave theory to consider non-linear effects.

A *modified non-linear theory* for the prediction of non-linear wave propagation is proposed. The non-linear output wave train and its characteristics at arbitrary positions in time and space are calculated iteratively from a linear or non-linear input wave train at an initial position. The technique serves as a practical tool for wave generation and transformation related to model tests such as capsizing tests.

The time step evaluation is based on the fact that short and high wave groups having strongly non-linear characteristics evolve from long and low wave groups which can basically be described by linear principles.

3.1 Linear aspects of non-linear wave propagation

Many non-linear aspects can already be introduced by linear wave theory if the particle motions are evaluated at the particles' real positions. Woltering (1996) develops the Lagrangian approach – such as introduced by the trochoid theory (Gerstner (1802)) – towards a non-linear wave description on the basis of linear wave theory.

In this spirit, to synthesize steep wave packets, Kühnlein (1997) proposes a method expanding linear wave theory by evaluating the equations of orbital motions at the particles' real positions and introducing an empirical term, which considers shallow water effects. The basic idea is the continuity of the information content of a wave group. The total energy of the wave group is invariant during propagation despite its local amplitudes, phase relations and total length are changing. For describing the propagation of the non-linear wave group the term "wave information" I is introduced — and assigned to the linear complex water particle surface velocity of a deep water wave ($z = \zeta$). The wave celerity c_I, i.e. the propagation velocity of wave information I, depends on linear celerity and an additional term due to non-linear convection effects,

$$c_I = c_{lin} + c_{add}. \tag{3.1}$$

The additional celerity c_{add} depends additionally on the the wave height which follows from the position of the wave group. The transformation of the wave information $I(t, x)$ from one position to any other location is similar to the transformation of a linear wave packet: only the linear wave celerity has to be replaced by the non-linear "information" speed $c_I(t, x)$. At selected positions a non-linear expansion is accomplished by integrating the mutually

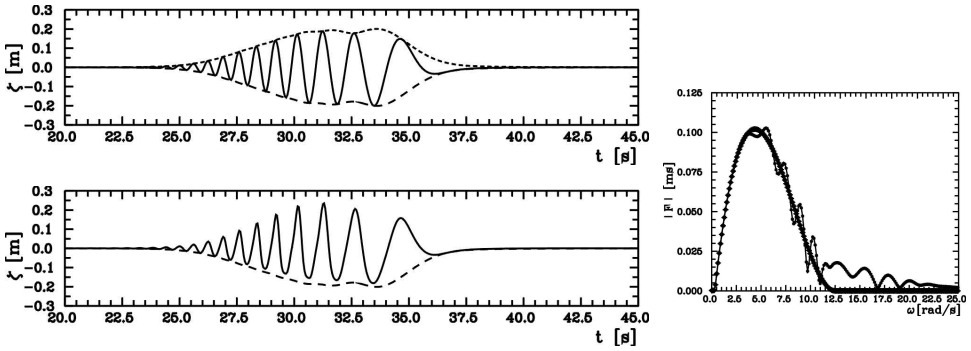

Figure 3.5: Linear wave elevation with envelope (above) and corresponding Stokes Third Order wave packet (below) as well as related Fourier spectra (smooth curve: linear wave train).

dependent particle motion equations in time domain, resulting in a numerical non-linear description of the transient wave train (Kühnlein et al. (2002)).

For the *modified non-linear theory* presented in the following section the idea of the wave information is adopted: In case of a transient wave packet, the corresponding long and low wave train, e. g. a registration close to the wave board, is defined as wave information. This wave information along with the adequate non-linear celerity, respectively wave number, at each time step gives the non-linear phase characteristics of the wave train. Stokes Third Order wave theory is applied. The iteration is carried out in the Eulerian reference frame. The detailed shape of the resultant wave train is developed at each time step considering the temporary steepness of the wave.

Figure 3.5 presents an example of a linear wave elevation and the corresponding Stokes Third Order wave packet. The Stokes wave packet shows significantly steeper wave crests. Comparing associated Fourier spectra it can be observed that the Stokes wave packet contains additional high frequency terms.

Concluding, the wave information for a given (linear or non-linear) wave train is the corresponding wave train according to Airy theory which gives the real wave train applying the *modified non-linear theory*.

E. g. for a regular Stokes Third Order wave the surface elevation is

$$\begin{aligned} \zeta(t) &= \zeta_a \cos\theta + \frac{1}{2}\zeta_a^2 k \cos 2\theta + \frac{3}{8}\zeta_a^3 k^2 \cos 3\theta, \\ \theta &= \omega t - kx. \end{aligned} \tag{3.2}$$

The linear first term $\zeta_a \cos\theta$ – the Airy wave – is modulated by small higher order terms which steepen the crest and induce a convective flow. Thus, for

a regular wave, the term $\zeta_a \cos\theta$ is the wave information.

3.2 Iteration scheme of the modified non-linear theory

Based on the wave information, the *modified non-linear theory* predicts non-linear wave propagation iteratively. To capture the growth or decay of non-linearities, the spatial steps have to be chosen accordingly. In contrast to linear theory, it is not possible to perform the transformation within one step. However, similar to linear wave theory, the wave train at the next spatial position is calculated by phase shift. The phase is adjusted according to Stokes Third Order dispersion. The shape of the wave train is developed according to non-linear wave theory as well. The entire process comprises the following steps:

1. Determination of wave information from initial wave train
2. Definition of non-equidistant spatial steps $(\triangle x)_l$ — step size decreases with increasing steepness of the considered wave group
3. Determination of corresponding non-linear wave train from information
4. Calculation of non-linear wave numbers for the non-linear wave train of step 3
5. Transformation of wave information to next spatial step using these wave numbers
6. Determination of corresponding non-linear wave train at the new position
7. Calculation of non-linear wave numbers and averaging of preceding and actual wave celerities to receive the adequate wave number values for the corresponding spatial step
8. Transformation of wave information from preceding step to actual spatial step using the wave numbers from 7
9. Repetition of steps 3-8 until the target position is reached where finally 6 has to be carried out to obtain the result

This procedure will be explained in detail in the following.

The method starts with wave information $\zeta_0(t)$, which is e. g. measured close to the wave maker. If it is not available, it has to be calculated from the input wave train (see section 3.4). Thus, as a first step, the initial wave train is checked with regard to applicability of Airy theory ($\frac{H}{L} < 0.05$) over the entire wave length range. As a further step in pre-processing the wave train is written as Fourier series and time mapped with respect to the Shannon theorem:

$$\zeta_0(t_i) = \sum_{j=0}^{n/2} A_j \cos(\omega_j t_i + \varphi_{0j}), i = 0, 1, \ldots n-1 \tag{3.3}$$

where

$$A_j = |F_j| \triangle\omega = \triangle\omega | \sum_{i=0}^{n-1} \zeta_0(t_i) e^{-i\omega_j t_i} \triangle t |, \tag{3.4}$$
$$j = 0, 1, \ldots n/2,$$

is the Fourier spectrum of $\zeta_0(t)$ with $\triangle\omega = \frac{2\pi}{n\triangle t}, \omega_j = j\triangle\omega$, and $i = 0 \ldots n-1$ denotes the initial time mapping. The corresponding initial phase spectrum φ_{0j} is also calculated by Fourier transform of the initial linear wave train.

The envelope $a(t_i)$ of the wave train is chosen as "wave amplitude" since in case of a regular wave the amplitude is equivalent to the envelope ($a_i = a(t_i) = \zeta_a$). The Hilbert transform is used to calculate the wave envelope a_i:

$$a_i = \mathrm{IFFT}\left(\sqrt{(\mathrm{FFT}(\zeta_0))^2 + (\mathrm{FFT}(\zeta_0)e^{i\pi/2})^2}\right) \tag{3.5}$$

where "(I)FFT" is abbreviate for the (inverse) Fast Fourier Transform algorithm. The IFFT gives:

$$\zeta(t_i) = \frac{1}{2\pi} \sum_{j=0}^{n/2} F_j e^{i\omega_j t_i} \triangle\omega, i = 0, 1, \ldots n-1. \tag{3.6}$$

As a test case serves a transient wave packet measured at two positions in the model basin (HSVA): The first location is close to the wave board ($x = 8.82$ m) where the wave train is linear. Fig. 3.6 shows the wave train and its envelope. At the second position ($x = 85.03$ m), the waves are already steeper and cannot be calculated by linear transform anymore.

According to Airy wave theory a wave train at an arbitrary position x is transformed to another position $x + \triangle x$ by phase shift (the Fourier spectrum

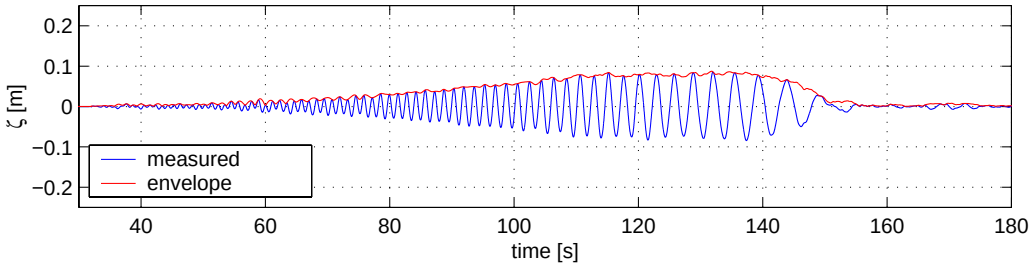

Figure 3.6: Transient wave packet measured close to the wave board at $x = 8.82$ m and corresponding envelope calculated by Hilbert transform: Linear wave theory is still applicable for its description.

remains the same):

$$\zeta(t_i, x + \triangle x) = \sum_j A_j \cos(\omega_j t_i + \varphi_{0j} - k_j \triangle x). \tag{3.7}$$

Fig. 3.7 shows the wave train from Fig. 3.6 transformed to $x = 85.03$ m by means of linear wave theory. It can be seen that Airy theory is not adequate. Particularly, the higher frequencies – which are relatively steeper – deviate obviously since they propagate faster than predicted by linear wave theory. Also the shape does not correspond with the measured wave train (flat troughs, steep crests).

In contrast, the non-linear iteration accounts for an increase of propagation velocity with instantaneous wave height. The non-linear wave train at another position is calculated from the initial wave train and the wave information. Since the chosen initial wave train can be described by linear wave theory it is used as wave information. The iteration is performed in time and

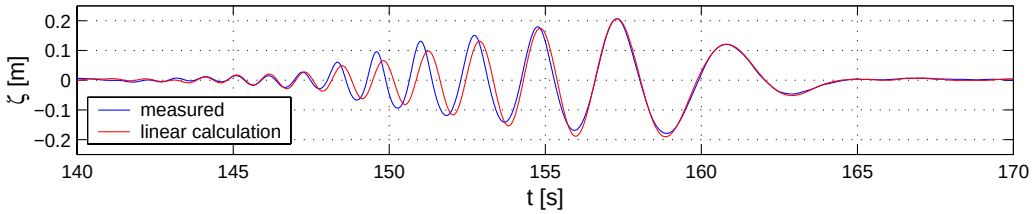

Figure 3.7: Transient wave packet at $x = 85.03$ m: Comparison of registration with linear calculation (linear transformation from $x = 8.82$ m — see Fig. 3.6) illustrates that linear wave theory gives inaccurate results.

frequency domain in adequate spatial steps to capture the growth (or decay) of non-linearities.

Adapting Eq. 3.7, the phase C_{ij} – which is the initial phase spectrum φ_{0j} in the beginning – is adjusted to the non-linear wave celerity as a function of non-linear wave numbers k_{ij}:

$$C_{ij} = \varphi_j - (\triangle x)_l k_{ij}. \tag{3.8}$$

The modified phase C_{ij} is calculated from Stokes Third Order wave theory. For each step l in space, x_l, the iteration scheme for the non-linear wave train has to be run. The following equations have to be solved with respect to k_{ij} (see chapter 2):

- Deep water, $d/L_0 \geq 0.5$:

$$\omega_j^2 = g k_{ij}(1 + (k_{ij} a_i)^2) \tag{3.9}$$

  (Stokes Third Order) — solved by Cardan formulae

- Intermediate water depth, $0.15 < d/L_0 < 0.5$:

$$\omega_j^2 = g k_{ij} \tanh(k_{ij} d) \left(1 + (k_{ij} a_i)^2 \frac{\cosh(4 k_{ij} d) + 8}{8 \sinh^4(k_{ij} d)}\right) \tag{3.10}$$

  (Stokes Third Order) — solved by fix point iteration

- Shallow water, $d/L_0 \leq 0.15$, $H/L_0 < 0.05$:

$$\omega_j^2 = g k_{ij} \tanh(k_{ij} d) \tag{3.11}$$

  (Airy) — solved by fix point iteration

The wave tanks referred to throughout the thesis are characterized by deep water or intermediate water depth conditions. Therefore, the considered wave components in shallower water have a low steepness and the wave numbers are determined by linear wave theory.

The test case wave packet is measured at the towing tank of HSVA with a water depth of $d = 5.6$ m. Thus, deep water limit frequency is $\omega = 2.34$ rad/s, shallow water limit frequency $\omega = 1.28$ rad/s.

k_{ij} is subject to the envelope a_i since the wave envelope for the particular x_l represents the instantaneous "wave amplitude" at a particular point in time and space. It also considers the fact that non-linearities gain more and

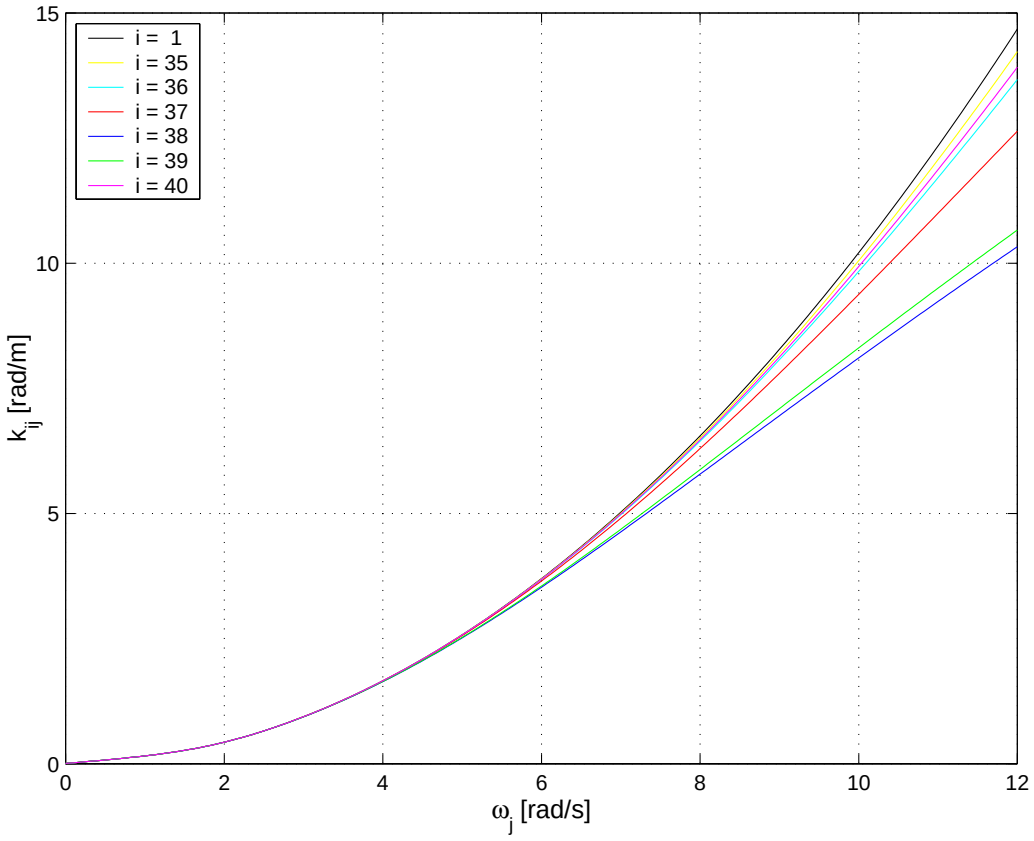

Figure 3.8: Calculation of wave numbers $k_{ij}(\omega_j, a(t_i))$ as function of the instantaneous wave envelope a_i at time step i for one spatial step x_l. Propagation velocity $c_{ij} = \omega_j / k_{ij}$ increases with "wave amplitude" a_i (see Eqs. 3.9 and 3.10).

more influence as the converging wave train travels through the tank with increasing wave height. Fig. 3.8 gives an impression of the iteration of the k_{ij}.

"Stokes Third Order components" at x_l are defined as:

$$\begin{aligned}
\zeta_{l,1}(t_i) &= \sum_{j=0}^{n/2} A_j \cos(\omega_j t_i + C_{ij}), \qquad (3.12)\\
\zeta_{l,2}(t_i) &= \frac{1}{2} a_i k_{ij} \sum_{j=0}^{n/2} A_j \cos(2\omega_j t_i + 2C_{ij}),\\
\zeta_{l,3}(t_i) &= \frac{3}{8} (a_i k_{ij})^2 \sum_{j=0}^{n/2} A_j \cos(3\omega_j t_i + 3C_{ij}).
\end{aligned}$$

After summation of these components,

$$\zeta_l = \sum_{k=1}^{3} \zeta_{lk}, \qquad (3.13)$$

the preliminary instantaneous wave envelope at the position x_l is given. Note that this scheme is applied locally to get the adequate "wave amplitude" for the calculation of wave numbers at each spatial step. The non-linear wave-wave interaction is considered implicitly in the spatial iteration. To obtain the final shape of the wave train, it is developed according to section 3.4.

The calculation of C_{ij}, Eq. 3.7-3.12, is repeated twice to average celerities from the first and second step:

$$k_{ij} = \frac{2k_{ij1}k_{ij2}}{k_{ij1} + k_{ij2}}. \qquad (3.14)$$

The accuracy of the wave celerities is determined by correct application of the adequate dispersion relation and the spatial discretization and influences the phase shift significantly: Even a deviation of less than 5% gives completely wrong results.

The $(\triangle x)_l$ are chosen such that they decrease with increasing non-linearity. In our example the iteration is done with 105 steps in space and 1024 steps in time. Fig. 3.9 presents some iteration steps.

3.3 Results

The result of the calculation procedure is shown in Fig. 3.10 and compared to the measured wave train. Agreement with the measured time series is

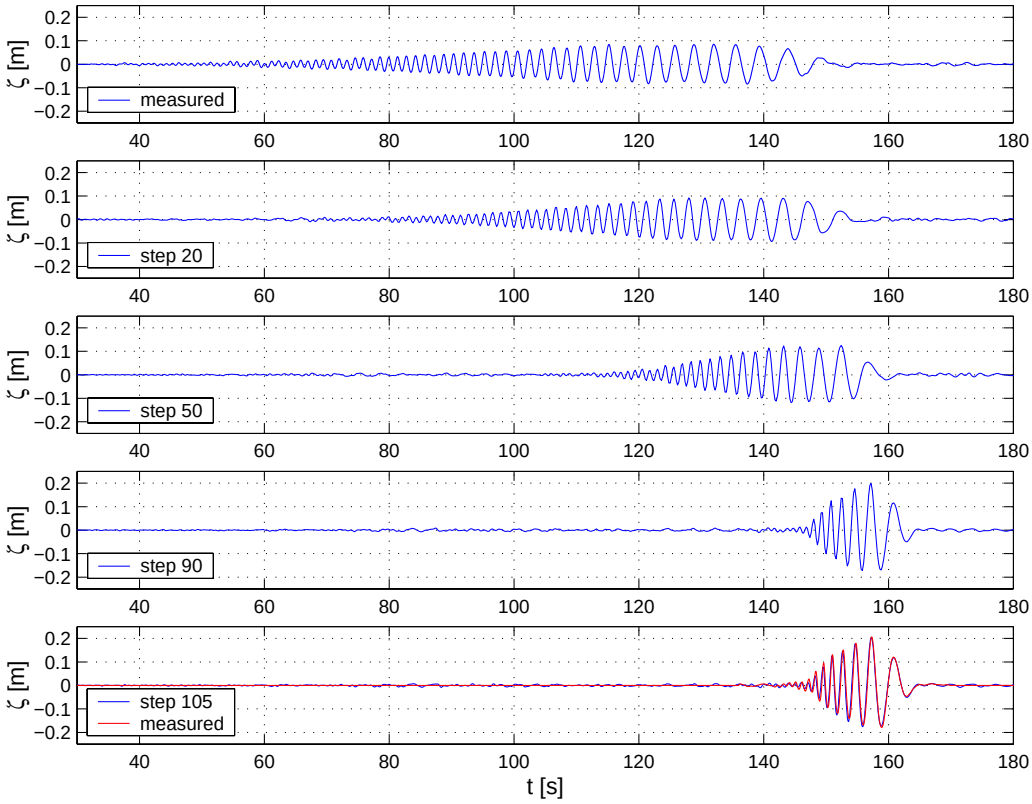

Figure 3.9: Non-linear transformation of wave train in Fig. 3.6 to downstream positions (showing selected iteration steps, $d = 5.6$ m): Agreement with measured data at $x = 85.03$ m is very good (see also Fig. 3.10).

good. Compared to Fig. 3.7 the higher frequency terms show the adequate propagation speed and a more pronounced non-linear shape with steeper crests.

Fig. 3.11 shows the transformation result for a steeper wave train. The phase relations are modelled very well by the non-linear approach whereas the results from linear theory show significant phase deviations if compared to the registration. Note that the iteration was performed over a distance of 76.21 m.

Fig. 3.12 presents the Fourier spectra at selected positions of the iteration process corresponding to Fig. 3.11. Slight modifications in the higher frequency band can be observed as the wave train becomes steeper. Fig. 3.13 comprises the Fourier spectra at all iteration steps of the wave tank. The

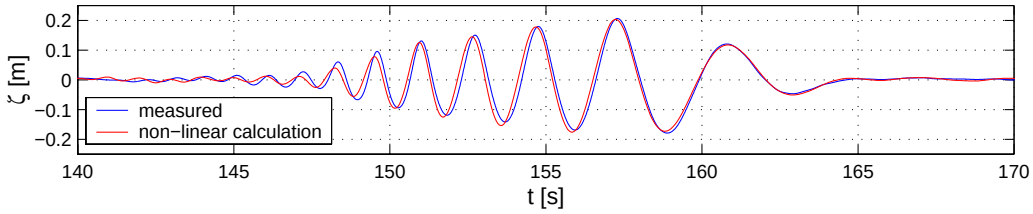

Figure 3.10: Transformation of wave packet in Fig. 3.6 ($x = 8.82$ m) to position $x = 85.03$ m using the described non-linear calculation procedure (iteration step 105). Although the transformation comprises more than 76 m, the result agrees very well with the registration.

colors are assigned to different spectral values. It can be seen the spectrum remains almost constant during the iteration. However, at the target position ($x = 85.03$ m), the colour changes indicate an "energy shift" to higher frequencies due to non-linear wave-wave interaction.

3.4 Non-linear wave shape and wave information

In the final iteration step, the non-linear shape of the target wave train has to be developed. I. e. the linear wave train – with correct non-linear phase – is subject to a function which gives the final non-linear wave train. In the example given here, the second order model of the sea surface – as given by Longuet-Higgins (1963) for water of infinite depth and extended to intermediate water depths by Hudspeth (1975) (uni-directional waves) and Sharma and Dean (1979) – is applied. The sea surface is extended to second order accuracy through a perturbation expansion,

$$\zeta = \zeta_1 + \zeta_2, \tag{3.15}$$

where

$$\zeta_1 = \sum_j A_j \cos\theta_j \tag{3.16}$$

(for one location) as given in subsection 2.4.2. The second order components added to the first order surface are then

$$\zeta_2 = \sum_j \sum_m A_j A_m (H_1 \cos(\theta_j - \theta_m) + H_2 \cos(\theta_j + \theta_m)), \tag{3.17}$$

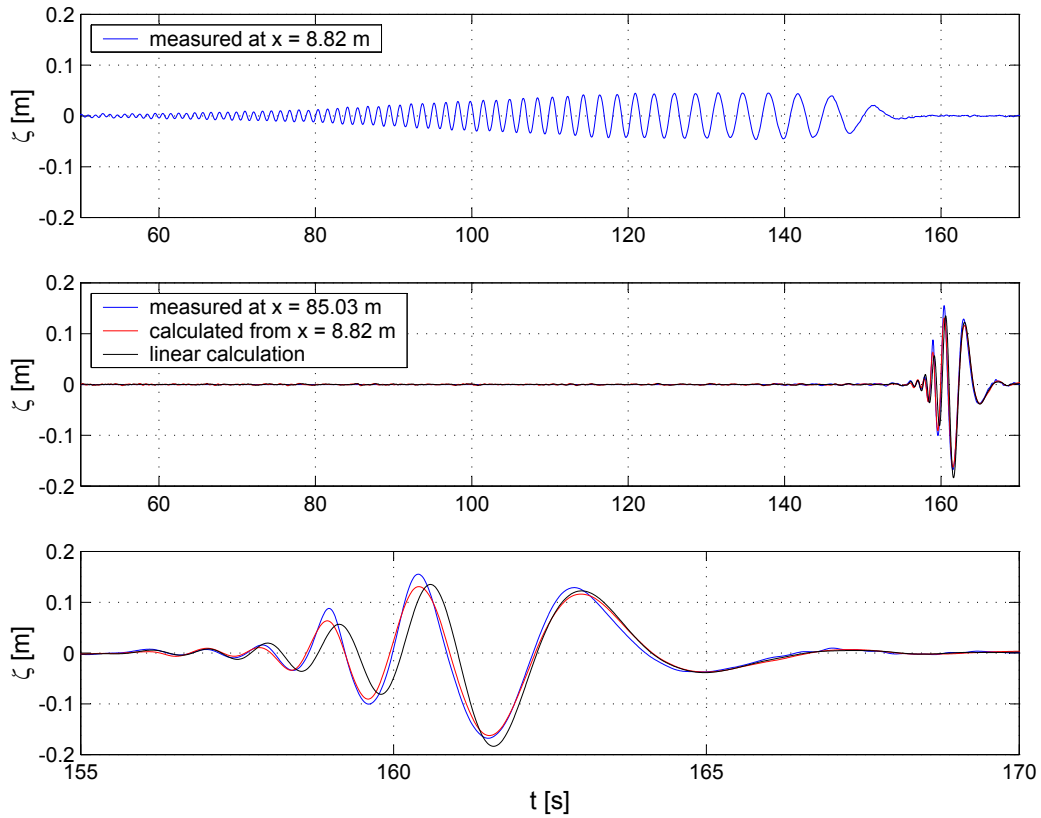

Figure 3.11: The wave train on top ($x = 8.82$ m) is transformed to position $x = 85.03$ m using the *modified non-linear theory* and compared to the linear result as well as the registration at that position.

where $\theta_{j,m}$ are the phase functions of the wave components and H_1 and H_2 are the positive and negative interaction terms. Alternatively, the Creamer transform (Eq. 2.66) may be applied to the linear wave train at the final location.

If a non-linear wave train is given as initial input of the iteration, the corresponding wave information has to be determined. It is not an easy task to obtain a linear sea surface from a given non-linear wave train – neither by application of the Creamer transform nor considering Second Order wave theory. Thus, as initial approximation, Eq. 3.13 is solved iteratively with respect to A_j which results in a smooth spectrum of wave information.

The problem of determination of wave information can be illustrated by the example of steep regular waves: Given the time series of surface elevation,

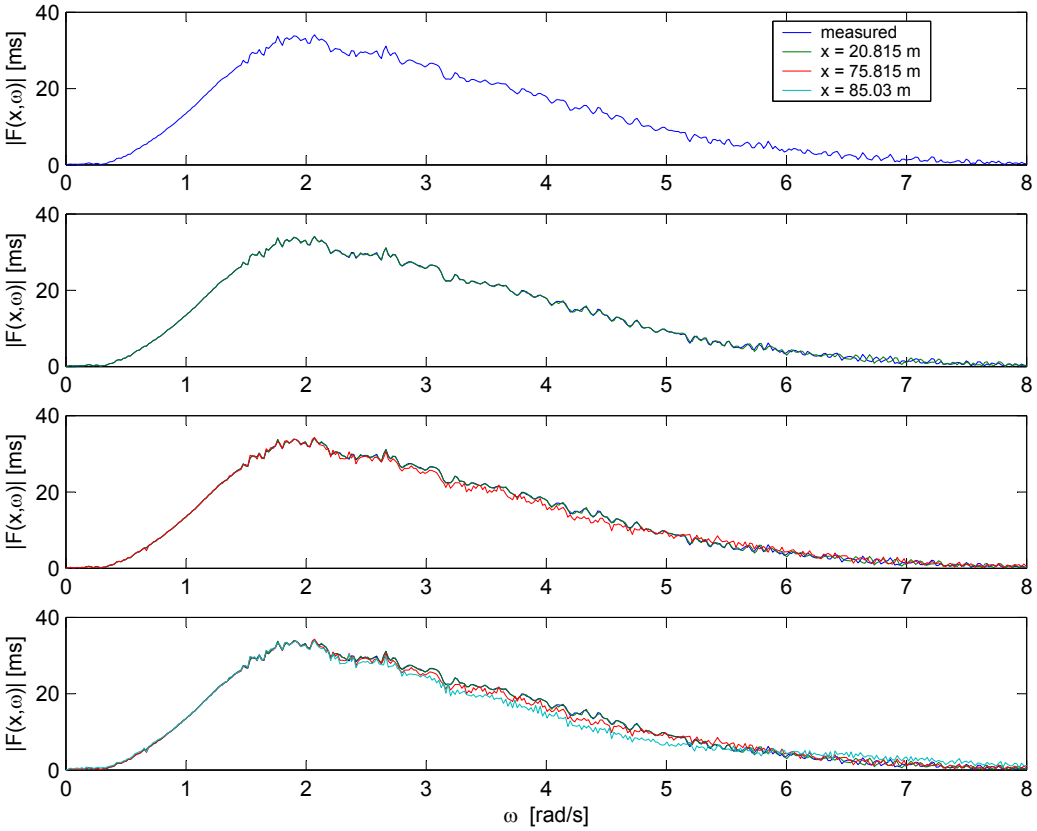

Figure 3.12: Fourier spectra at selected positions of the iteration corresponding to Fig. 3.11.

the wave height H is the difference of wave crest elevation ζ_c and trough elevation ζ_{tr}, $H = \zeta_c - \zeta_{tr}$, where $\zeta = \zeta_a \cos\theta + \frac{1}{2}\zeta_a^2 k \cos 2\theta + \frac{3}{8}\zeta_a^3 k^2 \cos 3\theta$. The wave information is $\zeta_a \cos\theta$ which refers to the corresponding amplitude of an Airy wave. Thus, Eq. 2.46 (chapter 2) has to be solved with respect to ζ_a to obtain the adequate wave information from the non-linear wave train.

3.5 Conclusions

The presented numerical method can be applied both to downstream and upstream prediction of wave trains. It confirms experimental observation that high and steep waves

- are faster and longer than waves which are small in height,

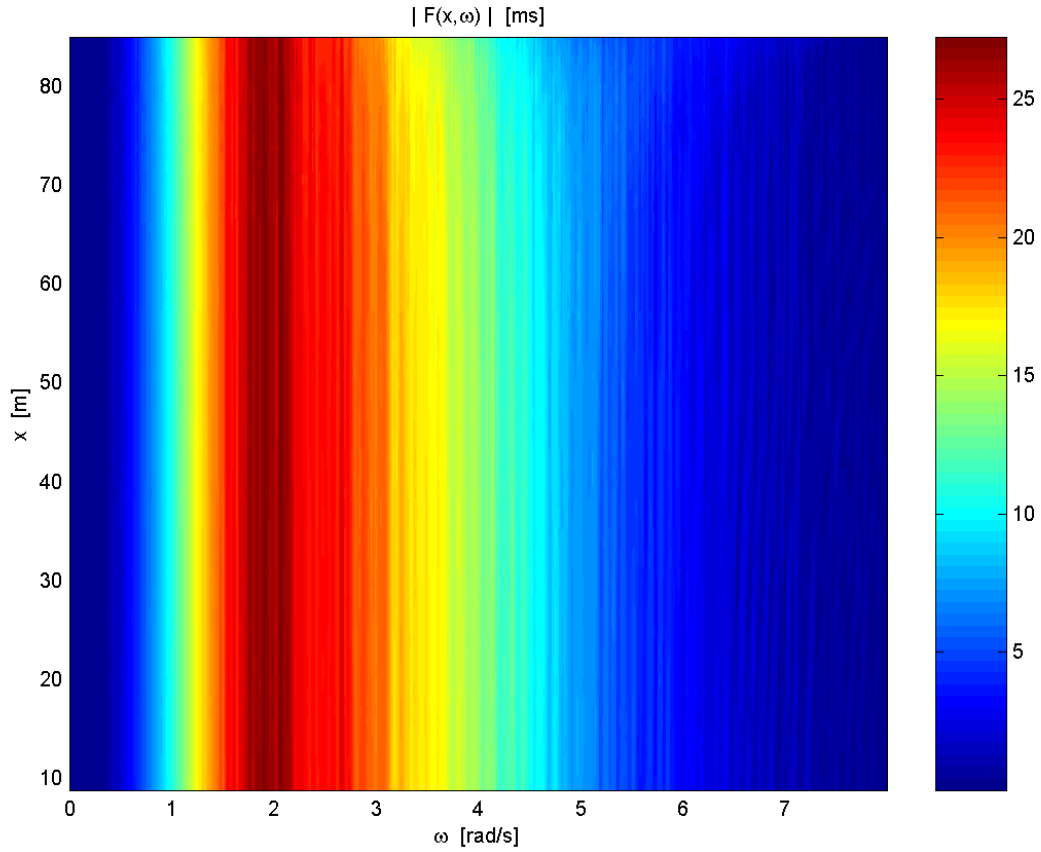

Figure 3.13: Fourier spectra at all test tank positions of the iteration shown in Fig. 3.11.

- show a crest-trough asymmetry increasing with wave height.

The approach uses terms from Stokes Third Order wave theory which can be considered satisfactory for deep water to intermediate water depth. However, they can also be replaced by other terms from different theories such as Stokes Fifth Order or shallow water theory. Empirical terms are also adequate as semi-empirical models are commonly used to overcome the gap between results of existing models and the results expected from reality (Buchner (2002)).

By application of various concepts – such as given in chapter 2 – also the wave kinematics can be calculated from the local linear wave train. Thus, the method can be adapted easily for new requirements.

The presented iteration allows for modelling the considered wave with high accuracy while the FFT-based algorithm leads to $O(N \log N)$ CPU costs. The examples given here take approximately half an hour computing time if implemented in *Matlab* or *VEE Pro* on a standard notebook. Short computing time and easy software installation allow an application of the *modified non-linear theory* for model testing.

As will be shown in chapter 4, a unique feature of the proposed procedure is the upstream transformation given target wave trains to the location of the wave maker. With this technique, wave sequences are also transformed into the moving reference frame of a cruising vessel which allows the analysis of wave scenarios from the point of view of a sailing ship. In conclusion, the *modified non-linear theory* is fast and precise and applicable in day-to-day use for experimental investigations.

Chapter 4

Generation and Transformation of Deterministic Wave Sequences

The described *modified non-linear iterative theory* allows for the following transformations of time series of surface elevation $\zeta(t)$:

$$\zeta(t, x_1) \leftrightarrow \zeta(t, x_2) \tag{4.1}$$
$$\zeta(t, x(t)) \rightarrow \zeta(t, x(t) + \triangle x) \tag{4.2}$$
$$\zeta(t, x_1) \rightarrow \zeta(t, x(t)) \tag{4.3}$$
$$\zeta(t, x_1) \leftrightarrow \zeta(t_1, x) \tag{4.4}$$

where x_1 and x_2 are fixed positions in space. $x(t)$ is a varying reference point, e. g. the keel point of a ship sailing at non-constant speed. $\triangle x$ is a constant distance between two measuring points.

Transformation of the type 4.1 enables generation of tailored deterministic wave sequences for model tests (upstream analysis). For the experimental investigation of wave-structure interaction of stationary offshore structures, it might be important to determine the exact wave train at the model position through downstream transformation since measurements close to the model are disturbed by radiation and diffraction.

Transformation 4.2 is applied to wave sequences between moving reference points of constant distance. Transformation 4.3 is used to calculate the wave sequence in the moving reference frame of a vessel cruising at non-constant speed – given an undisturbed registration at a fixed location. This allows for wave analysis to investigate non-linear wave-structure interaction in time

domain.

Transformation 4.4 switches the wave train representation from time to space domain and vice versa.

In the following section, examples of deterministic wave sequences are given. In section 4.2, the generation of deterministic wave sequences in a model basin is explained. Section 4.3 deals with wave transformations of the kinds 4.2-4.4. Finally, some applications of wave sequences for model tests are given.

4.1 Deterministic wave sequences

The wave generation technique based on the *modified non-linear theory* allows for the deterministic wave tank generation of all kinds of tailored waves. These model seas are called "deterministic wave sequences". Since the generation of most deterministic wave sequences is based on the transient wave technique most attention is directed to transient wave packets. The following examples are discussed here:

- Transient wave packets and single wave events
- Sea state realizations with defined embedded wave sequences at several positions in time and space
- Regular waves with high wave groups (*Three Sisters*)
- Wave tank realization of observed wave records (*New Year Wave*)

According to the type of model sea the wave train is defined by the following parameters:

- Target location x_{target} in the model basin: The characteristics of the wave sequence refer to this location.
- Wave frequency band $\omega_{beg} \ldots \omega_{end}$ and peak frequency ω_P or e. g. peak period T_P or zero-upcrossing period T_0 for sea states
- Characteristic wave elevation ζ_a (amplitude for regular waves), ζ_{max} (maximum elevation of a wave packet in the concentration point) or significant wave height H_s for sea states

4.1.1 Transient wave packets as single wave events

A *wave packet* is defined as a superposition of two-dimensional waves with different frequencies which is concentrated in space and diverges with time due to dispersion. The propagation velocity of the wave packet is called group celerity. Dispersion is related to the fact that phase velocity and group celerity are not equal (Walz (2001)).

A *transient* wave packet is a wave packet consisting of subsequent waves with increasing propagation speeds so that all "components" meet in the so-called concentration point. After that point, they diverge in opposite order. The related mathematical problem is called Cauchy-Poisson problem. An example for a transient wave packet is given in Fig. 4.1.

Transient waves for model excitation were originally proposed by Davis and Zarnick (1964) and further developed by Takezawa and Hirayama (1976) and Mansard and Funke (1982). Clauss and Bergmann (1986) recommended a special type of transient waves called Gaussian wave packets which have the advantage that their propagation behavior can be predicted analytically (Chakrabarti and Libby (1988)). With increasing efficiency and capacity of computers the restriction to a Gaussian distribution of wave amplitudes has been abandoned, and the entire process is performed numerically (Clauss and Kühnlein (1995)). Since they have a short extension and consequently a small sensitivity with regard to disturbing frequencies they can be used to determine the RAOs of models within only one test run. The shape and width of the wave spectrum can be selected individually for providing sufficient energy in the relevant frequency range. Clauss and Kühnlein (1997b) extended the linear approach to the generation and analysis of very high transient wave packets.

The wave packets generated throughout the thesis are defined by the following function for the Fourier spectrum:

$$|F(\omega)| = \frac{27(\omega - \omega_{beg})(\omega - \omega_{end})^2}{4(\omega_{end} - \omega_{beg})^3}. \tag{4.5}$$

For very steep waves the function can be modified:

$$|F(\omega)| = \left(1 - \left(\frac{\omega - \omega_P}{\omega_{end} - \omega_P}\right)^2\right) \frac{27(\omega - \omega_{beg})(\omega - \omega_{end})^2}{4(\omega_{end} - \omega_{beg})^3}. \tag{4.6}$$

Transient wave packets are characterized by well-defined periods and phase relations, and are therefore used to model deterministic wave sequences for

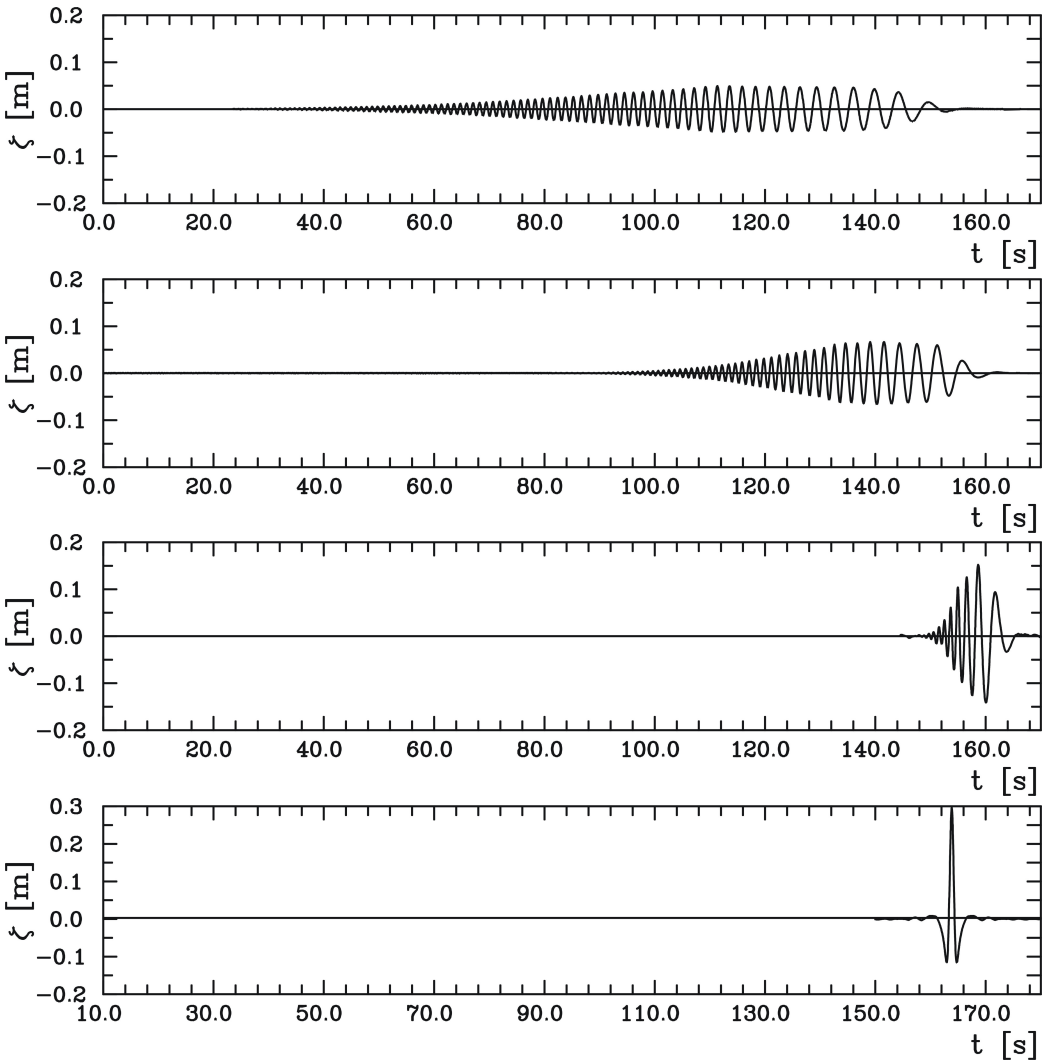

Figure 4.1: Generation of a transient wave packet in the model basin of HSVA: Registrations at x =5.88 m, 47.74 m, and 85.03 m, concentration point at x =95.00 m (bottom).

model tests (Clauss et al. (1996), Clauss and Kühnlein (1997a)). Thus, transient waves can be used for the generation of breaking waves on vertical cylinders (Wienke et al. (2001)). Kjeldsen (1983) investigated capsizing of smaller vessels by generation of large plunging breakers (freak waves). Wave packets are good laboratory equivalents to large ocean waves since they are transient and show frequency focusing. Focused component waves – even if still linear describable – behave in a fully non-linear manner in a relatively small region around the concentration point (compare also Chaplin (1996)).

4.1.2 Deterministic wave sequences in a sea state

Fig. 4.2 presents experimental data of a storm sea realization ($T_P = 14.6$ s, $H_s = 15.3$ m) which has been modelled at HSVA at a scale of 1:34.

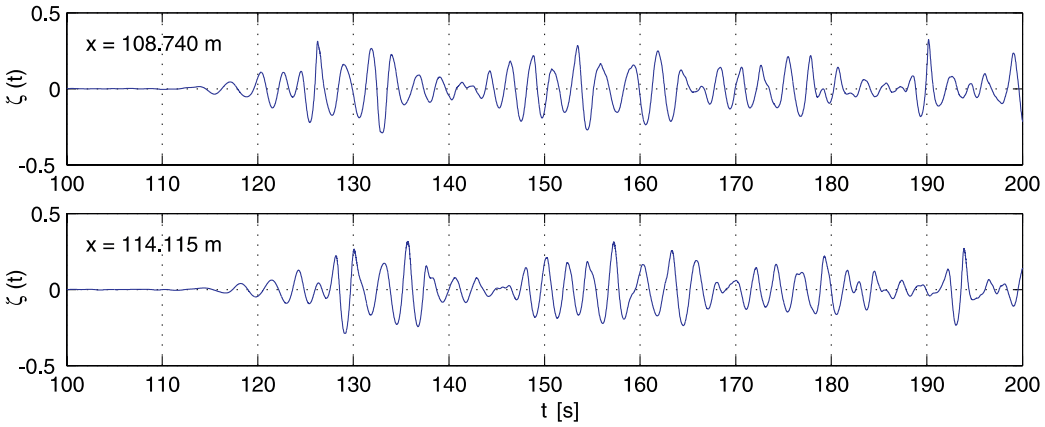

Figure 4.2: Registration of a storm sea at HSVA ($T_P = 14.6$ s, $H_s = 15.3$ m, scale 1:34).

For a given design spectrum of an uni-directional wave train, the phase spectrum is responsible for all local characteristics, e. g. wave height and period distribution as well as location of the highest wave crest in time and space. The most unfavorable event under storm conditions is the in-phase superposition of component waves in the seaway. Randomly, the time series may contain a dangerous wave sequence — a coincidence which would require a very extended test duration.

Applying the transient wave technique, a single wave event can be integrated in a random sea deterministically: Fig. 4.3 shows the realization of a JONSWAP sea state ($T_P = 2.2$ s, $H_s = 0.15$ m) at TUB. It also presents

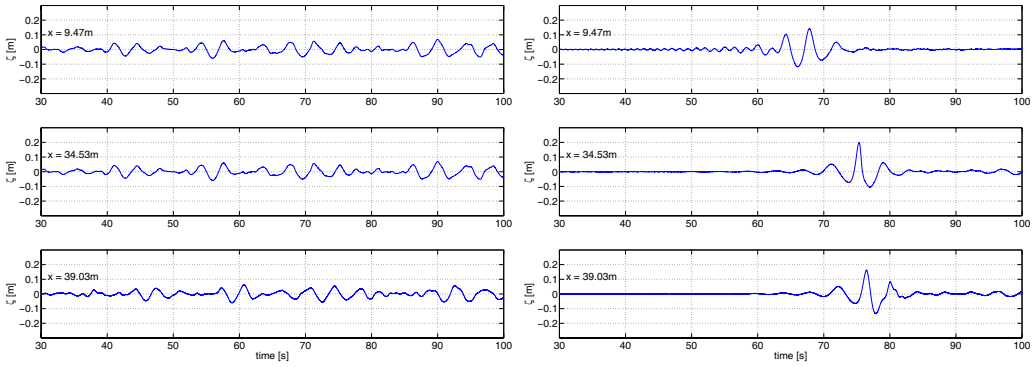

Figure 4.3: Registration of a JONSWAP sea ($T_P = 2.2$ s, $H_s = 0.15$ m) and a wave packet ($H_{max} = 0.35$ m) with same JONSWAP spectrum at TUB (scale 1:81).

the measurement of a wave packet with the same JONSWAP spectrum in the wave tank. Fig. 4.4 shows the wave tank simulation of the wave packet integrated into the irregular sea from Fig. 4.3. For these deterministic wave sequences, horizontal asymmetry is $\zeta_c/H_{max} = 0.7$, ratio of maximum to significant wave height is $H_{max}/H_s = 2.3$.

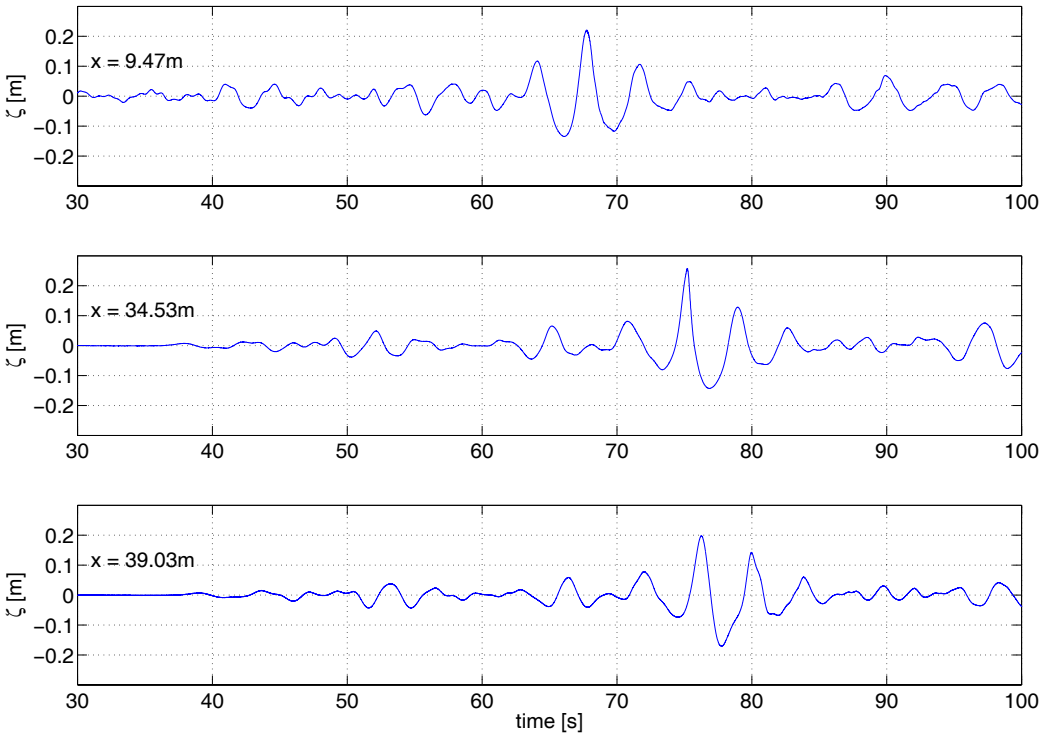

Figure 4.4: Irregular sea (JONSWAP spectrum, $T_P = 2.2$ s, $H_s = 0.15$ m) with integrated wave packet ($H_{max} = 0.35$ m) as a very steep *Three Sisters* wave at different positions in the wave tank (scale 1:81) – $\zeta_c/H_{max} = 0.7$, $H_{max}/H_s = 2.3$.

4.1.3 Regular wave sequences

Benney (1962) as well as Benjamin and Feir (1967) deal with the mathematical analysis of regular waves in wave tanks. They observe parasitic waves which are due to an increase of energy in sidebands while the wave train propagates through the tank. This leads to the disintegration of the wave train and is referred to as Benjamin-Feir instabilities. These instabilities can be reduced significantly by Second Order wave maker theory (Schäffer (1996), Huseby and Grue (2000)). Recommendations with respect to wave tank generation of regular waves can be found in ITTC (2002). This thesis is concerned with regular waves as a "carrier" of wave packets to model special deterministic wave sequences. Fig. 4.5 presents such a superposition of a regular wave train with a wave packet. This tailored wave sequence is used for the investigation of large roll motions and capsizing of ships (chapter 5). The "irregular" wave train turns out to become a rather regular wave with an integrated extreme *Three Sisters* wave if transformed to the moving reference frame of a cruising ship (Fig. 4.6).

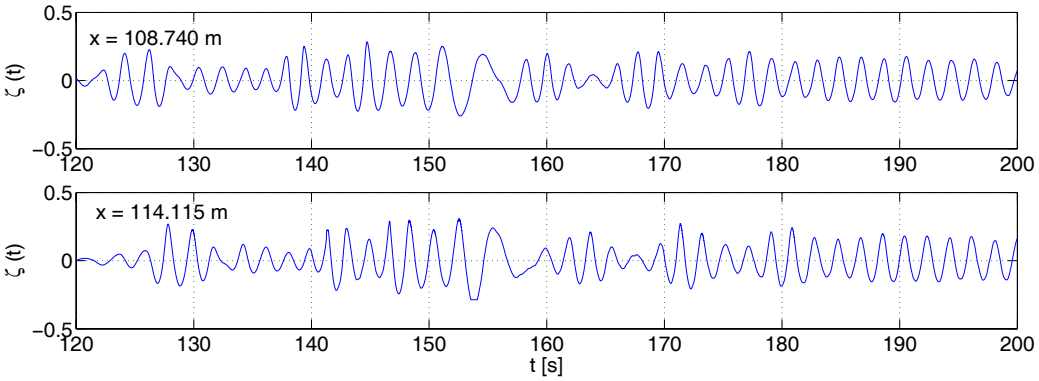

Figure 4.5: Regular wave with wave packet (*Three Sisters*) for the investigation of large roll motions and capsizing of ships (scale 1:29, see Fig. 5.11). The stationary registration shows a neither regular nor dangerous shape whereas its drastic character becomes evident after transformation into the moving reference frame (Fig. 4.6).

4.1.4 Wave tank realization of observed wave records

Some interesting wave events are reported and registered from radar or buoy measurements. Depending on water depth and ability of the wave maker, it is

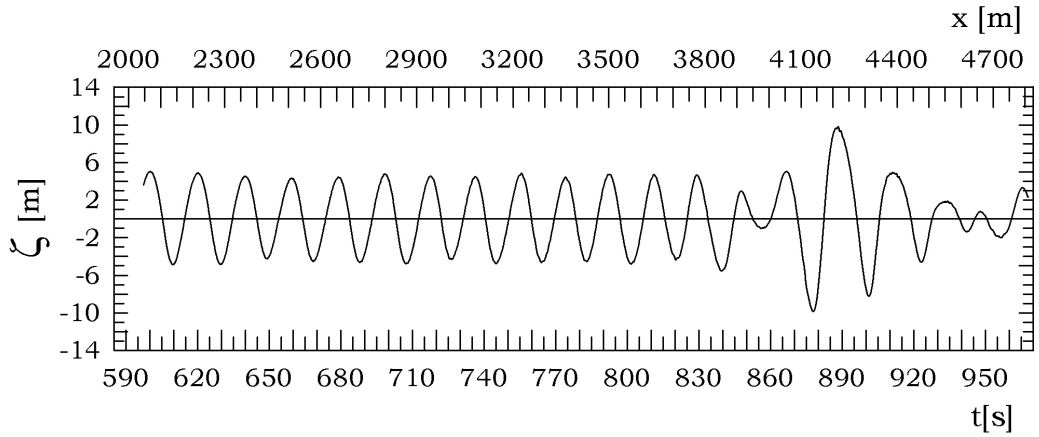

Figure 4.6: Regular wave with wave packet (*Three Sisters*) from Fig. 4.5 in the moving reference frame of a cruising ship – see chapter 5, Fig. 5.11.

possible to generate them in a model basin. As an example, Fig. 4.7 presents the so-called *New Year Wave* recorded in the North Sea – compare chapter 1 – and simulated in the wave tank using the *modified non-linear theory*. The measured wave train shows a good agreement with the target wave. Fig. 4.8 shows the wave tank evolution of the New Year Wave where $x_{target} = 28.95$ m is the target position of this rogue wave. The wave is modelled in the wave tank at scale 1:81. At the upstream position $x = 29.95$ m the New Year Wave results in significant higher structural response of an FPSO in terms of its vertical bending moments (Clauss et al. (2004c)).

4.2 Wave generation

For the generation of deterministic wave sequences in a model basin different types of wave makers are available which will be treated in subsection 4.2.3. The wave generation process as illustrated in Fig. 4.9 for a double flap wave maker can be divided into four steps:

1. Definition of the target wave train: The target position in time and space is selected – for example the position where the ship encounters the wave train at a given time. At this location, the target wave train is designed – based on defined parameters or a wave record (see previous section).

2. Upstream transformation $\zeta(t, x_{target}) \rightarrow \zeta(t, x_0)$: The target wave train

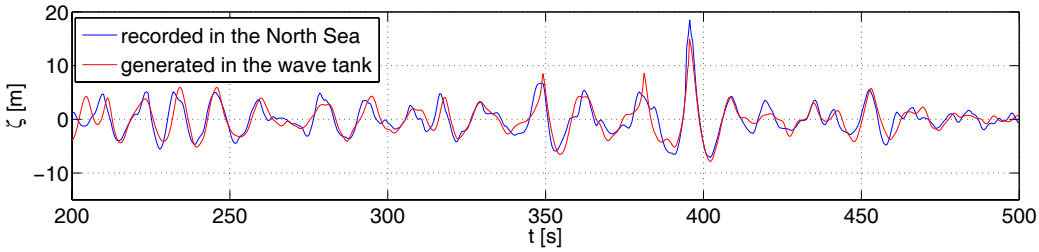

Figure 4.7: *New Year Wave*: Comparison of full scale data (registered on January 1, 1995, at the Draupner platform in the Norwegian Ekofisk field) and wave tank generation at the tank of TUB (scale 1:81). The measured wave train shows quite a good agreement with the target wave – $\zeta_c/H_{max} = 0.72$, $H_{max}/H_s = 2.15$.

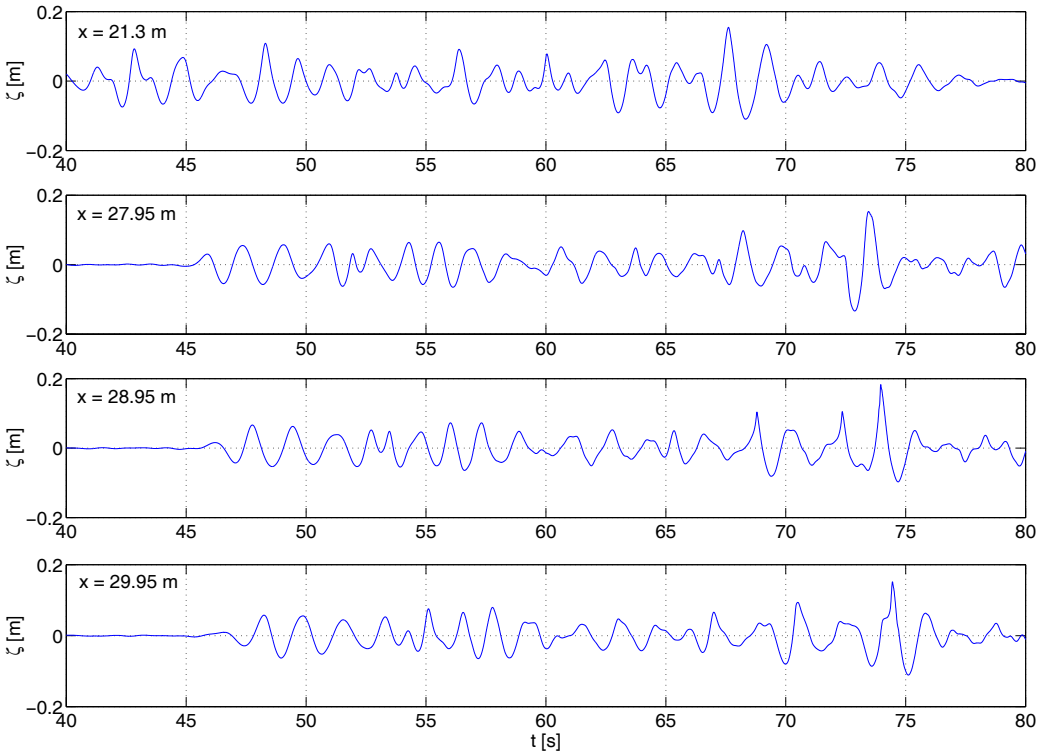

Figure 4.8: Wave tank evolution of the *New Year Wave*, target position at $x_{target} = 28.95$ m.

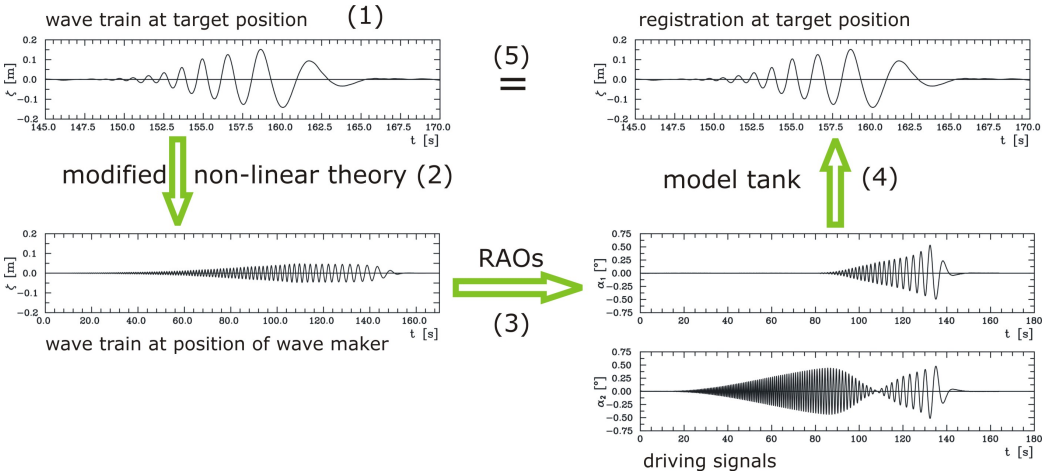

Figure 4.9: Process of wave generation: Calculation starts from the desired target wave train, defined by particular parameters (1). Modelling wave propagation properly, the wave train at the position of the wave maker (2) as well as the corresponding wave maker control signals (3) are calculated. The resultant wave train can be measured at the target position (4) and compared to the given target wave (5).

is transformed upstream to the position of the wave maker (see chapter 3).

3. Calculation of control signals: The corresponding control signals are calculated using adequate transfer functions of the wave generator (subsection 4.2.3).

4. Performance of model tests: The control signals are used to generate the specified wave train which is measured at selected positions in the tank. The ship model arrives at the target position by the corresponding target time (measured from the beginning of wave generation). Registration of the wave sequence at the target position confirms the compliance with the target wave parameters.

4.2.1 Definition of the target wave train

The definition of the target wave train depends on the type of model sea to be generated. Examples have been given in section 4.1. The target wave train can be defined by

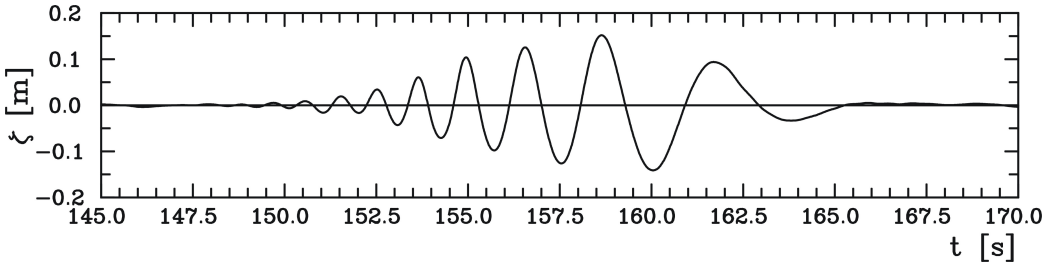

Figure 4.10: Generation of a transient wave packet at HSVA: Definition of the target wave train at $x = 85.03$ m (wave maker at $x = 0$).

- Parameters
- Spectra
- Time series.

As spectral representation both Fourier or energy density spectra are available. Since the *modified non-linear theory* is based on a Fourier spectrum representation, energy density spectrum S has to be rewritten as Fourier spectrum $|F|$:

$$|F(\omega)| = \sqrt{2S(\omega)\triangle\omega}. \tag{4.7}$$

In any case, the wave generation process starts with a time series which satisfies the desired wave train characteristics.

As an illustration of the wave generation procedure a transient wave packet generated at HSVA is chosen. The target wave train is shown in Fig. 4.10 ($x_{target} = 85.03$ m – which is 9.97 m in front of the concentration point – $\zeta_{max} = 0.3$ m, $\omega_{beg} = 0.5$ rad/s, $\omega_{end} = 10.0$ rad/s).

4.2.2 Upstream transformation of the target wave

The second step – upstream transformation of the wave train to the position of the wave board – is treated in chapter 3. For the test case the result is shown in Fig. 4.11.

For reducing the number of time steps until the wave maker starts to operate, the wave train – represented by its Fourier transform F – at the position of the wave maker is shifted by time t_{shift} (which shifts the time axis for the target wave as well):

$$\hat{F}(\omega_j, x_0) = F(\omega_j, x_0) \cdot e^{-i\omega_j t_{shift}}. \tag{4.8}$$

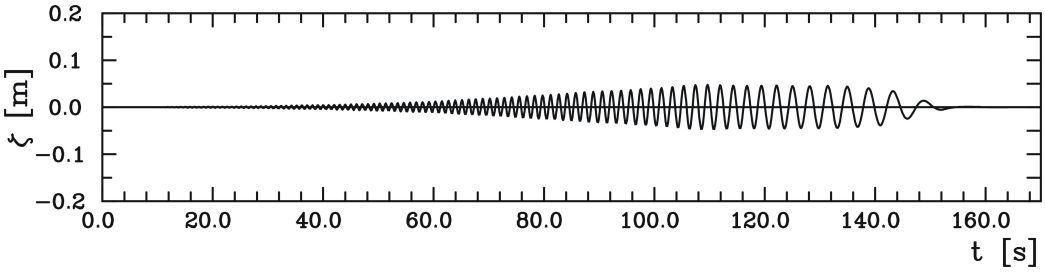

Figure 4.11: Generation of a transient wave packet at HSVA: Transformation of the target wave train (Fig. 4.10) to the position of the wave maker ($x = 0$).

4.2.3 Transfer functions relating wave train to wave maker control signals

Finally, the Fourier transform of surface elevation at the position of the wave maker is multiplied by adequate transfer functions to receive the corresponding wave maker control signal(s). Two types of transfer functions (RAOs) are considered:

1. Hydrodynamic transfer function relating wave elevation to wave board motion (Biésel transfer function).
2. Hydraulic-electrical transfer function which assigns the wave board motion to a voltage signal considering the properties of the engines and driving components.

Biésel transfer function for piston and flap type wave makers

The hydrodynamic transfer function depends on the type of wave maker. For piston and flap type wave makers (see Fig. 4.12) the hydrodynamic transfer function has been deduced by Biésel and Suquet (1951) and experimentally confirmed by Ursell et al. (1959) (for a piston type wave maker). The wave generation process is characterized by the following model (coordinate system as given in Fig. 4.13):

$$\begin{aligned}
\triangle\Phi &= 0 \quad \text{in} \quad \Omega && (4.9)\\
\zeta_t - \Phi_z &= 0 \quad \text{on} \quad z = 0 && (4.10)\\
\Phi_t + g\zeta &= 0 \quad \text{on} \quad z = 0 && (4.11)\\
\Phi_z &= 0 \quad \text{on} \quad z = -d && (4.12)\\
\Phi_x - h(z)T(t) &= 0 \quad \text{on} \quad x = 0 && (4.13)
\end{aligned}$$

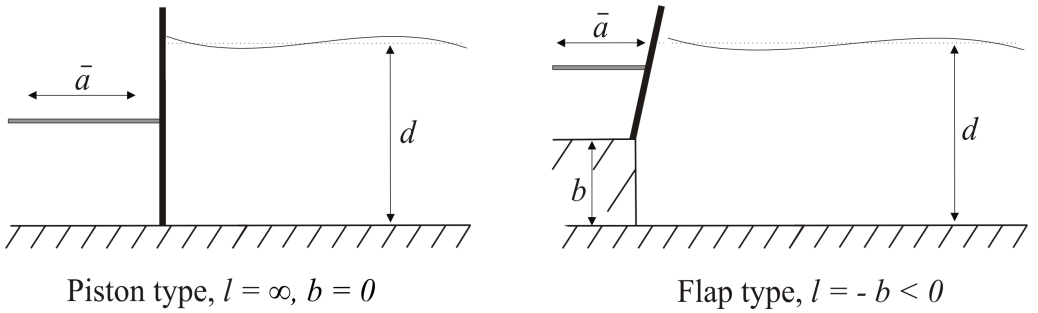

Figure 4.12: Types of wave makers with nomenclature.

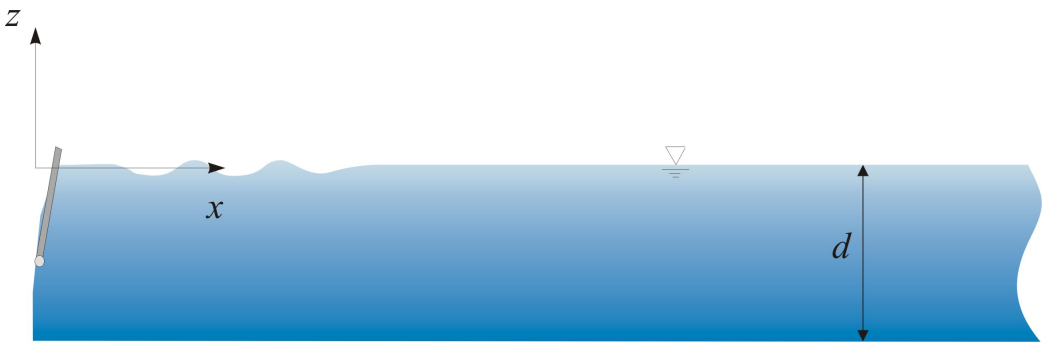

Figure 4.13: Coordinate system for modelling the wave maker.

with a radiation condition for $x \to \infty$. A linear model is assumed since both the kinematic and the dynamic boundary conditions as well as the stroke function of the wave board have been linearized. The type of wave maker is introduced by the function $h(z)$ in Eq. 4.13, defined as

$$h(z) = \begin{cases} 1 + \frac{z}{d+l} & \text{for} \quad -(d-b) \leq z \leq 0 \\ 0 & \text{for} \quad -d \leq z \leq -(d-b) \end{cases} \tag{4.14}$$

where d is the water depth, $z = -(d+l)$ is the center of rotation of the board and b is the elevation of the hinge above the bottom. l is introduced to distinguish between flap and piston type. If the center of rotation is below the bottom, then $b = 0$. As shown in Fig. 4.12, the flap type wave maker is described by the case $l = -b < 0$. The piston type wave maker corresponds to $l = \infty$, $b = 0$. The wave board stroke is denoted $\bar{a}$.

For a harmonic oscillating wave board, $T(t)$ is

$$T(t) = i\bar{a}\omega e^{-i\omega t}. \tag{4.15}$$

Thus, the general solution of the system 4.9-4.13 is given by

$$\Phi(x,z,t) = \frac{\bar{a}g}{\omega}\sum_{j=0}^{\infty} C_j \frac{\cosh(k_j(z+d))}{\cosh(k_j d)} e^{i(k_j x-\omega t)} \tag{4.16}$$

$$\zeta(z,t) = \bar{a}\sum_{j=0}^{\infty} C_j e^{i(k_j x-\omega t)}, \tag{4.17}$$

$$\tag{4.18}$$

where k_j are solutions of

$$\omega^2 = g k_j \tanh(k_j d). \tag{4.19}$$

The complex solutions of Eq. 4.19 do not only consist of the progressive (physical) real part solution k_0, but also of the so-called evanescent modes $k_j, j \geq 1$ which are the imaginary solutions of the dispersion relation. These modes have to be taken into account for higher order wave maker theories (Schäffer (1996),Westhuis (2001)). Here, only the linear wave maker theory is applied, and the coefficient C_0 – the Biésel transfer function – is given by

$$C_0 = \sinh k_0 d \frac{\Lambda_1(k_0)}{\Lambda_2(k_0)} \tag{4.20}$$

with

$$\begin{aligned} \Lambda_1(k_0) &= \sinh(k_0 d) - \frac{b+l}{d+l}\sinh(k_0 b) + \frac{1}{d+l}\frac{\cosh(k_0 b)-\cosh(k_0 d)}{k_0} \\ \Lambda_2(k_0) &= \frac{1}{2}[k_0 d + \sinh(k_0 d)\cosh(k_0 d)]. \end{aligned} \tag{4.21}$$

The Biésel transfer function C_0 relates the amplitude $\bar{a}$ of the wave board stroke to the amplitude a of the progressive wave:

$$a = C_0 \bar{a}. \tag{4.22}$$

The wave board stroke $\bar{a}$ corresponds to the horizontal oscillation of the wave board of the piston type wave maker. For a flap type wave maker $\bar{a}$ refers to the intersection point of the flap with the undisturbed water level. For the wave generation process described here, C_0 has to be applied as reciprocal, $\bar{a} = a/C_0$, since the wave board motion is looked at. As an example, the Biésel transfer function for the piston type wave maker at TUB is given in Fig. 4.14 for water depth $d = 1.5$ m. It is compared to the Biésel function of the main flap at HSVA with elevation of hinge over bottom $b = 3.44$ m and $d = 5.6$ m.

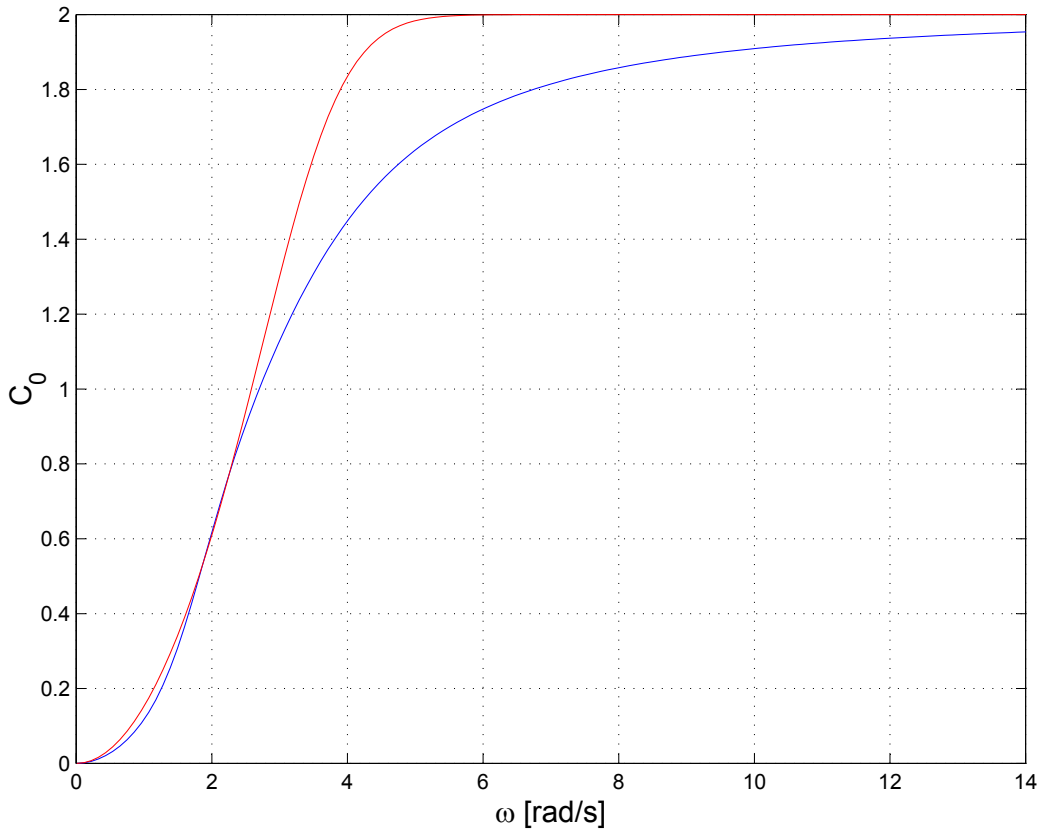

Figure 4.14: Biésel transfer function for wave generation with a flap type wave maker (blue graph, main flap HSVA, $b = 3.44$ m, $d = 5.6$ m) respectively piston type wave maker (red line, TUB, $d = 1.5$ m).

The water depth has to be considered accurately to determine the adequate transfer function: Depending on the particular frequency, a slight reduction of water depth of about 5 % might result in wave height reduction up to 50 %!

Double flap wave maker

For the case of a double flap wave maker, such as the wave maker W45 at HSVA, the hydrodynamic transfer functions for both flaps have to be considered. The motion of the total flap – denoted as α_{mf+uf} – has to be assigned appropriately to the flap angles of main and upper flap, α_{mf} and

α_{uf}:

$$\alpha_{uf} = \tau\alpha_{mf+uf}, \tag{4.23}$$
$$\alpha_{mf} = (1-|\tau|)\alpha_{mf+uf} \tag{4.24}$$

with a splitting function τ depending on wave length λ

$$\tau(\lambda) = \begin{cases} 1 & \text{for} \quad \lambda < \lambda_0 \\ 1.5e^{-0.055(\lambda-\lambda_0)^2} - 0.5 & \text{for} \quad \lambda \geq \lambda_0, \end{cases} \tag{4.25}$$

$\lambda_0 = 2$ m at HSVA.

Hydraulic and electrical RAO

In general, transfer functions can be used to represent the characteristics of the electrical devices and the hydraulic engines if the entire system is linear. Thus, the hydraulic-electrical transfer function is determined by measurements with a small transient wave packet covering the entire frequency range. The wave packet serves as control signal $U(t)$, which is measured simultaneously together with the corresponding wave board motion $\alpha(t)$ (or $\bar{a}(t)$, respectively). The hydraulic-electrical transfer function is given by Fast Fourier Transform (FFT):

$$H_{hydrl} = \frac{\mathrm{FFT}(U)}{\mathrm{FFT}(\alpha)}. \tag{4.26}$$

Thus, the control signals are calculated from the wave board motion as follows:

$$U(t) = \mathrm{IFFT}(H_{hydrl}\mathrm{FFT}(\alpha)). \tag{4.27}$$

If the system is suspected to behave non-linearly, the small transient wave packet can be scaled to rather high values. For a linear system, this must result in phase identical wave board motions, thus identical transfer functions.

Final control signals

After application of all required transfer functions, the calculated control signals are checked with regard to maximum motions of the wave board. Fade-in and fade-out of the signal are provided by the following function:

$$f_r(t) = \begin{cases} \frac{1}{2}(\cos(\pi + \frac{t}{T_r}\pi) + 1) & 0 \leq t \leq T_r \\ 1 & T_r < t < T_{meas} - T_r \\ \frac{1}{2}(\cos(\frac{t-T_{meas}+T_r}{T_r}\pi) + 1) & T_{meas} - T_r \leq t \leq T_{meas} \end{cases} \tag{4.28}$$

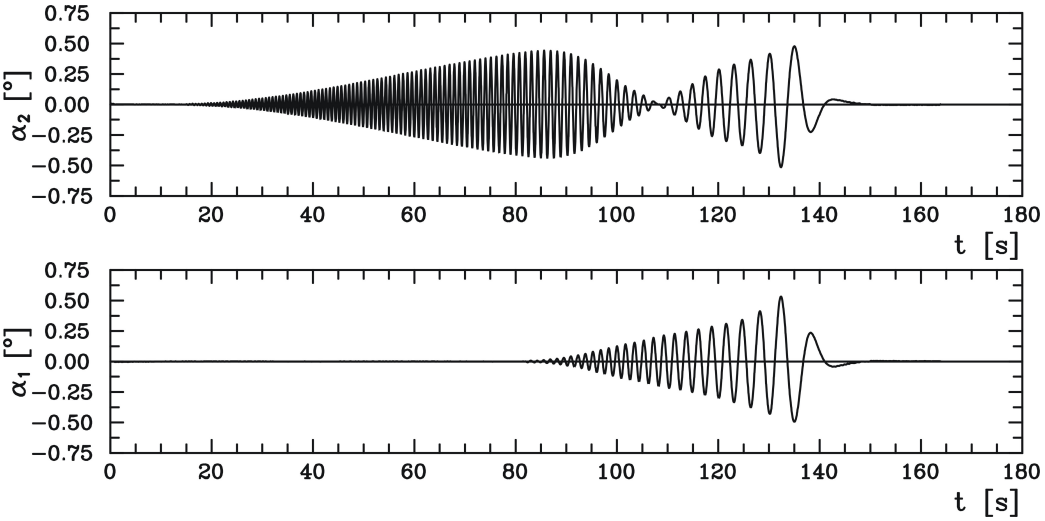

Figure 4.15: Generation of a transient wave packet at HSVA: Control signals for upper flap (top) and main flap (bottom), calculated from the wave train in Figure 4.11.

T_{meas} is the duration of the full signal, T_r is the fade-in or fade-out duration, respectively. Fig. 4.15 shows the final control signals of the test case for main and upper flap at HSVA. Waves with a length up to 2 m are generated by the upper flap only. Thus, the signal starts with high frequency operation of the upper flap. The main flap begins to operate in phase with the upper flap later on, and the angles of the upper flap decrease again until the motion changes to paraphase with the main flap. Thus, a transient wave packet illustrates the operating mode of a double flap wave maker very well. Fig. 4.16 shows the resultant wave train at the target position.

4.3 Wave transformation

For the deterministic analysis of motions and forces of ships and offshore structures the wave excitation denotes the beginning of a complex cause-reaction chain. Wave probes can be installed at defined positions, but usually not at the position of the model (due to relative motions and disturbances). Therefore, the measured wave train has to be transformed to a reference position of the model. For stationary model locations, the transformation is of the kind 4.1: $\zeta(t, x_1) \rightarrow \zeta(t, x_2)$ and the *modified non-linear theory* according to chapter 3 applies. The problem gets complex when the structure is moving at constant or non-constant speed, as stationary measurements in

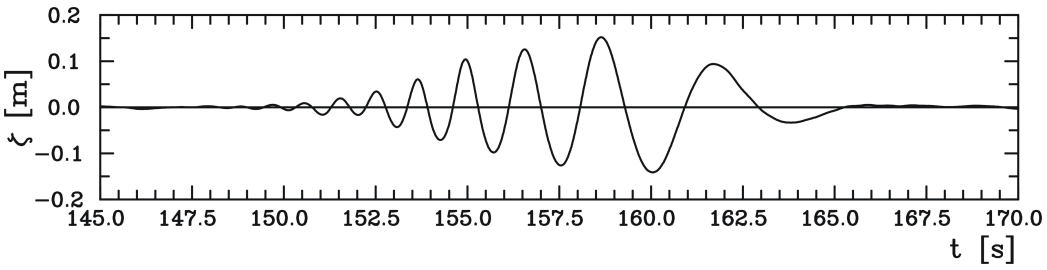

Figure 4.16: Generation of a transient wave packet at HSVA: Registration of the wave train at the target position x =85.03 m as a result of the wave maker motion shown in Fig. 4.15.

a model tank do not provide the wave train in the moving reference frame of a cruising ship.

4.3.1 Transformation of measured wave trains into the moving reference frame

For converting measured surface elevations linearly to another constantly moving location – transformations $\zeta(t, x(t)) \rightarrow \zeta(t, x(t) + \triangle x)$ (4.2) and $\zeta(t, x_1) \rightarrow \zeta(t, x(t))$ (4.3) – the following scheme is applied:

$$\omega_j = \omega_{ej} + k(\omega_j) \cdot v_M(t_i) \cdot \cos\mu(t_i) \tag{4.29}$$

$$\zeta(t_i, x + \triangle x(t_i)) = \frac{1}{2\pi} \sum_j F(\omega_j, x) \cdot e^{i(\omega_j t_i - k_j \triangle x_i)} \triangle\omega \tag{4.30}$$

where $\triangle x_i$ stands for the time varying distance between both locations. ω_{ej} is the encounter frequency which is obtained at a moving measuring point (v_M) due to the Doppler effect. Considering well-defined time windows during the test, this technique can be applied to all types of linear model seas.

For steep wave sequences, the non-linear k_j and the adequate $F(\omega_j, x_l)$ from the *modified non-linear theory* have to be calculated at the position of the model reference point $x(t_i)$ at each time step in order to get the non-linear moving reference frame wave train.

Fig. 4.17 confirms the accuracy using these tools for non-linear calculation: The wave train (transient wave packet) is measured at a stationary wave probe close to the position of the wave maker (x = 8.74 m) as well as at a downstream position of the wave tank (x = 85.03 m). Finally, the lower diagram presents the wave train as registered on board of the towing carriage

(mean velocity 1.65 m/s). Transformation of the first wave train to the fixed downstream position as well as to the moving wave probe travelling with the carriage is also shown. Agreement of registration and calculation (stars) is excellent.

4.3.2 Application to time-space correlation

The wave train can be transformed from a function of time $\zeta(t, x_0)$ at a fixed location x_0 to a function of space $\zeta(t_0, x)$ at a given time t_0 applying the *modified non-linear theory* where all wave trains at given spatial steps up to the target position are calculated subsequently. Thus, the space information is calculated implicitly and can be applied e. g. to transform data in space domain – as given by radar and satellite images of the wave field (compare Fig. 6.12) – to time domain. These time series allow the realization of spatial observation as wave sequences in a model basin.

4.4 Application of deterministic wave sequences

Apart from the examples given later on (capsizing tests), deterministic wave sequences can be used for various applications in model testing:

- RAOs of a model or of a wave maker can be determined by only one test run as a transient wave packet covers the entire frequency band. For this purpose, the wave train has to be small in height and steepness.
- The wave generation technique is used as a validation tool for two numerical wave tanks by providing special control signals and wave data (Clauss et al. (2004a) and Clauss et al. (2004b)). Also wave-structure interaction modelled by a RANSE solver is validated using deterministic wave sequences (Xing et al. (2001a), Xing et al. (2001b)).
- Wave sequences calculated by the *modified non-linear theory* are successfully applied to the experimental and numerical investigation of the influence of rogue wave impacts on a semisubmersible (Clauss et al. (2003c)), a stationary crane vessel (Clauss et al. (2003b)), and an FPSO ship (Clauss et al. (2004c)). Guedes Soares et al. (2004b) analyze the structural design wave loads on the FPSO and compare the vertical bending moment at midship induced by rogue waves with rule values.

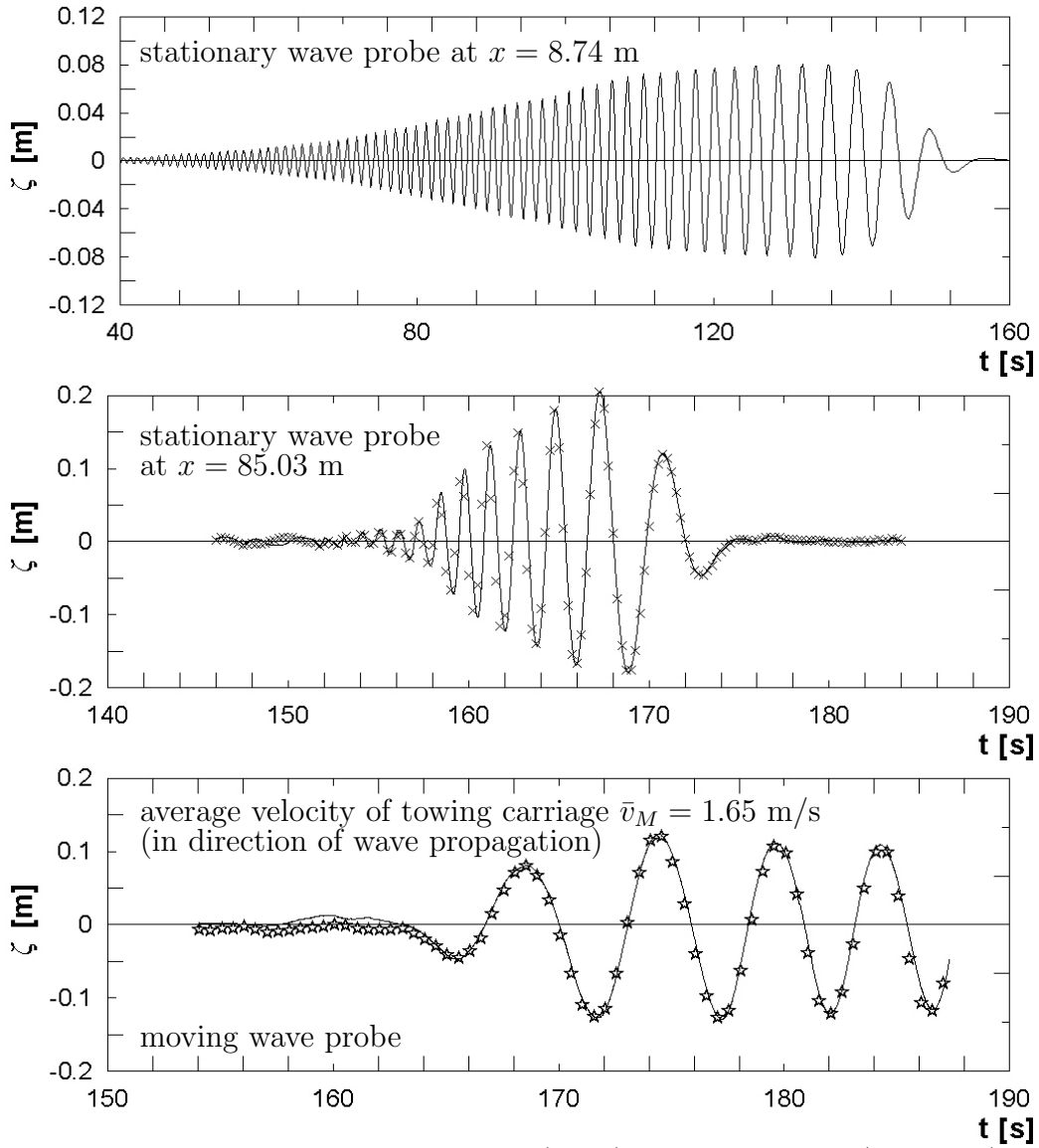

Figure 4.17: Comparison of calculation (stars) and registration (solid line) of a wave packet at stationary wave probes and at a moving probe: The wave packet at the stationary wave probe close to the wave maker is transformed to a position farther downstream and compared to the registration of a wave probe at 85.03 m. The stationary registration is also transformed into the moving reference frame of a wave probe installed at the towing carriage (average speed of 1.65 m). Agreement of calculation and registration is very good.

To investigate the sensitivity of the structural response to the wave sequence, the FPSO is exposed relatively to the incoming freak wave further downstream or upstream. Surprisingly, the *New Year Wave* results in higher bending moments at a position upstream confirming the importance of time and phase information and the need for precise simulations and model tests (Clauss et al. (2004c)).

For an improved design of ships and offshore structures with regard to their behaviour under severe weather conditions, wave height and steepness as well as the shape of the wave profile have to be considered. Thus, the *New Year Wave* is varied with respect to wave height and period using the *modified non-linear theory*. As an example, Fig. 4.18 shows the wave tank realization (scale 1:81) of the *New Year Wave* as original wave train and elongated in wave period. The elongation factor is 1.2 for the local wave period. The global wave characteristics remain the same. Since the relative steepness of the *New Year Wave* elongated in period decreases, wave breaking is less severe. Thus, the wave becomes higher than in the original registration. The elongated wave train is also scaled to larger wave height (scaling factor 1.25). Heave and pitch of a moored FPSO are measured as a response to the three wave trains and compared: Both heave and pitch motion increase due to the elongated local wave period. If the wave height is increased additionally, the response of the FPSO is scaled to higher values. Thus, non-linear wave effects can be investigated.

Concluding, the *modified non-linear theory* can be used for different kinds of wave transformations – in particular it is applied to the generation of all kinds of deterministic wave sequences and various types of model tests. It is also applicable in various model basins and for different types of wave makers.

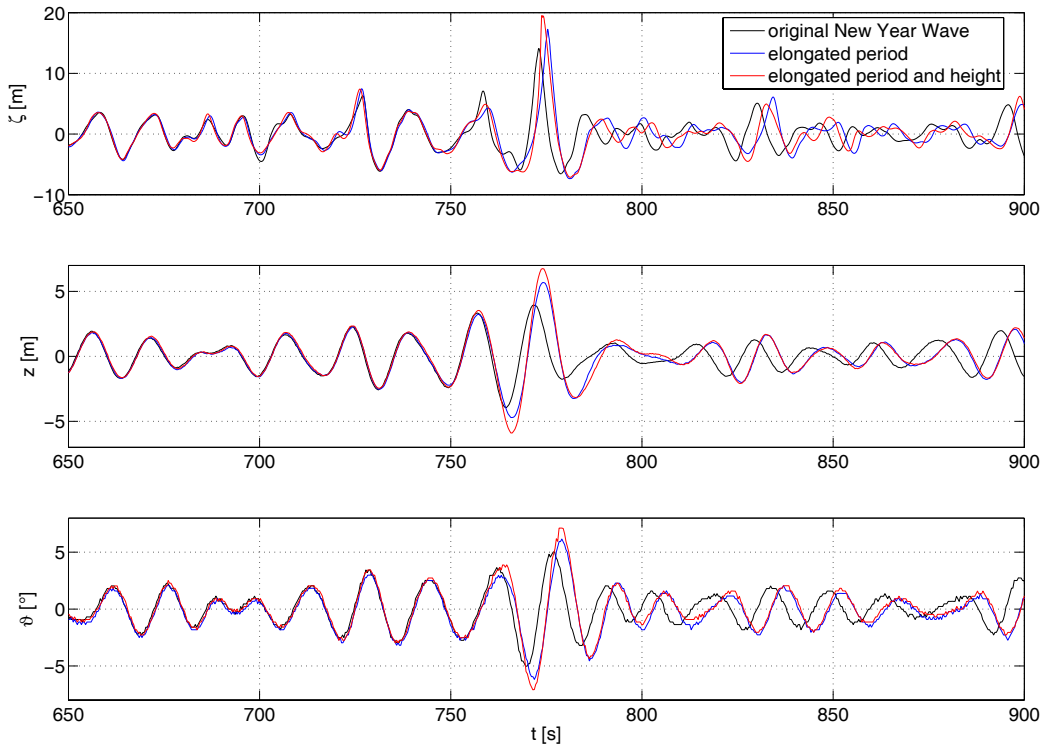

Figure 4.18: Heave and pitch of an FPSO due to the original and locally modified *New Year Wave*: The original wave train is compared to wave tank realizations with locally elongated wave period and height (top). The response increases with wave period and height as can be observed in the lower diagrams showing heave and pitch motion. The global environment is not influenced by the locally modified wave train, and also the response remains identical farther upstream and downstream.

Chapter 5

Capsizing Tests with Deterministic Wave Sequences

In this chapter, the wave generation and transformation techniques are applied to a new deterministic capsizing test procedure at the Hamburg Ship Model Basin. The fully computer controlled test procedure allows for highly accurate and reproducible investigations of various intact stability phenomena. Deterministic wave sequences are generated with respect to an exact time-space correlation of ship encounter. In this chapter, wave sequences in the moving reference frame of different ship models are compared to the measured ship motions which allows for analyzing large roll motions and capsizing as a cause-reaction chain.

The capsizing tests are performed to get a detailed understanding of the underlying mechanisms of large roll motions and capsizing and to develop methods to evaluate ship safety. For ship approval by authorities, model tests are required to prove the ship's performance with regard to seakeeping safety if the design is not covered by rules and regulations. Additionally, the deterministic test technique allows for proceeding one step further in the development of ship assessment which will be shown in chapter 6.

5.1 Categorization of rolling and capsizing

Different mechanisms leading to large roll motions and capsizing can be distinguished (de Kat and Paulling (2001)):

- Resonant excitation: The roll motion increases as the dominant en-

counter wave frequency ω_e coincides with the ship's resonance frequency ω_R. ω_e can be determined from the ship speed v, course μ and the predominant wave frequency ω (together with the dispersion relation):

$$\omega_R = \omega_e = kv_{rel} = \omega - kv\cos\mu. \tag{5.1}$$

$\mu = 0$ means sea from astern. ω is not necessarily the frequency of e. g. a swell, but can also be the frequency of an envelope of a wave sequence (Kjeldsen (1983)).

- Parametric excitation: The roll angle increases dangerously due to nonlinear processes (disturbances) which cause roll motions at half the frequency of the exciting wave. The ship rolls with twice the period of the pitch motion (which is approximately the encountered wave period). Fig. 5.1 gives an example of severe damage to cargo due to parametric excitation. The following factors contribute to parametric roll:
  - Encounter period close to one-half of the natural roll period
  - Large waves
  - Wave length comparable to the ship length
  - Wide, flat sterns in combination with pronounced bow flare, as this increases the stability variations as the wave passes along the hull.
- Impact excitation such as caused by rogue waves
- Loss of stability at the wave crest. This refers to the quasi-static loss of transverse stability (associated with an excessive righting arm reduction) in the wave crest. This mode occurs typically in regular or irregular following to quartering waves with low encounter frequencies. The ship can capsize when it experiences temporarily a critically reduced (possibly negative) righting arm for a sufficient period of time, while the wave crest overtakes the ship slowly and the ship is surging or surf-riding periodically. In irregular waves, one encountered wave of critical length and steepness is sufficient to cause the sudden catastrophic event.
- Broaching/loss of course stability due to
  - Successive overtaking waves while the ship is travelling at low speed
  - Low frequency, large amplitude yaw motions

Figure 5.1: Massive damage of cargo due to parametric roll.

  - Single wave
  - Reversed water flow at rudder, due to particle motion in waves

  Broaching has to be distinguished clearly from lying abeam. The latter is quite often considered dangerous, although model test results and in particular reports by experienced seamen confirm that lying abeam is a method of choice to survive a severe storm. The problem is rather to "get there without broaching".

- Combined modes based on additional factors.

With regard to the model test results, extreme and resonance phenomena are investigated: Examples for parametric excitation, loss of stability at the wave crest and impact excitation are treated. Apparently, the definition of a "dangerous" wave sequence depends significantly on the rolling scenario modelled. It is not a trivial task to determine a "dangerous" wave sequence: The highest wave is not necessarily the most dangerous and already the definition of "high" depends on the definition of wave height – whether it be measured by zero-upcrossing or zero downcrossing. Here the wave heights differ significantly. However, it can be concluded by experience that "dangerous" wave sequences are often related to a wave length L which coincides roughly with the ship length L_{pp}. Generally, quartering seas at approximately 30° course seem to provide the highest capsizing risk (Blume and Hattendorff (1984)).

5.2 Correlation of wave excitation and ship motions

In order to correlate wave excitation and ship motions from experimental investigation exactly, both technical synchronization within an accurate test procedure and knowledge of the (non-linear) wave train in the moving reference frame of the sailing ship are required. This is realized by:

- Computer controlled test procedure
- High accuracy at measurement and control units
- Optical motion measurement and automatic course tracking
- Self-propelled radio controlled ship model
- Deterministic wave generation
- Non-linear transformation of wave trains measured at stationary positions to the moving reference frame of the ship model.

Briefly spoken, test setup and procedure have to ensure that the ship model encounters the wave train at a defined position in time and space. Thus, the test conditions can be varied deterministically.

In order to investigate the reproducibility of such tests, preliminary tests are carried out. In place of a ship, a wave probe is installed at the towing carriage and meets a transient wave packet. Figure 5.2 presents the results of two test runs with identical parameters – $v_M = 1$ m/s, $\mu = 180°$. The registrations as well as related Fourier spectra agree very well. The transfer function relating both test results serves as an indicator for good reproducibility.

The exact timing of ship-wave encounter is an unique feature of the new capsizing test procedure with deterministic wave sequences. Former systematic capsizing investigations did not provide an accurate time-space correlation (Blume and Hattendorff (1984)).

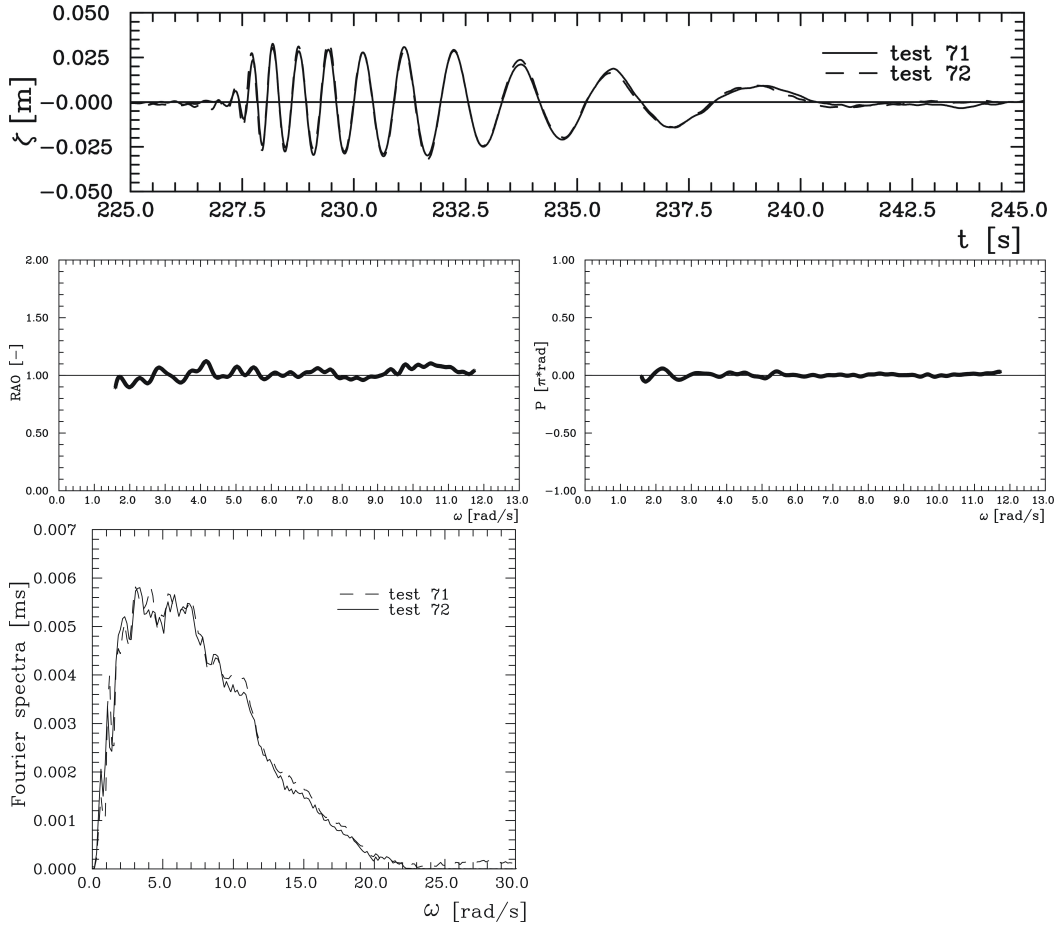

Figure 5.2: Registrations of a sonic wave probe encountering a transient wave packet at a speed of 1.00 m/s and course of 180°. The time series and related Fourier spectra of encounter agree very well which is reflected in the RAO relating the two identical test runs 71 and 72.

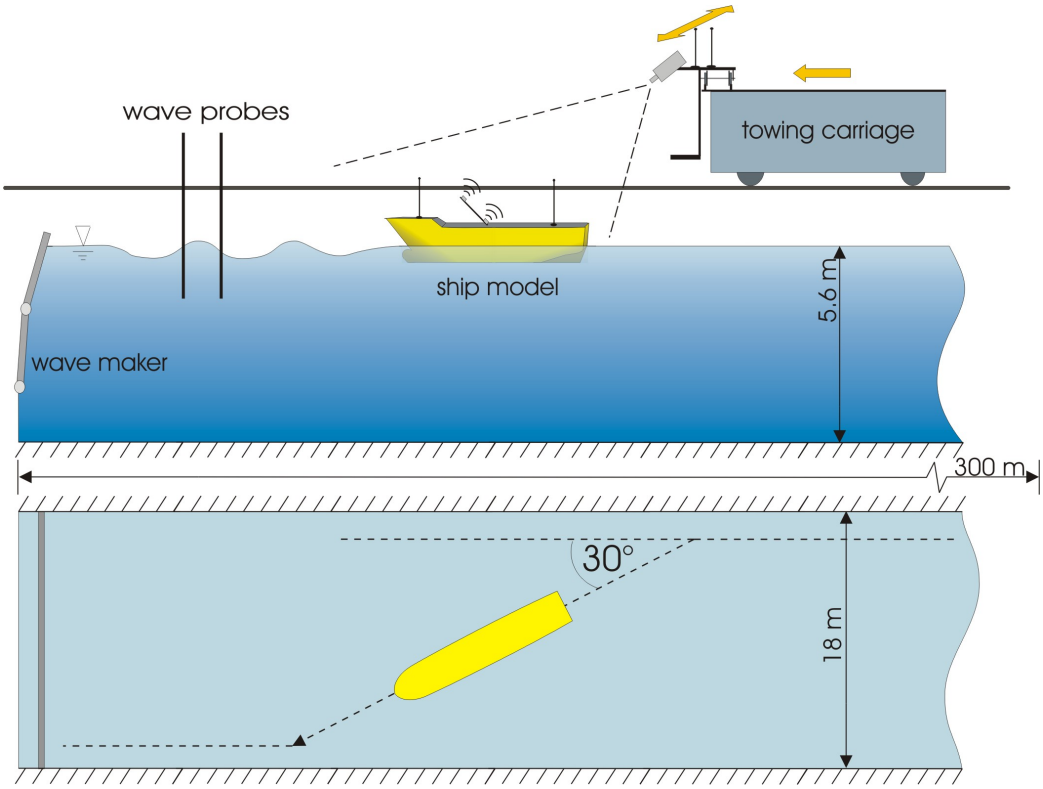

Figure 5.3: Configuration of computer controlled capsizing tests at HSVA.

5.3 Deterministic test procedure

Fig. 5.3 shows the basic test configuration of a new deterministic capsizing test technique implemented at HSVA (Kühnlein and Brink (2002)). Three main system components are coordinated:

- Wave maker
- Towing carriage (including the horizontal carriage)
- Ship model.

The master computer at the towing carriage surveys and controls the other system components transferring the necessary parameters.

For model tests in head seas, the starting position of the ship is at the side wall at the end of the towing tank. For experiments in seas from astern, the ship model has to wait close to the wave maker until a defined sequence of

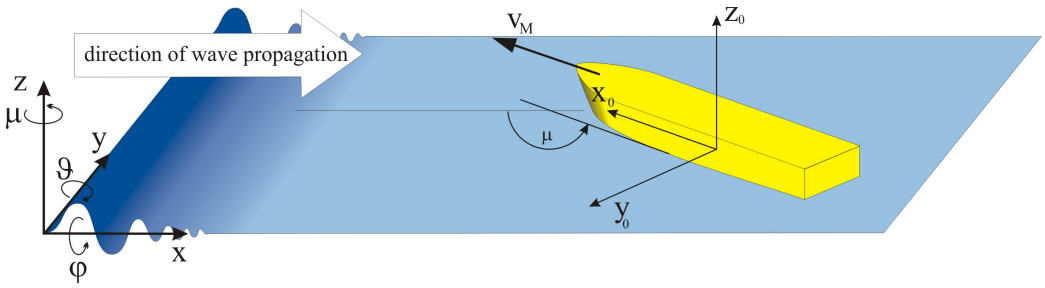

Figure 5.4: Coordinate system for capsizing tests: The measured motions (six degrees of freedom) and the wave train (both in the stationary and moving reference frame) refer to the global coordinates. The reference point at the ship model is the keel point.

the wave train has passed. Fig. 5.4 shows the definition of the coordinate systems. The motion registrations and the wave train in the moving reference frame refer to a reference point at the sailing ship model. This point is chosen to be the keel point. A course angle of 0° means following seas, and 180° denotes head seas.

As illustrated in Fig. 5.5 the test procedure starts with the definition of test parameters such as wave frequency ω (either given as single frequency or given as entire band), characteristic wave height (e. g. the maximum wave crest elevation ζ_{max}) and the target position x_e of the ship encountering the tailored wave train related to the position of the maximum wave elevation x_c. These parameters are fed into both the wave generation program WaveGen and the test simulation program WaveShipSim. As a first step, the control signals for the double flap wave maker are calculated, which corresponds to the flap angles α_{uf} and α_{mf} as time series. Preprocessing includes the calculation of the encounter point in time and space where the ship meets the wave train under defined conditions. WaveShipSim returns the time t_e at which the ship will reach the encounter position x_e (depending on the average ship velocity v_M and course μ).

The double flap wave maker generates the deterministic wave train. The model starts to sail through the tank in such a way that it reaches the encounter position at the predefined instant. The ship moves in parallel with the tank side wall at a safety distance.

Ship motions in six degrees of freedom are registered precisely by the optical motion tracking system and evaluated by the master computer to control by telemetry the ship's z-manoeuvre at a constant average course angle and model velocity. Computer controlled guidance of both, the towing and the

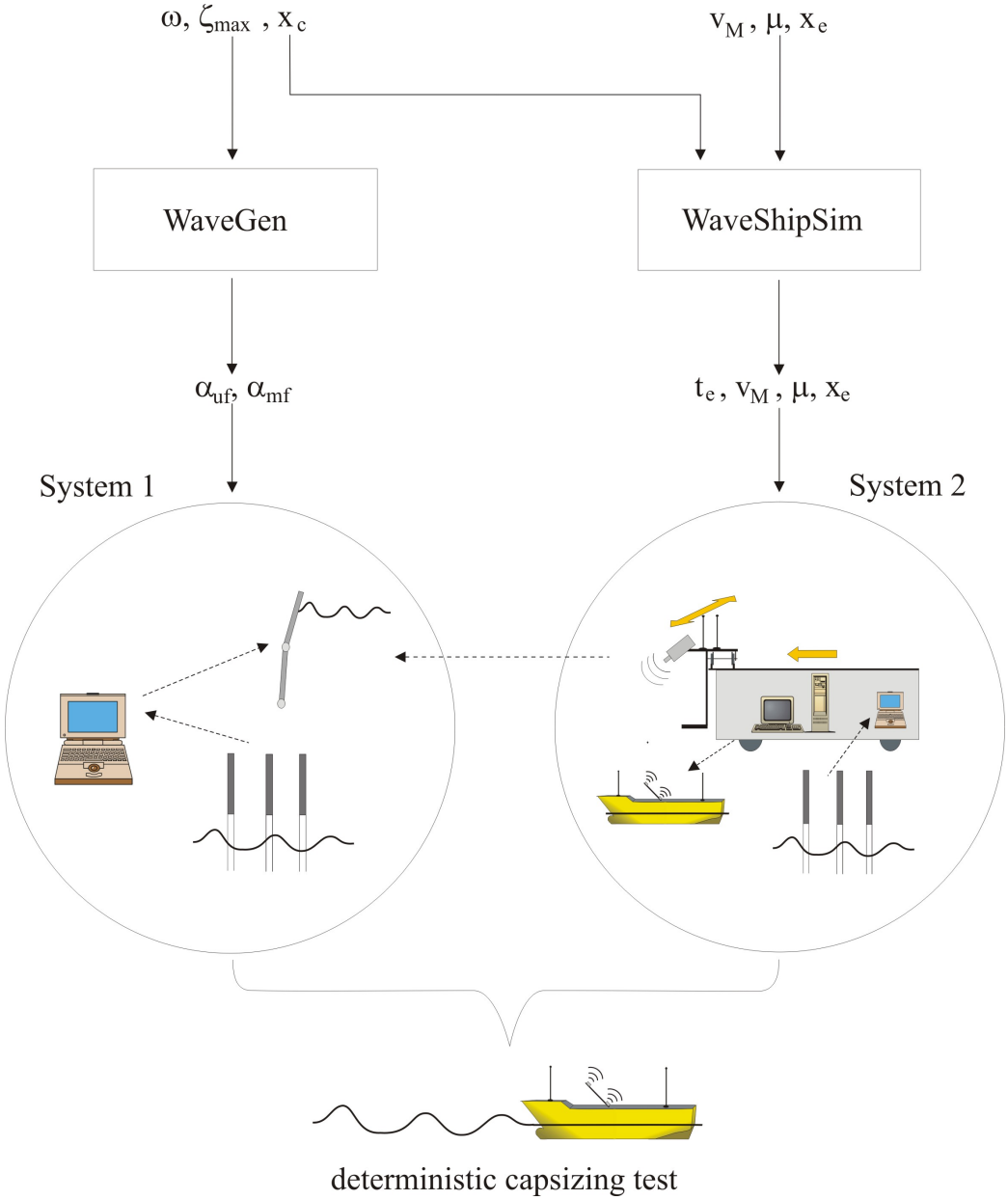

Figure 5.5: Computer controlled capsizing test procedure.

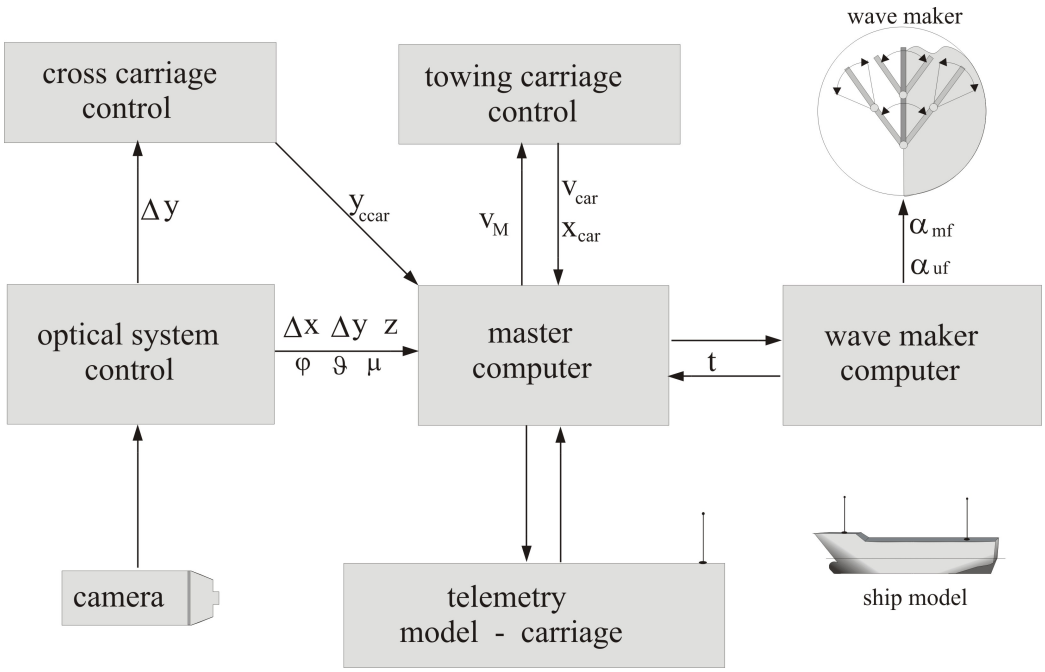

Figure 5.6: Communication scheme for computer controlled capsizing tests.

horizontal carriage by real-time evaluation of all relevant parameters ensures that the ship model stays in the field of view of the line cameras during the entire test run. This is illustrated in the communication scheme in Fig. 5.6. Additionally, the wave train is measured at several fixed positions in the wave tank. When the model reaches the critical distance to the wave maker or the absorbers at the opposite side of the tank, the ship and the carriage stop automatically.

Thus, the test is realized by a deterministic course of test events which allows a reproducible correlation of wave excitation and ship motion. Fig. 5.7 shows the importance of high accuracy in control and measurement: Encountering a wave packet slightly differently induces clearly distinguishable effects in vessel motions. The wave train is presented in the moving reference frame of the ship. The resultant roll motion shows a completely different behaviour towards the end of the registration. For more complex wave sequences such as wave groups within a sea state, the effect becomes even more significant. In particular, a reproducible test technique is indispensable not to miss a predefined wave sequence during the test.

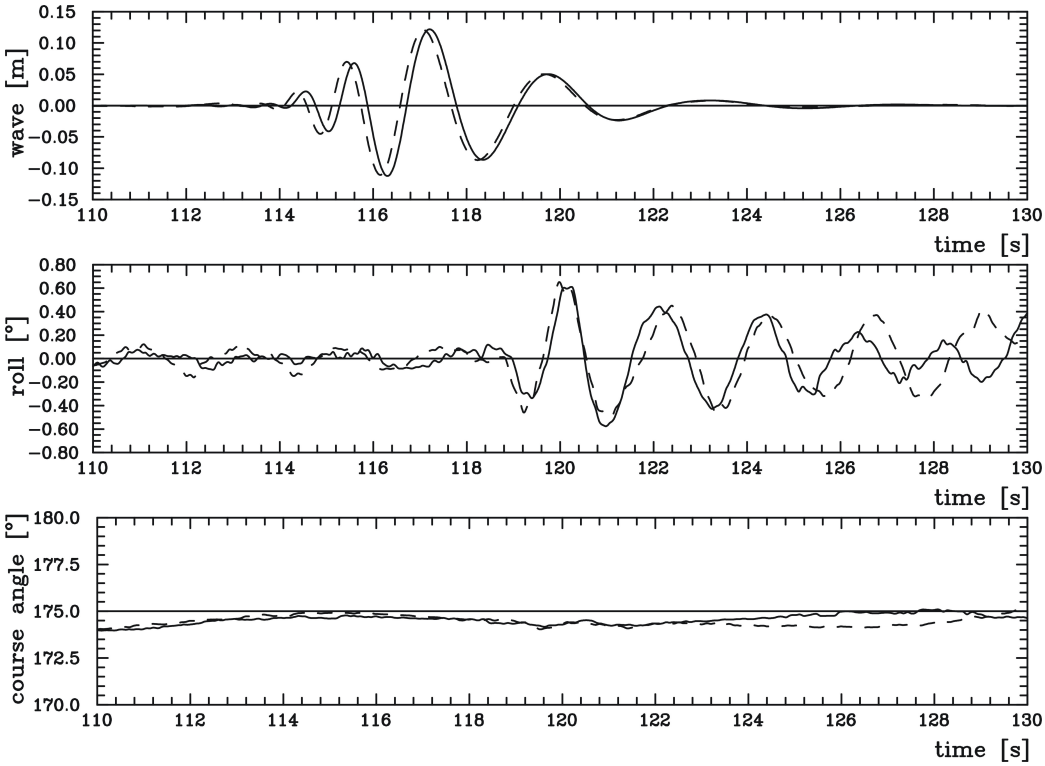

Figure 5.7: Transient wave packet (top – in the moving reference frame) encountering the self-propelled ship model with optical registration of roll motion and course angle (bottom): Comparison of two tests with slightly different conditions of encounter (the ship encounters the wave packet at 0.4 s time shift) demonstrates the importance of high accuracy and reproducibility in the test procedure.

5.4 Results of capsizing tests with deterministic wave sequences

According to the expected rolling mode and occurrence of resonance, the experimental conditions are varied with respect to the following parameters:

- Metacentric height GM of the ship model – varies mainly around the current limits as given by IMO's Code on Intact Stability (IMO (2002)).
- Average model velocity v_M
- Target course μ
- Type of deterministic wave sequence

  - regular waves – with or without embedded *Three Sisters* rogue wave
  - irregular waves with deterministically embedded high wave sequences

- Characteristic wave frequency and height with respect to encounter frequency

- Time and position of encounter of ship and wave

The model tests are performed according to Froude's law, i. e. for a given scale λ, length is scaled by λ, time and velocity by $\sqrt{\lambda}$, and frequency by $1/\sqrt{\lambda}$.

Different ships – designed by Flensburg Shipyard – are investigated:

- Multipurpose container vessel (C-Box, Fig. 5.8) with $L_{pp} = 145.75$ m, $B = 23.60$ m, $T = 9.00$ m, and $C_B = 0.7395$ (model scale 1:29),

- RO-RO vessel A (Fig. 5.9) with $L_{pp} = 182.39$ m, $B = 26.00$ m, $T = 5.70$ m, and $C_B = 0.5686$ (model scale 1:34),

- RO-RO vessel B (Fig. 5.10) with $L_{pp} = 190.29$ m, $B = 26.50$ m, $T = 7.35$ m (model scale 1:34) – twin screw propulsion,

- RO-RO vessel C – similar design as vessel B, but single screw propulsion.

The models are self-propelled - C-Box and RO-RO vessel C with one, RO-RO vessels A and B with two propulsion systems, which are radio controlled by the master computer at the towing carriage.

Stationary wave registrations complete the test instrumentation. As the wave cannot be measured directly at the cruising ship model, for all model test results given here, stationary wave registrations are transformed to the moving reference frame of the sailing ship. The transformation is based on the exact registration of the horizontal ship position in the model basin. Thus, the wave train as encountered by the ship model is directly compared to the resultant ship motions and the underlying mechanism of large roll motions and/or capsizing is revealed.

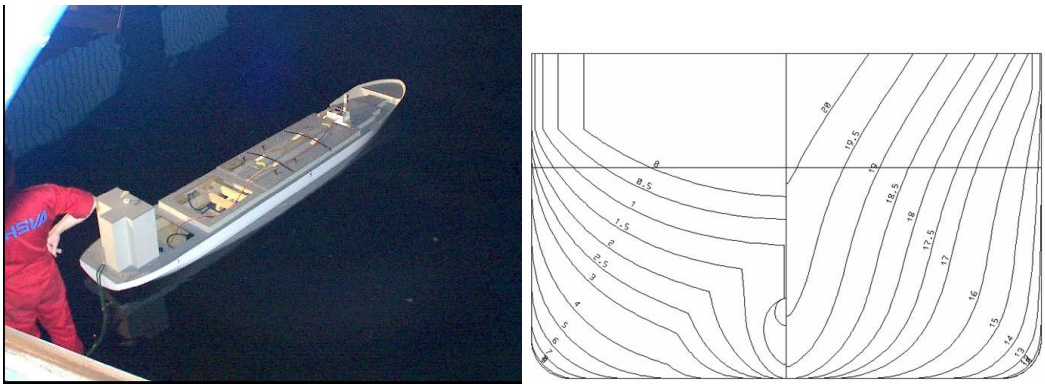

Figure 5.8: Investigated ship model C-Box and corresponding ship lines – model scale 1:29.

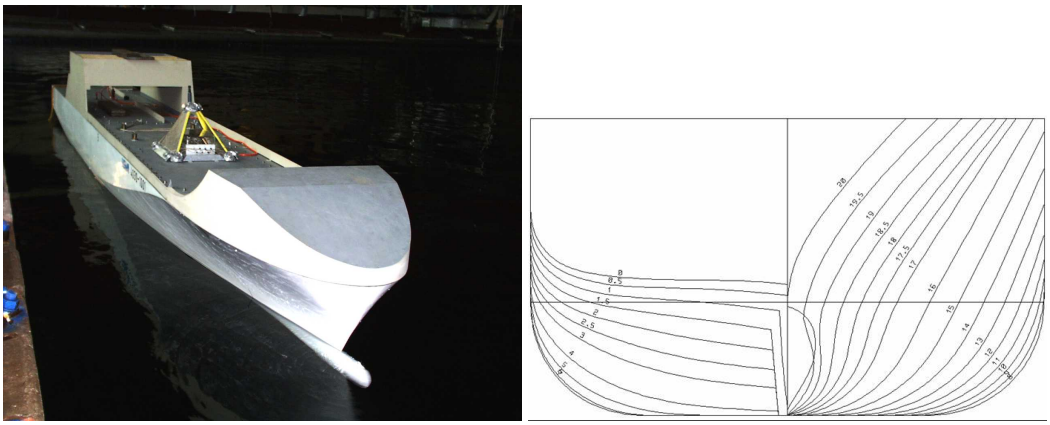

Figure 5.9: Investigated ship model RO-RO vessel A – model scale 1:34.

5.4.1 Large roll angles induced by a Three Sisters wave sequence from astern

As a special application of deterministic wave sequences, a regular wave which is superimposed with a rogue wave sequence – a so-called *Three Sisters* wave – is generated in the towing tank at HSVA. Fig. 5.11 shows the test results for the C-Box ($GM = 0.44$ m, $v = 14.8$ kn and $\mu = \pm 20°$) measured in waves from astern ($L/L_{pp} = 1.1$). The first figure shows a wave packet within a regular wave measured at a stationary wave probe close to the wave board ($x = 8.76$ m, model scale 1:29). The wave train looks unsuspicious and rather chaotic than regular. Transformation to the moving reference frame of the cruising ship discloses the wave's real character: The resultant wave sequence is quite regular and contains the target *Three Sisters* wave at the

Figure 5.10: RO-RO vessel B – model scale 1:34 – in a high wave sequence from astern which finally leads to capsizing.

location of interaction with the cruising ship. The regular wave train at the keel point (moving frame) develops from an apparently irregular wave train (see wave registration close to wave maker). The wave crests seem to be flat whereas the troughs look steeper than compared to stationary registrations of high wave groups. This is due to the ship surf-riding on top of the wave crest. Thus, it experiences the wave with longer crests than can be revealed from a stationary reference frame. Ship motions at all degrees of freedom are registered and processed by the optical system – position, roll, pitch, and course are presented here. The roll angles which were quite small due to the regular wave train increase dramatically as the ship encounters the *Three Sisters* wave. This test case illustrates the advantage of using deterministic wave sequences: The ship behaves inconspicuously until it encounters the rogue wave sequence. Applying the *modified non-linear theory* to transform the stationary wave train into the moving reference frame, ship behaviour

can be clearly related to the encountered wave sequence.

5.4.2 Parametric roll in regular head seas

Figs. 5.13 and 5.12 illustrate the ship motion characteristics of RO-RO vessel A ($GM = 1.36$ m, natural roll period $T_R = 19$ s, $v = 8.4$ kn) in high regular head seas ($H = 10.2$ m, $L = 218$ m, $T = 11.65$ s, $L/L_{pp} = 1.2$), with a target course angle of $\mu = 173°$. During the first half of the test duration, the roll motion is inconspicuous (see photos in Fig. 5.12 at model time $t = 220$ s). Suddenly, beginning at model time $t = 240$ s, parametric roll with twice the wave encounter period is starting, with increasing rolling angles up to critical values of 40° (see Fig. 5.12: photos at model time $t = 260$ s and $t = 290$ s). Note that the pitch motions keep the same value and agree with the encounter frequency.

5.4.3 Parametric roll in deterministic wave sequences from astern

Apart from large container ships, also other modern ship designs are susceptible to parametric excitation such as RO-RO, RoPax, ferries and cruise vessels. An example for parametric roll due to a high deterministic wave sequence from astern ($H_s = 9.36$ m, $T_P = 11.66$ s) is given Fig. 5.14. The test conditions for the RO-RO vessel B (GM=1.27 m, $v = 10.4$ kn, $\mu = 3°$) are simulated prior to the test (see chapter 6). In both test runs, the ship encounters the wave train at almost identical conditions (top) and shows a similar roll response. However, in the first test (blue graph) the ship roll motions exceed 50° but the capsize occurs only in the second run (green graph). This is also an example for both the high reproducibility of capsizing tests with deterministic wave sequences and the sensitivity of the mechanism leading to capsizing. It has to be noted that in reality, a capsize at a roll angle of more than 50° might have occurred though – eventually due to shift of cargo, vehicles – or engines.

Another example of parametric roll is given in Fig. 5.15 for RO-RO vessel B ($GM = 1.05$ m, $v = 11.3$ kn, $\mu = 3°$). The wave sequence is varied in height – $H_s = 7.14$ m for the blue graph, $H_s = 8.84$ m for the green graph

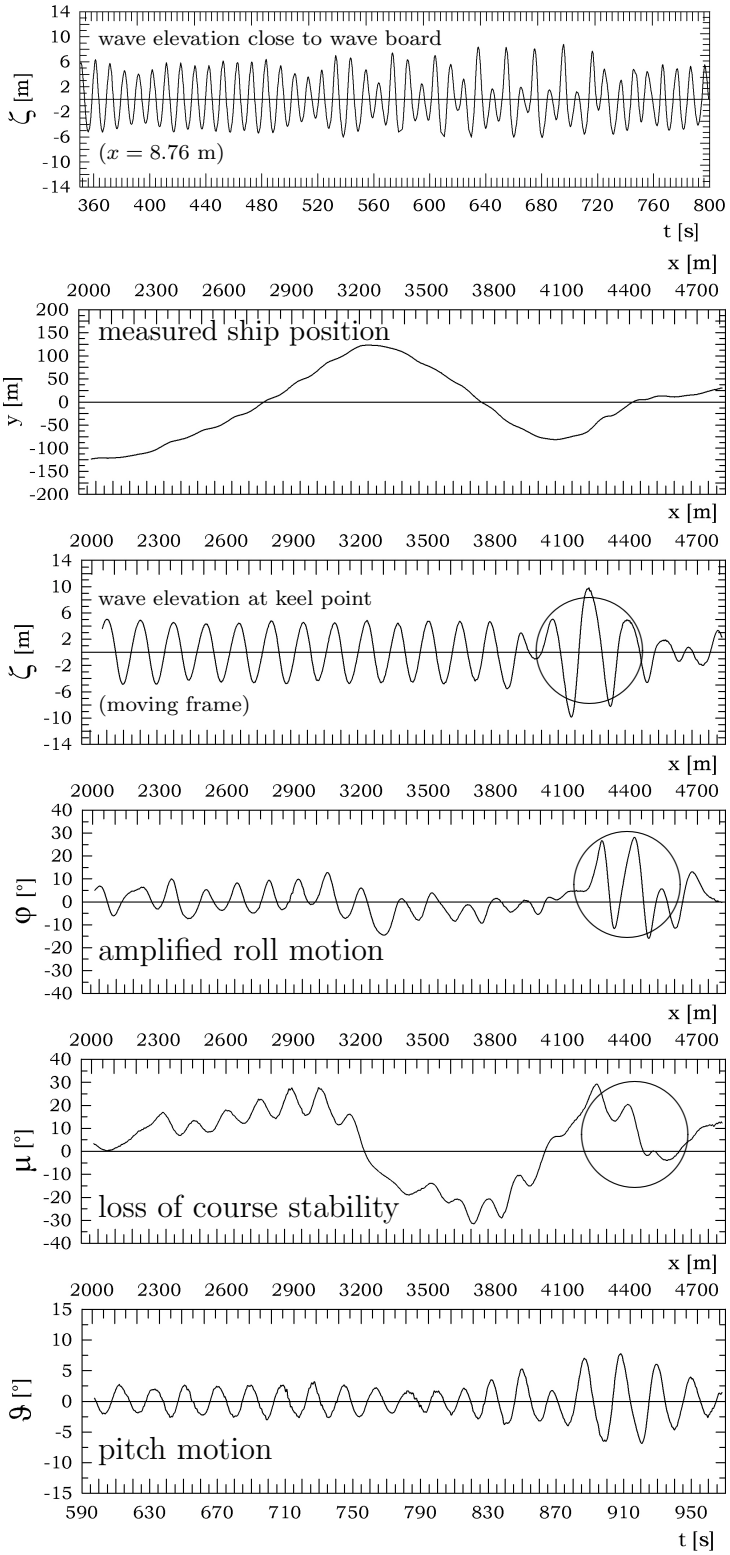

Figure 5.11: Roll motion of the C-Box ($GM = 0.44$ m, $v = 14.8$ kn und $\mu = \pm 20°$) in a regular wave from astern ($L = 159.5$ m, $\zeta_c = 5.8$ m) with embedded *Three Sisters* wave which induces dangerously increased roll motions. Transformation of the stationary wave train (top) to the moving reference frame (third graph) reveals the regular and rogue character of the wave sequence encountered by the ship. Model scale is 1:29. The x-axis refers to the mean position of the cruising ship.

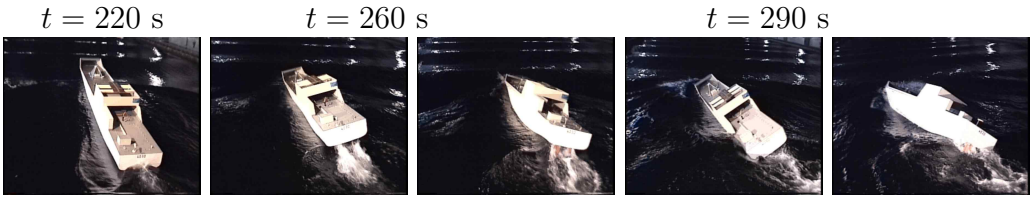

Figure 5.12: Parametric excitation of the RO-RO vessel A (compare Fig. 5.13) — model scale 1:34.

– $T_P = 11.66$ s for both. The wave phase encountered by the ship is similar in both cases (top), and parametric roll occurs (bottom). However, in the lower wave train (blue graph), the vessel motions exceed 50° whereas only in the second test run subsequent capsizing is observed.

The scenario of parametric roll given in Fig. 5.14 is reproduced for the RO-RO vessel C (single screw propulsion). The ship model capsizes in the same deterministic wave group (Fig. 5.16) – blue graph: vessel C, green graph: vessel B.

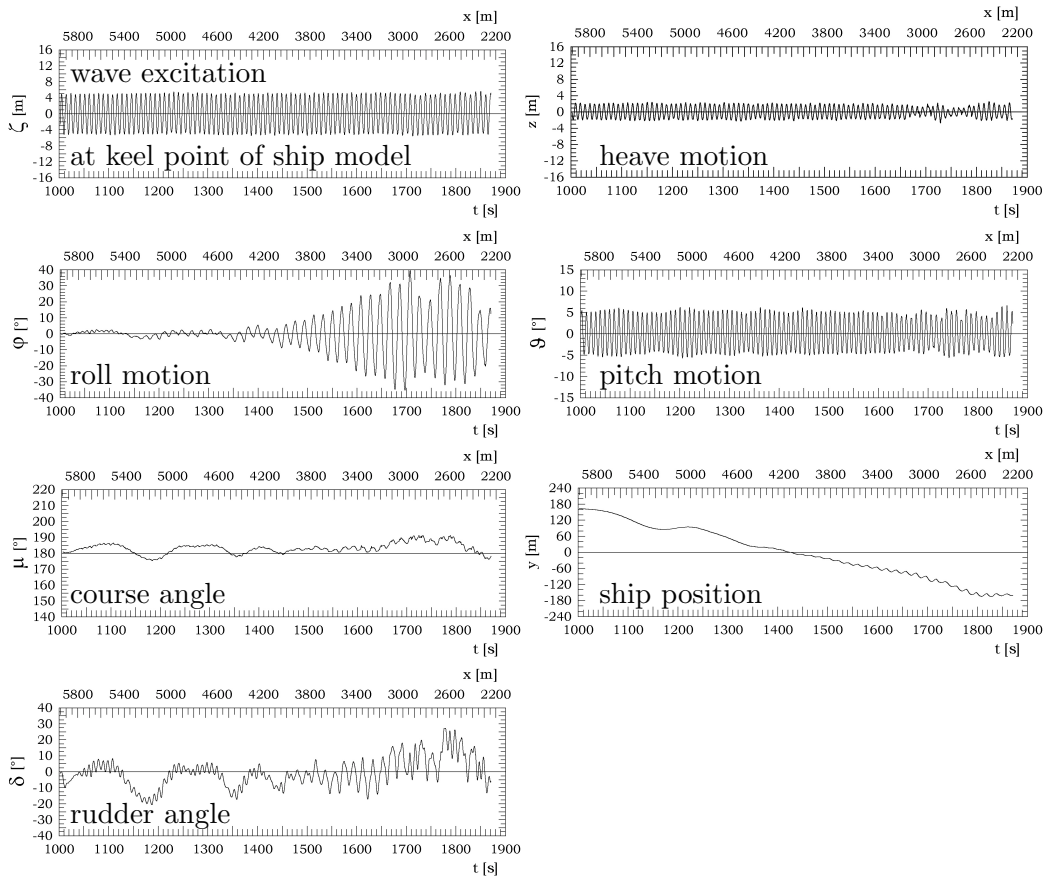

Figure 5.13: Parametric excitation of the RO-RO vessel A ($GM = 1.36$ m, $v = 8.4$ kn) in regular head seas ($\mu = 173°$, $L/L_{pp} = 1.2$). Wave height is $H = 10.2$ m at wave period of $T = 11.65$ s, encounter period $T_e = 9.5$ s; period of roll resonance: $T_R = 19$ s.

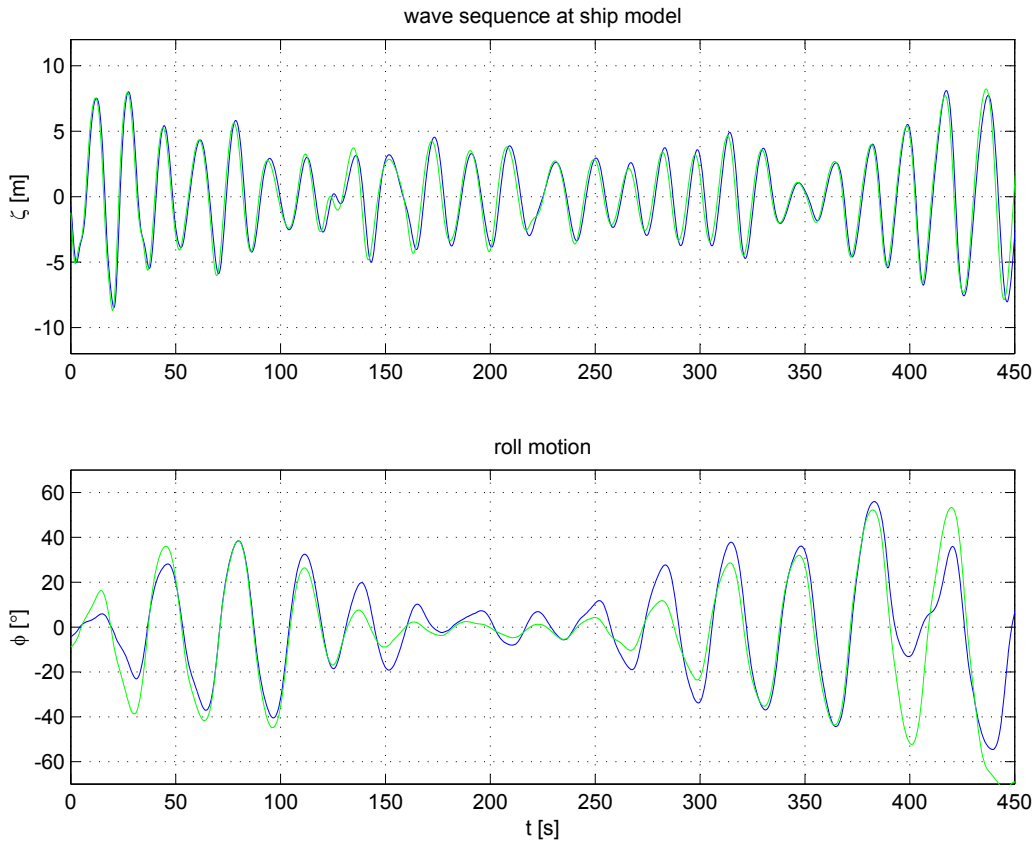

Figure 5.14: Comparison of two capsizing test runs in deterministic wave sequences from astern inducing parametric roll ($v = 10.4$ kn, $\mu = 3°$): The encounter of ship and wave train demonstrates the very good reproducibility of capsizing tests with deterministic wave sequences: The wave train is encountered under identical conditions. However, the sensitivity of capsizing processes is obvious – although the conditions and resultant motions are almost identical, the RO-RO vessel B ($GM = 1.27$ m) capsizes during the second test run only (green graph, bottom).

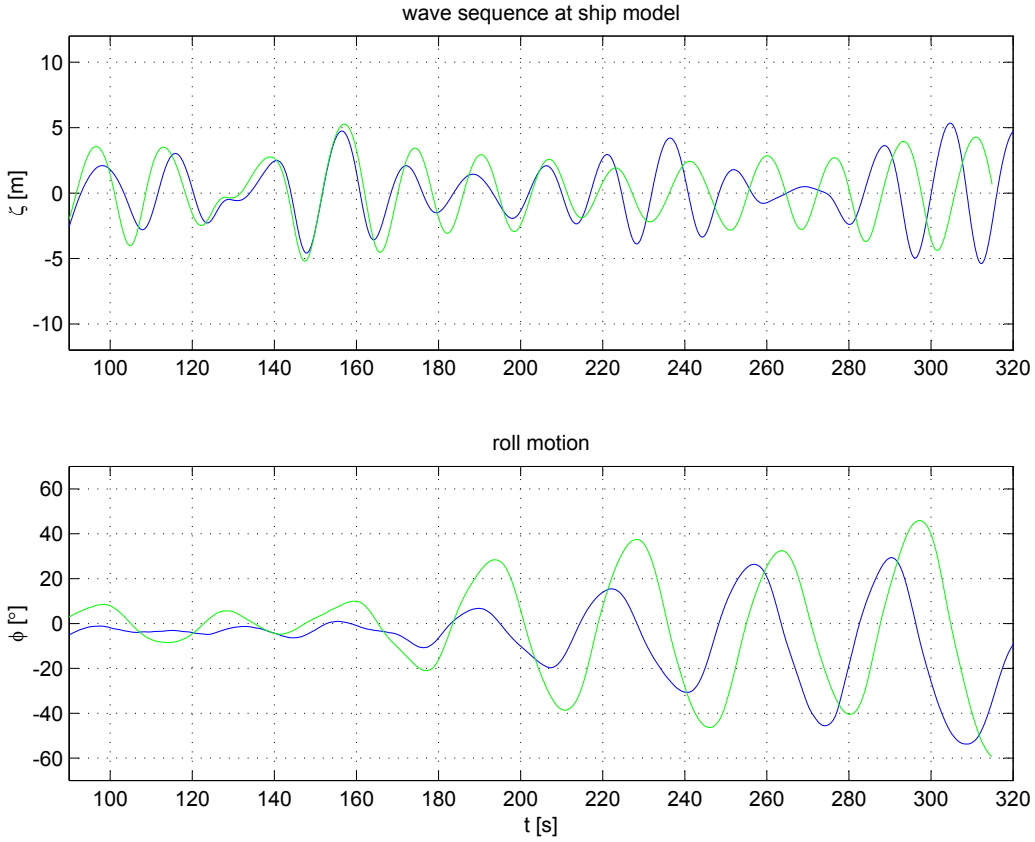

Figure 5.15: Comparison of two capsizing test runs in deterministic wave sequences from astern inducing parametric roll to RO-RO vessel B ($GM = 1.05$ m, $v = 11.3$ kn, $\mu = 3°$): The wave train is varied in height ($H_s = 7.14$ m for the blue graph, $H_s = 8.84$ m for the green graph) which leads to a capsize only for the higher wave train although the wave encounter is similar by phase.

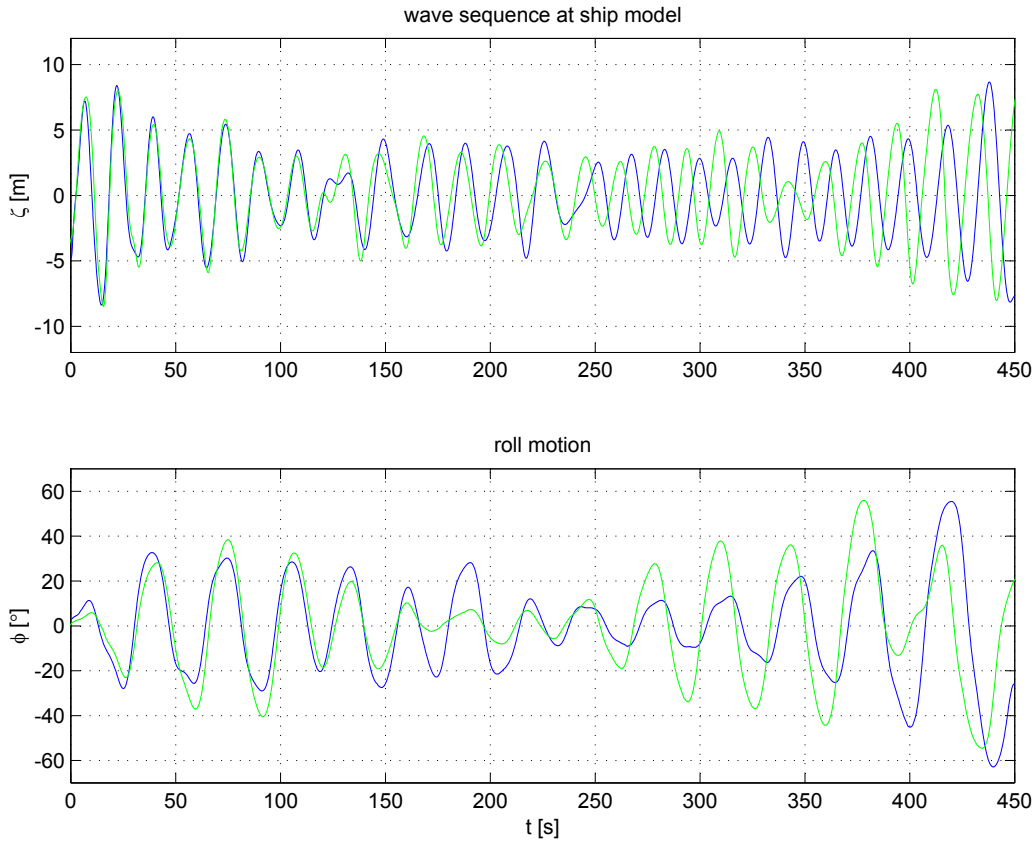

Figure 5.16: Capsizing of RO-RO vessel C ($GM = 1.24$ m, blue graph) due to parametric roll in the same deterministic wave sequence ($H_S = 9.36$ m, $T_P = 11.66$ s) as in Fig. 5.14 ($v = 11.3$ kn, $\mu = 3°$). Comparison of results from the test with model B (green graph) demonstrates reproducibility even for different models.

5.4.4 Loss of stability at a wave crest in high wave sequences from astern

Using transient wave packets any deterministic wave sequence can be embedded in irregular seas. Thus, Figs. 5.17 and 5.18 present results of model tests with RO-RO vessel A ($GM = 1.36$ m, natural roll period $T_R = 19.2$ s, $v = 15$ kn) in high seas from astern (JONSWAP spectrum with $H_s = 15.3$ m, $T_P = 14.6$ s, Z-manoeuvre: target course $\mu = \pm 10°$). The upper diagram (Fig. 5.17) presents the registration at a stationary wave probe. As the waves are quite high the associated crests are short and steep, followed by flat and long troughs. In contrast, the cruising ship – see wave elevation at keel point (moving reference frame)– apparently experiences extremely long crests and short troughs with periods well above 20 s, as the vessel is surfing on top of the waves of the high deterministic sequence. Consequently, the ship looses stability, and finally capsizes as the vessel roll motions exceed 40° (Fig. 5.18). Note, that the wave elevation refers to the moving reference frame at the keel point of the cruising ship and can be directly correlated to the ship motions by magnitude and phase. As a consequence, the seakeeping behaviour and even the mechanism of capsizing can be deduced and explained on the basis of cause-reaction chains.

The presented results from deterministic capsizing tests document that different roll phenomena – extreme situations as well as resonance effects – can be investigated reproducibly applying deterministic wave sequences. All seakeeping scenarios are modelled realistically choosing the model sea and test conditions accordingly. Permanent control and registration of the exact ship position allows for the transformation of stationary wave registrations to the moving reference frame.

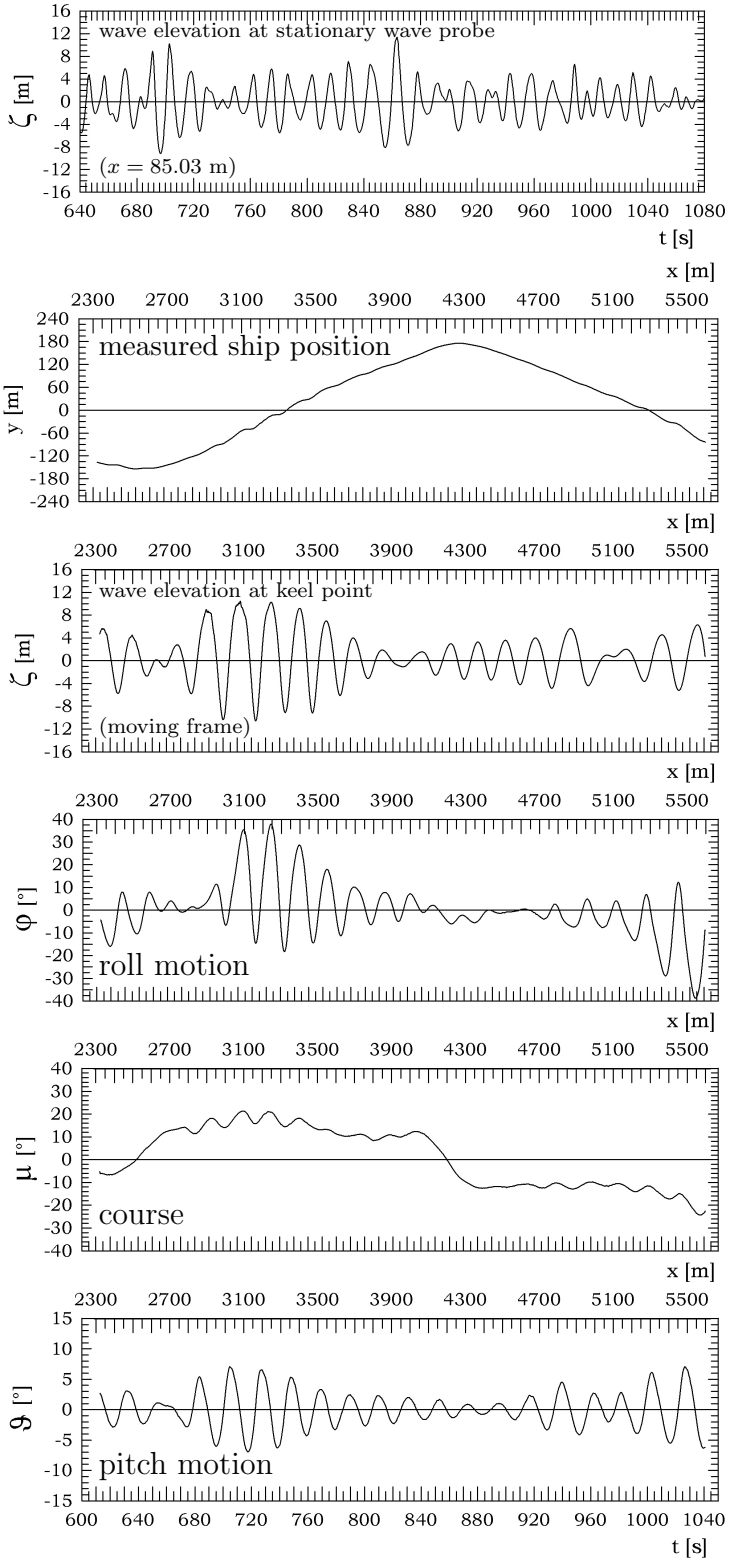

Figure 5.17: Capsizing of the RO-RO vessel A (GM = 1.36 m, v = 15 kn, Z-manoeuvre at $\mu = \pm 10°$) due to deterministic high waves within harsh seas (T_p = 14.6 s, H_s = 15.3 m). Transformation of the stationary wave registration to the moving frame of the cruising ship reveals the extreme wave sequence encountered by the sailing ship.

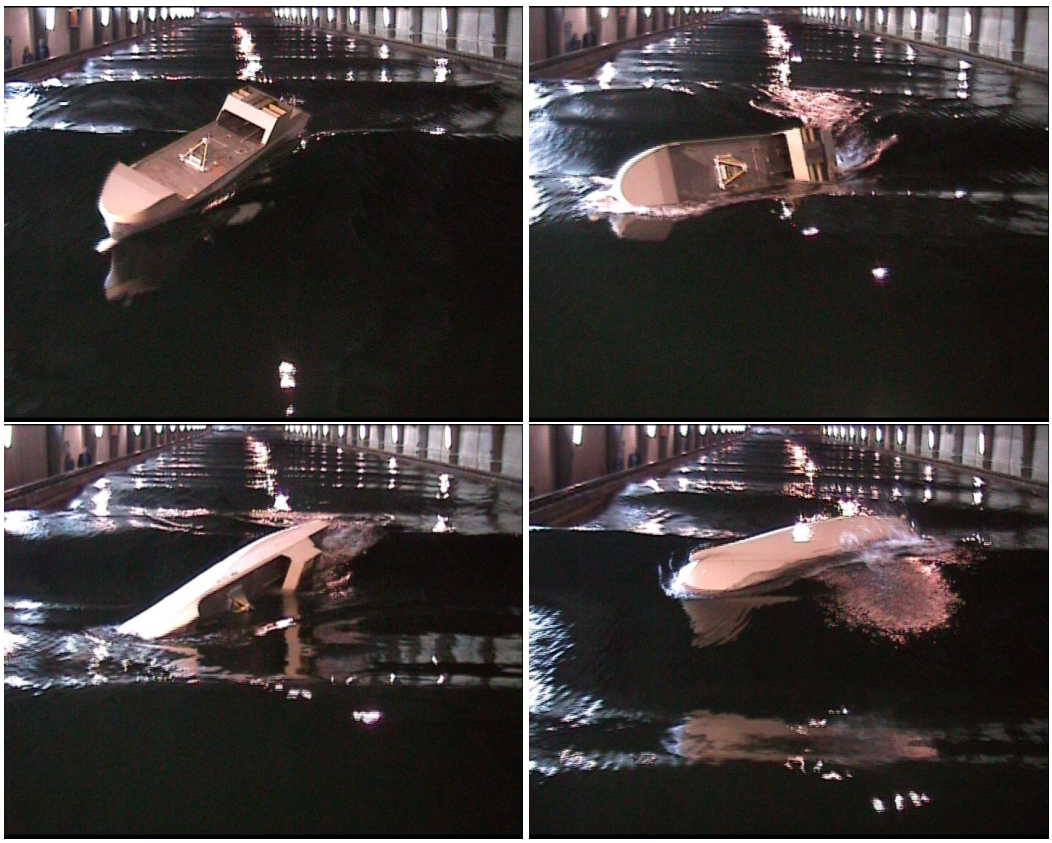

Figure 5.18: Capsize of RO-RO vessel A due to a high wave sequence in a severe model storm (compare Fig. 5.17) – model scale 1:34.

Chapter 6

Validation of Numerical Motion Simulations by Deterministic Wave Sequences

Faulkner (2003) deplores that ships are not at present designed to withstand severe weather conditions. He cites a sample of deep ocean abnormal wave reports from 115 ship incidents where many waves were of 25 m height or more, whereas normal design uses linear waves equivalent to no more than 10 m to 15 m. He continues, that ship capsize rules may not be adequate to face loss of stability phenomena. As a consequence, a *survival design* approach in addition to normal ship design is suggested where computer controlled test tank simulations can be conducted to measure ship response and loads for *survival design*.

Also Kjeldsen (2001) recommends a more realistic adaptation of the rules and regulations – e. g. provided by classification societies and the International Maritime Organization (IMO) – with regard to design wave height and model tests. Cramer and Tellkamp (2003), Cramer et al. (2004a) pinpoint the drawbacks of existing stability criteria which do not include some potentially dangerous situations related to parametric excitation and changes of stability in waves. For modern ship design, the application of the current intact stability code (IMO (2002)) seems not to provide a reliable basis for the assessment of ship safety in rough seas – as confirmed by many examples of ship design and operation. The international discussion evidences the demand for methods, suitable to evaluate the seakeeping performance of ship designs.

Possible methods to investigate seakeeping behaviour and ship safety are

model tests – such as shown in chapter 5 – and numerical simulations. Numerical assessments are faster and less expensive than experiments but require a thorough validation by model tests as the required quality of numerical simulation tools is not agreed upon by rules and regulations.

In this chapter, a state-of-the-art numerical method for the simulation of ship motions in realistic seas is validated by capsizing tests with deterministic wave sequences. The new type of validation allows for comparison of time series from model tests and numerical simulations in all degrees of freedom directly in the moving reference frame of the ship. The validation is based on the exact modelling of deterministic wave sequences both in the numerical and experimental simulation.

6.1 Numerical simulation of ship motions

Various numerical motion simulation programs exist worldwide – from rather simple linearized tools to sophisticated non-linear codes. All simulation methods are based on assumptions and simplifications in their mathematical model in order to reduce computing time. Still some of the highly non-linear methods have longer computing times than simulated time, which strongly reduces their practical applicability for safety assessments.

Simulation programs have improved significantly during the last years and are considered routinely in the design process at shipyards and for the basic investigation of ship safety (Cramer and Tellkamp (2003)). First results from test calculations for existing ships are presented by Krüger (2002), and the conclusions from numerical motion simulations regarding seakeeping capabilities of different ships correlate well with operational experience. Many examples show, that simulation tools are well suited to investigate accidents, see e. g. France et al. (2001), McTaggart and de Kat (2000), Söding (1987a). With respect to design optimization it can furthermore be demonstrated that the consequent application of numerical investigations in the early design phase allows to efficiently improve the design with respect to intact safety. Numerical motion simulations are a valuable tool for ship design, investigation of accidents and operational guidance if they are used appropriately.

The numerical motion simulation tool *rolls* is based on a methodology developed by Kröger (1987) and Petey (1988) further developed by Söding (1987b), and others (Cramer and Krüger (2001)). *Rolls* simulates the motion of intact and damaged ships in time domain in all six degrees of freedom in regular waves and irregular long or short crested seas. For heave, pitch, sway and

yaw, response amplitude operators (RAO) are used – calculated linearly by means of strip theory. Yaw is considered as a mean value and linearized. The surge motion is simulated assuming a hydrostatic pressure distribution under the water surface for the determination of the surge-inducing wave forces. The roll motion is simulated non-linearly with the righting arm in waves which is determined for every time step using Grim's effective wave as modified by Söding (1987a). The underlying theoretical model (Cramer and Krüger (2001)) allows for very short simulation times and is basically able to predict the following mechanisms of large roll motions and capsizing very well (Clauss et al. (2005)):

- Resonance excitation
- Parametric excitation
- Loss of stability phenomena
- Combinations of the above

6.2 Method of validation

Validation denotes the process of testing the ability to accurately model a physical phenomenon (whereas verification refers to the process of testing the accuracy of numerical implementations of a mathematical model). Validation of numerical methods such as *rolls* by model tests commonly comprises the following approaches:

- Comparison of amplitudes and phases in regular waves
- Analysis of statistical results in irregular waves
- Investigation of basic ability to model the phenomenon qualitatively

A validation by direct comparison of time series is frequently used for regular waves but not for irregular waves as the exact correlation of time and position for wave excitation and ship motion is not available in standard test set-ups. Additionally, a direct comparison of measured and simulated time series is extremely complicated if all six degrees of freedom are considered: Small deviations in the ship reaction might add up over time. Thus, a small deviation in the surge motion changes the wave trains encountered in the movings reference frame of the vessel.

Based on deterministic wave sequences and and fully automated capsizing tests the wave elevation is known at all tank positions and instances – i. e. in the moving reference frame of the ship. Thus, it is possible to extent the validation to more details.

In the following section, numerical investigations are used to identify critical conditions with respect to resonance phenomena or pure loss of stability. Corresponding wave sequences are generated – in particular with respect to timing between waves and vessel – and realized in the model basin. It is shown that the numerical tool is able to model the basic mechanism of large roll motions (qualitative validation).

Secondly, the measured scenario is re-modelled in the numerical simulation to allow the direct – quantitative – comparison of model test and numerical motion simulation.

6.3 Realization of a numerically simulated scenario in the model basin

Possibly dangerous situations with regard to large roll motions are simulated in *rolls*. The investigated ship is the twin screw RO-RO design B (L_{pp} = 190.29 m, B = 26.50 m, T = 7.35 m) from chapter 5. The modelled test conditions correspond roughly to stability values around the current limits as given by IMO's Code on Intact Stability ($GM = 1.24$ m). Fig. 6.1 shows an example of the occurrence of parametric roll in a JONSWAP sea state with $T_P = 11.5$ s and $H_s = 10$ m. The sea state is represented by energy equivalent spectral components at the beginning of the simulation. The ship encounters the wave sequence from astern ($\mu = 5°$) at a speed of $v = 10$ kn. In the simulation, the ship capsizes in the simulated wave sequence.

The spectral wave data from *rolls* refer to the beginning of the simulation which is defined $x_0 = 0$ and $t_0 = 0$ both for head and following seas. At (t_0, x_0), ship speed and course take already the target values. The unidirectional wave sequence $\zeta(t, x_0)$ is represented by its Fourier coefficients A_j and the initial phase φ_{j0} at x_0:

$$\zeta(t, x_0) = \sum_{j=0}^{n/2} A_j \cos(\omega_j t + \varphi_{j0}). \tag{6.1}$$

During the simulation, linear wave theory serves as wave model which means that the amplitudes A_j remain constant at any position and instance and

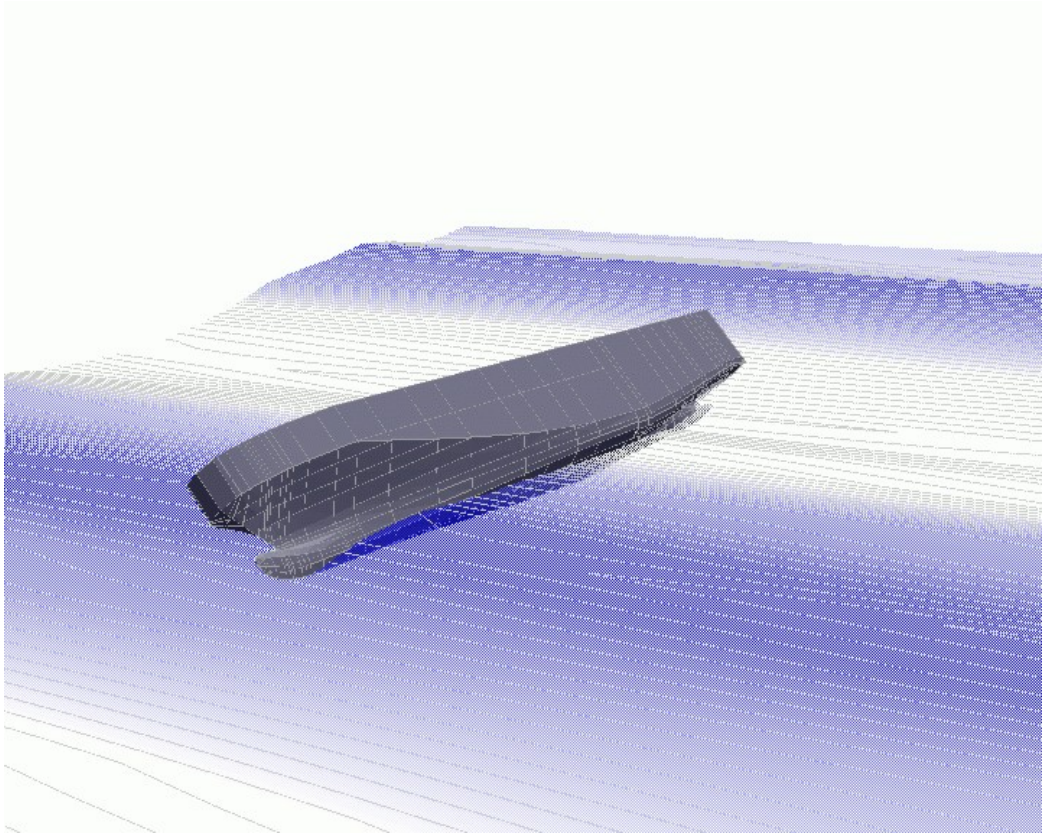

Figure 6.1: Simulated scenario of parametric roll of RO-RO ship B in a wave sequence of the JONSWAP sea state $T_P = 11.5$ s, $H_s = 10$ m.

the phase is adopted according to linear dispersion:

$$\zeta(t, x_0 + \triangle x) = \sum_{j=0}^{n/2} A_j \cos(\omega_j t + \varphi_{j0} - k_j \triangle x) \tag{6.2}$$

$$\omega_j^2 = k_j g \tanh(k_j d). \tag{6.3}$$

$\triangle x$ is calculated from the ship speed at the given position and the surge motion s_1 from the numerical simulation:

$$\triangle x(t) = \sum_{t=0}^{t_{end}} v(t)t + s_1(t). \tag{6.4}$$

The full scale wave train from the numerical simulation is given as target wave train for the model tests by inverse Fourier transform (Fig. 6.2, top)

and is transformed to model scale 1:34. The encounter time t_e is the time the wave train needs from the test beginning to arrive at the encounter position. The waves have to be generated as long as the ship sails through the towing tank, plus the time the waves need to the end position. The position x_e of encounter of ship and wave, which is equivalent to the simulation beginning, has to be defined.

For head seas at HSVA, the position is $x_{target} = x_e = 215$ m from the wave maker. At this position the ship model takes the desired calm water course and speed. This is the position where the wave train at the beginning of the simulation refers to.

In following seas, the ship either tends to sail out of the wave field or the waves may overtake the ship model — depending on group velocity of the waves and ship speed. Thus, it has to be ensured that at the beginning of the simulation "enough waves" are in the tank as the simulation starts with this condition as well. E. g. the target position is at $x_e = 67$ m, and here the target wave train appears after 100 s plus the time the wave needs to reach this position starting from the wave maker.

Now the *modified non-linear theory* is applied to obtain the wave train at the position of the wave maker. For the transformation zero values are added in order to deal exactly with the desired wave train – wrap-around resulting from the Fast Fourier Transform would give mistakes in the wave tank simulation. After this manipulation the wave train has to be transformed to the target position again to get the new encounter time t_e of ship and wave. This value is put into the master computer of the towing carriage to ensure that the model will arrive at x_e at instance t_e after the start of the test.

From the wave train at the position of the wave maker, the corresponding control signals (for upper and main flap of double flap wave maker at HSVA) are calculated (Fig. 6.2, bottom). Now the experiment is started, and the wave train is generated. The wave train needs time t_e to reach position x_e. The automated test procedure as explained in chapter 5 ensures that the model reaches this target position in time.

The wave train is verified by wave probe registrations during the test. In the example given in Fig. 6.3, the generated wave train is registered at a stationary wave probe close to the wave maker and transformed to $x = 125$ m (compare target wave train in Fig. 6.2).

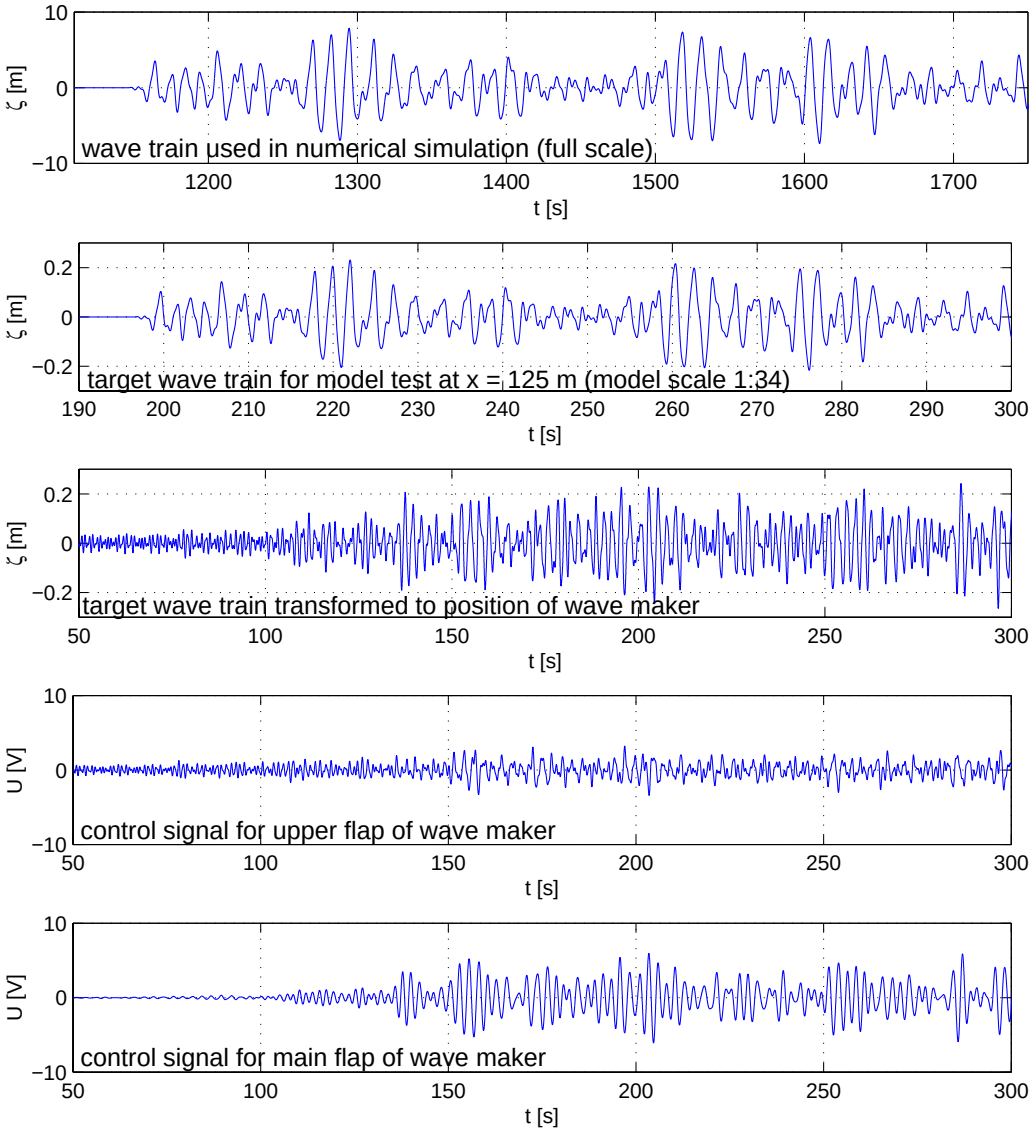

Figure 6.2: Experimental realization of dangerous wave sequences from numerical capsize simulations: Starting with the target wave train, the wave at the position of the wave maker is calculated using the *modified non-linear theory* to get the corresponding control signals.

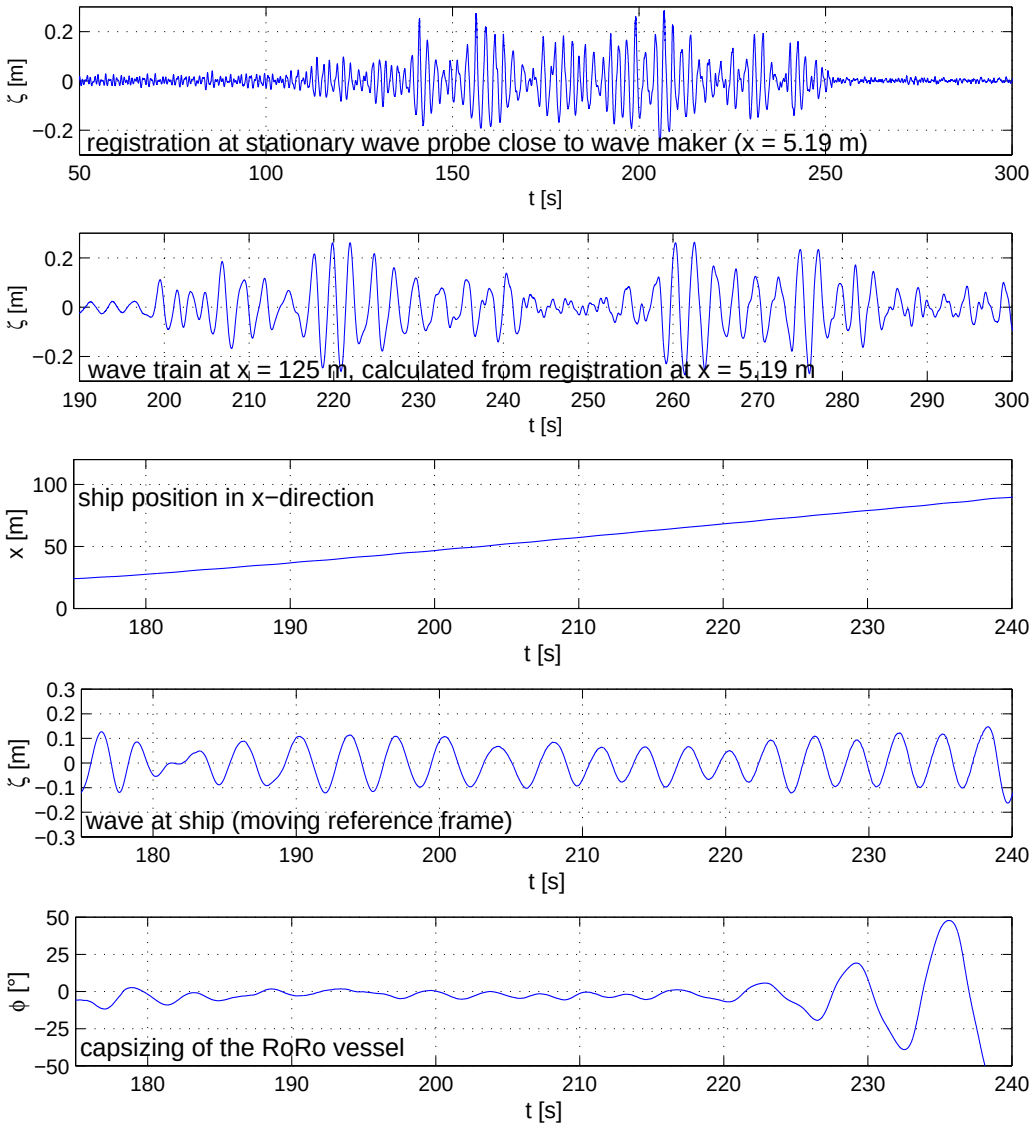

Figure 6.3: From registration at a stationary wave probe close to the wave maker the stationary wave train at $x = 125$ m is calculated by the *modified non-linear theory* (compare target wave in Fig. 6.2) and transformed into the moving reference frame of the ship model (scale 1:34). This allows for a direct relation to the roll motion of RO-RO vessel B which subsequently capsizes.

The motion simulation is carried out for the same load condition as in the model test, $GM = 1.24$ m. The ship position is measured during the test. Thus, the stationary wave registration can be transformed into the moving reference frame of the ship model to obtain the wave as experienced by the ship. The wave shows a rather regular pattern after 220 s which induces parametric excitation. The resultant (measured) roll motion can be directly related to this wave train (Fig. 6.3 bottom). The roll motion increases significantly and the ship capsizes.

Visual (qualitative) comparison of results from numerical simulation and model test proves that the numerical method models the underlying basic mechanism of parametric excitation and subsequent capsizing very well (Fig. 6.4). The fact, that the motions are simulated *before* the corresponding model test, enhances the credibility of the given qualitative validation scheme.

6.4 Re-simulation of model test scenario

The exact realization of the numerical simulation in the model test is not possible since the track of the ship model in the tank differs slightly from the simulated track due to disturbances or other small variations. A comparison of two capsizing test runs reveals that the beginning of encounter of wave and ship is reproducible which results in the same wave sequence at the test beginning (Fig. 6.5, top). The ship response is quite similar as reflected in the first part of the roll registration (bottom), whereas the mentioned variations lead to different encountered wave sequences, thus different instances of capsize. Therefore, the following procedure is applied to re-model the test conditions in a new numerical simulation run for direct comparison.

As a first step, the measured x-position of the ship model is modified with respect to starting position and instant. The first measuring point in the time series is defined as instant $t = 0$ and assigned to starting position $x = 0$ instead of the measured real starting position (Fig. 6.6):

$$x_{sim}(t_{sim}) := x_{meas}(t_{meas} - t_0) - x_{meas}(t_{meas} = 0). \tag{6.5}$$

Accordingly, the measured wave train at an undisturbed stationary position $x_{meas} = x_0$ is transformed to the starting position of the ship model and the time axis is shifted accordingly (Fig. 6.7). Now, the wave train is calculated

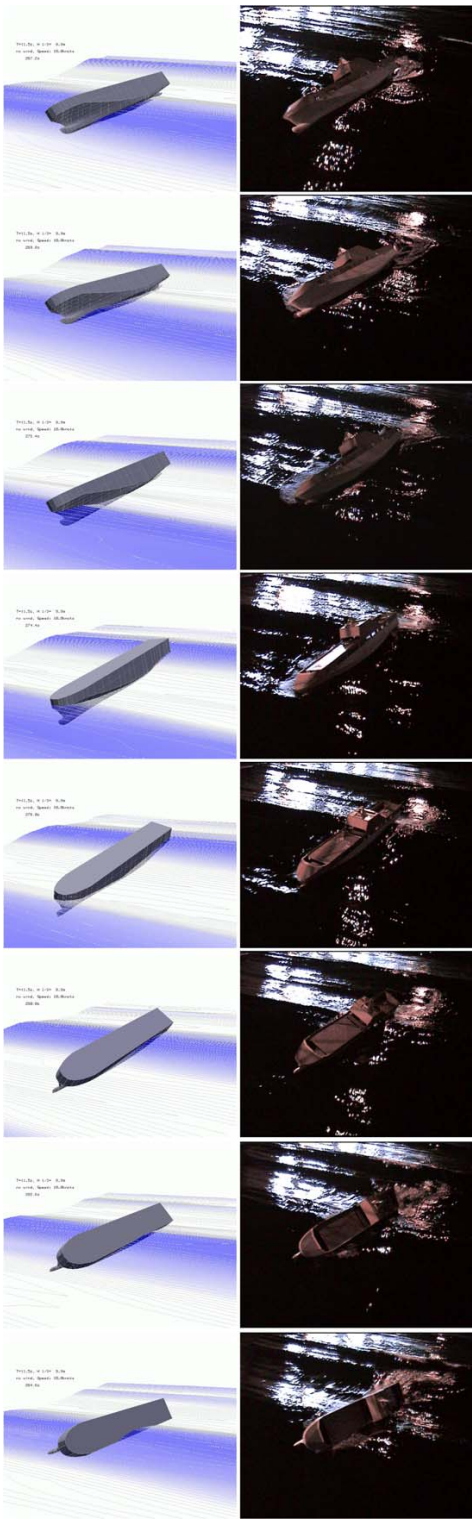

Figure 6.4: Qualitative comparison of numerical simulation and experimental realization of capsizing due to parametric excitation (compare Figs. 6.2 and 6.3).

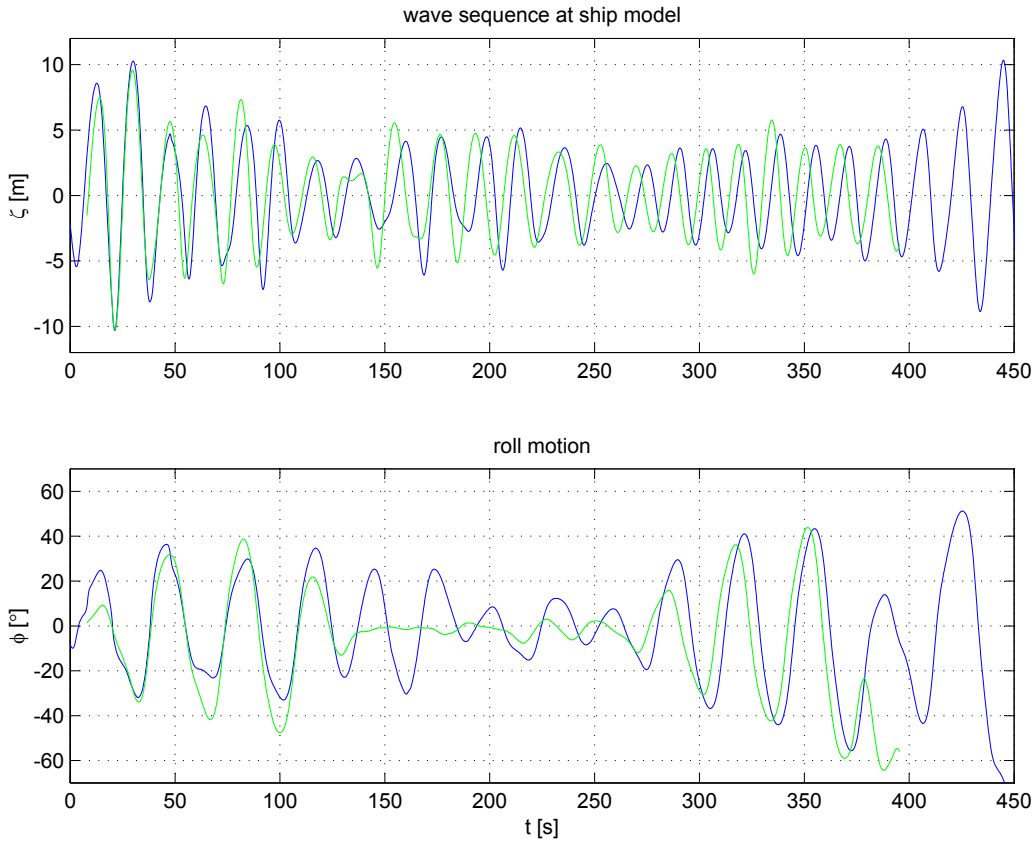

Figure 6.5: Comparison of two different capsizing test runs with reproducible conditions in the beginning of encounter of wave and ship: The wave sequences deviate more and more as the ship response, thus track, is slightly different: This leads to a different course of capsize.

at full scale and represented by 50-100 Fourier coefficients after adequate reduction of time data to reduce the simulation duration.

Based on the deterministic capsizing test procedure, the exact ship position is known at every time step of the model test and the wave train is calculated at the position of the ship. The chosen time window – the simulation duration – has to be a multiple of the longest occurring wave in the simulation, $T_{sim} = 2\pi/\omega_{min} \approx \sqrt{\lambda_{max}/1.56}$. Also the roll motion (and all other results) from the model tests have to be modified with respect to the time axis.

Now, the simulation can be run with the calculated wave spectrum and x data. The vessel is usually simulated in all six degrees of freedom. Even small disturbances lead to significant variations of x-position versus time which

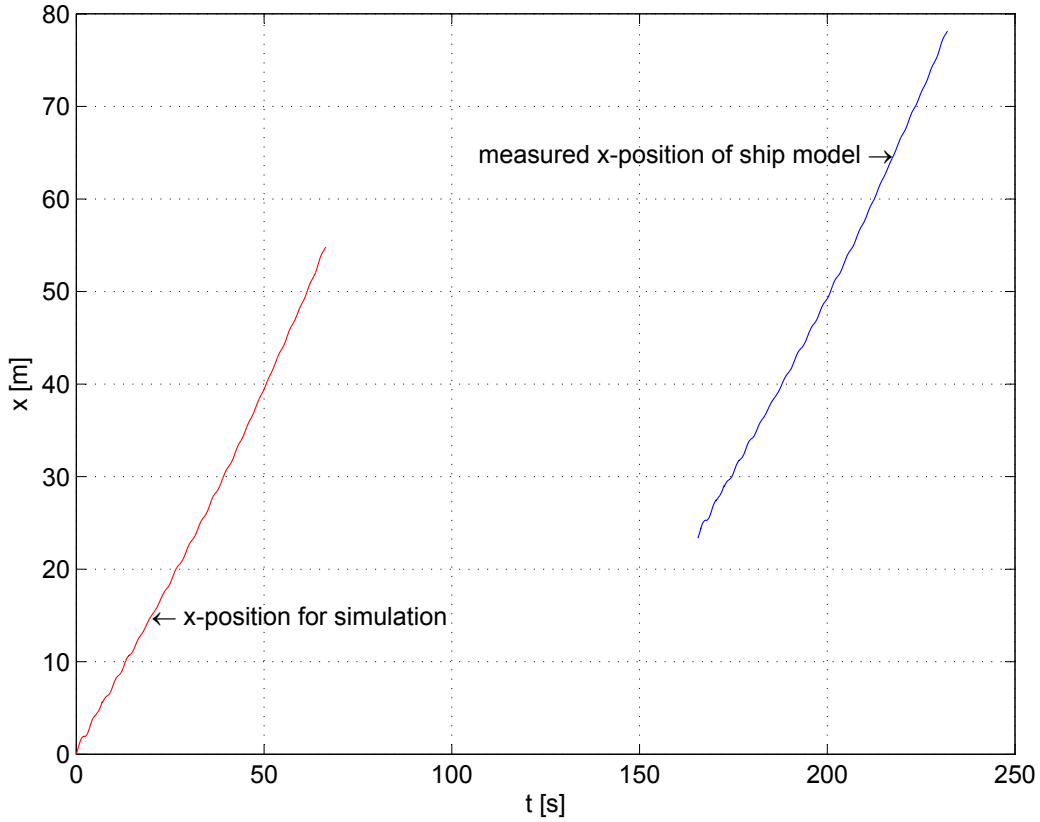

Figure 6.6: The measured track data (x-coordinate) of the ship model is referred to the starting position in the simulation.

changes the wave train encountered by the ship. Thus, the ship is guided with regard to the longitudinal position over time – exactly as measured in the experiment. Consequently, the wave train encountered in the simulation corresponds well with the wave train from the experiment.

6.5 Results of validation

The results for two different model test runs with slightly different starting conditions are given in Figs. 6.8 and 6.9. The measured stationary wave sequence from a JONSWAP sea state with $T_P = 11.5$ s and $H_s = 10$ m (model scale 1:34) is transformed to the moving reference frame of the ship sailing at average speed of 10.4 kn and target course of 3°. The course changes close to the wall (due to z-manoeuvre in the model tests) are neglected in

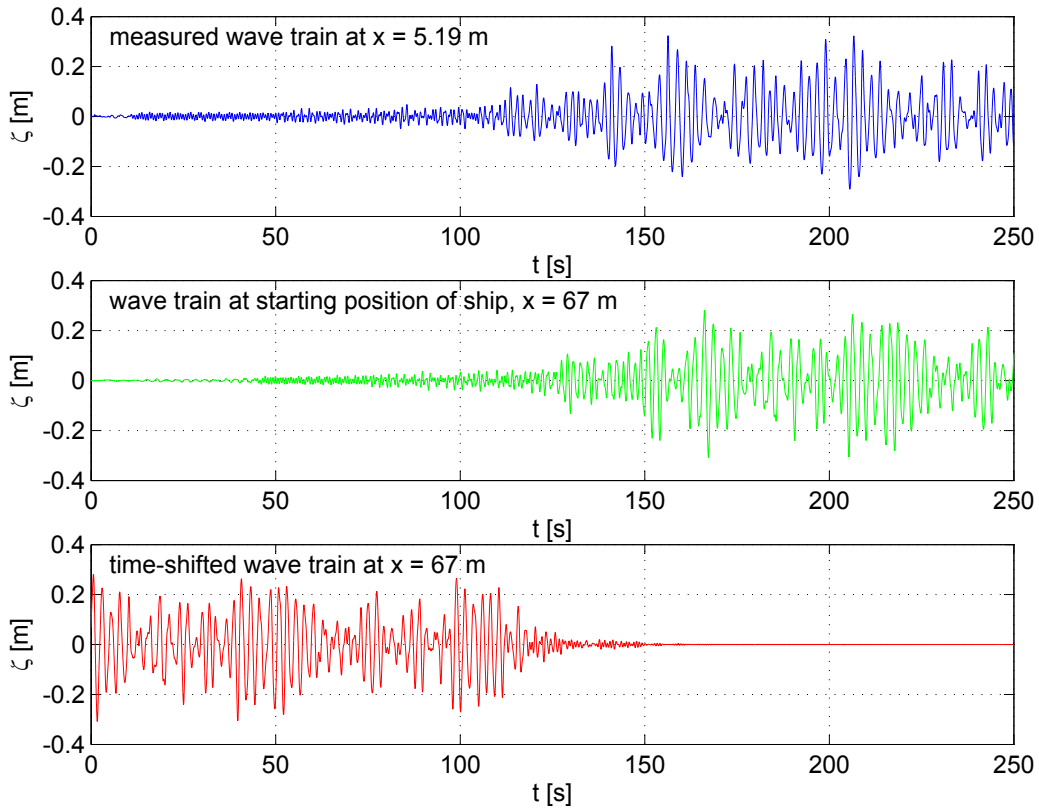

Figure 6.7: Transformation of wave train corresponding to modified ship track data: The blue graph – according to the track data of same colour in Fig. 6.6 – is registered and transformed to the starting position of the ship (green graph). After time shift, the wave train (red graph) corresponds to the modified red x-position of the ship (Fig. 6.6).

the simulation.

Fig. 6.8 shows the model test result for this wave sequence in comparison with results from two numerical simulations in the same wave train but with slightly different initial conditions. The two simulation runs look very similar – except for the actual capsize which occurs with a difference of one wave crest. Comparison with the model test results shows a good agreement in the first wave group. Further in time, the simulation seems to damp the roll motion too fast. A further investigation into the model test data shows, that the model performed a course change due to the z-manoeuvre at this time. This influences the development of the roll motion for quite some time, while the roll response in the wave group leading to the actual capsize shows a good

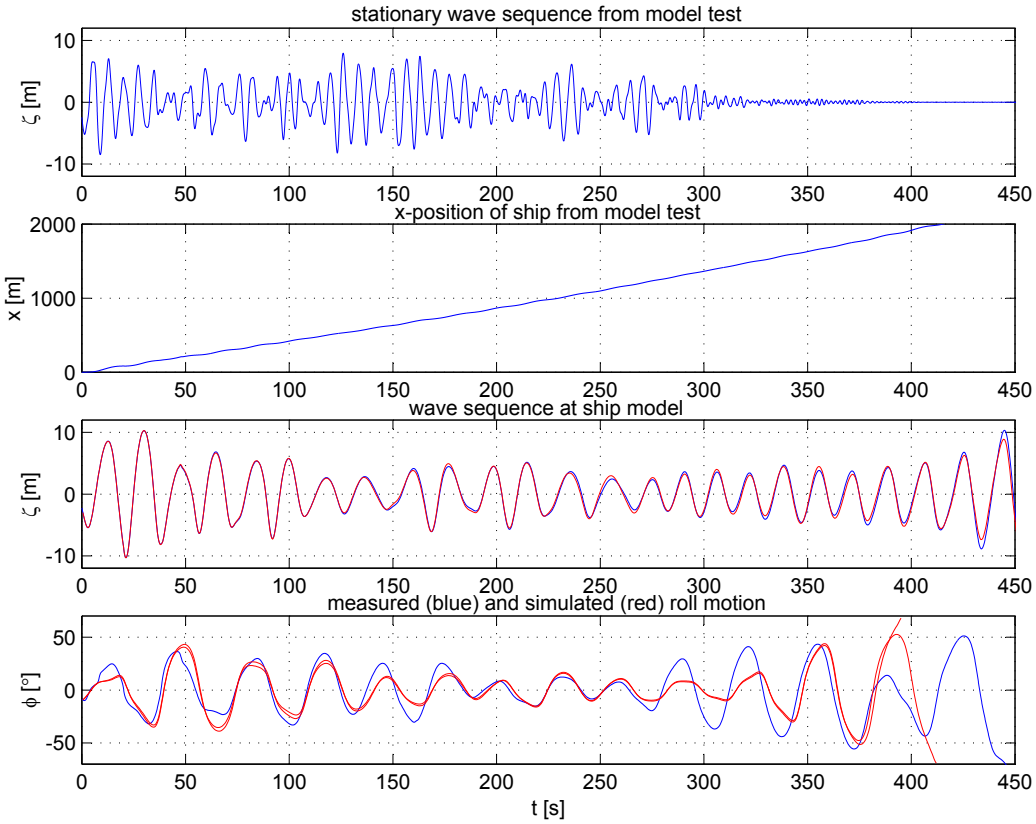

Figure 6.8: Comparison of time series from numerical simulations (red) and deterministic test results (blue) of capsizing due to parametric excitation ($T_P = 11.5$ s and $H_s = 10$ m).

agreement between model test and simulation again around 350 s. Following the next roll peak the tank model caught water on the upper deck which leads to a rather sudden roll damping until the water flooded out again. Water on deck is not included in the simulation. Nevertheless, the vessel is not safe in the model test either and capsizes shortly afterwards.

In Fig. 6.9 can be observed that the ship model encounters the wave sequence slightly differently compared to the previous test run. Again, the roll responses from model test and simulation agree well in the first wave group. After approximately 100 s, a course change is performed by the model. This leads to a rather sudden decrease of roll motion which is not observed in the numerical simulation as rudder forces are disregarded. Nevertheless, the roll response in the "fatal" wave group (300 s and later) corresponds well with

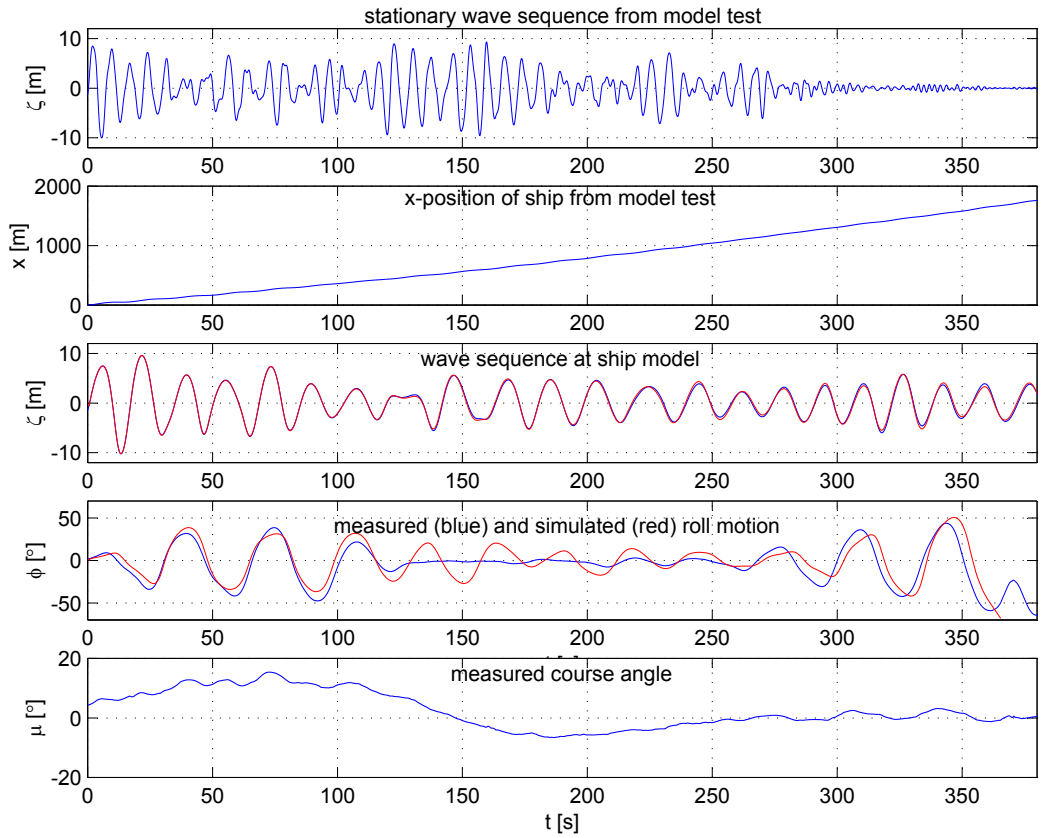

Figure 6.9: Comparison of time series from numerical simulation (red) and deterministic test results (blue) of capsizing due to parametric excitation ($T_P = 11.5$ s and $H_s = 10$ m).

the model test result.

A comparison of the two model test runs shows the reproducibility of the capsizing scenario applying deterministic wave sequences and the special model test technique (Fig. 6.5). The vessel encounters both wave groups under almost identical conditions and therefore rolls and capsizes accordingly. The comparison also documents the influence of course changes and of slight differences in the ship track on the roll motion in between the wave groups where the period of encounter does not match the ship's natural period of roll. In one case, the roll motion is enforced, in the other case damped. Nevertheless, the capsize in the second wave group is independent of this history.

Concluding, the roll responses (and the capsize) are reliably predicted by the

numerical simulation as long as resonance and stability loss effects dominate the roll motion while the effect of the course change as well as the water on deck leads to differences between model test results and numerical investigations. This is not surprising, as rudder forces and water on deck are not accounted for in the numerical simulation.

It can be summarized, that capsizes due to resonance and stability variations are reliably predicted, not only qualitatively but also quantitatively. When investigating intact safety, numerical tools need to be validated and the theoretical limits of the theory must be evaluated regarding their potential influence on quantitative results. Deterministic wave sequences and capsizing experiments provide a reliable means to investigate wave phenomena endangering ships and deliver a basis for detailed validation and improvement of numerical tools.

6.6 Safer ship design and operation

Ship design, ship approval and ship operation determine the safety of a vessel in rough sea conditions. Based on systematic experimental validation as explained above, numerical simulation of ship motions is a valuable tool for ship design evaluation. A sufficient number of simulations provides a data basis for polar plots to judge the ship's situation in a sea state - defined by significant wave height and characteristic period - with respect to load case, encounter angle and ship speed.

As an example, Fig. 6.10 shows polar plots for two different load cases illustrating at which course and speed the considered RO-RO ship is cruising safely (Clauss et al. (2003a)). The most critical regions of resonance motions as well as of parametric roll are identified. A change of trim by only 1 m to stern (see right hand side) reduces the capsizing risk considerably.

Furthermore, guidelines for ship operation can be based on polar plots. Experience from ship operation shows, that the safety of a vessel and its crew relies strongly on the ability of the crew to judge the vessel's performance and limits. Based on results from a numerical design evaluation carried out at Flensburg Shipyard a so-called "operational performance" booklet was developed to summarize the findings and communicate these to the ship crew. Fig. 6.11 shows an example extracted from such a manual (Cramer et al. (2004b)). In these polar plots the danger of occurrence of sliding of unlashed cars is presented for two different load cases and different significant wave lengths.

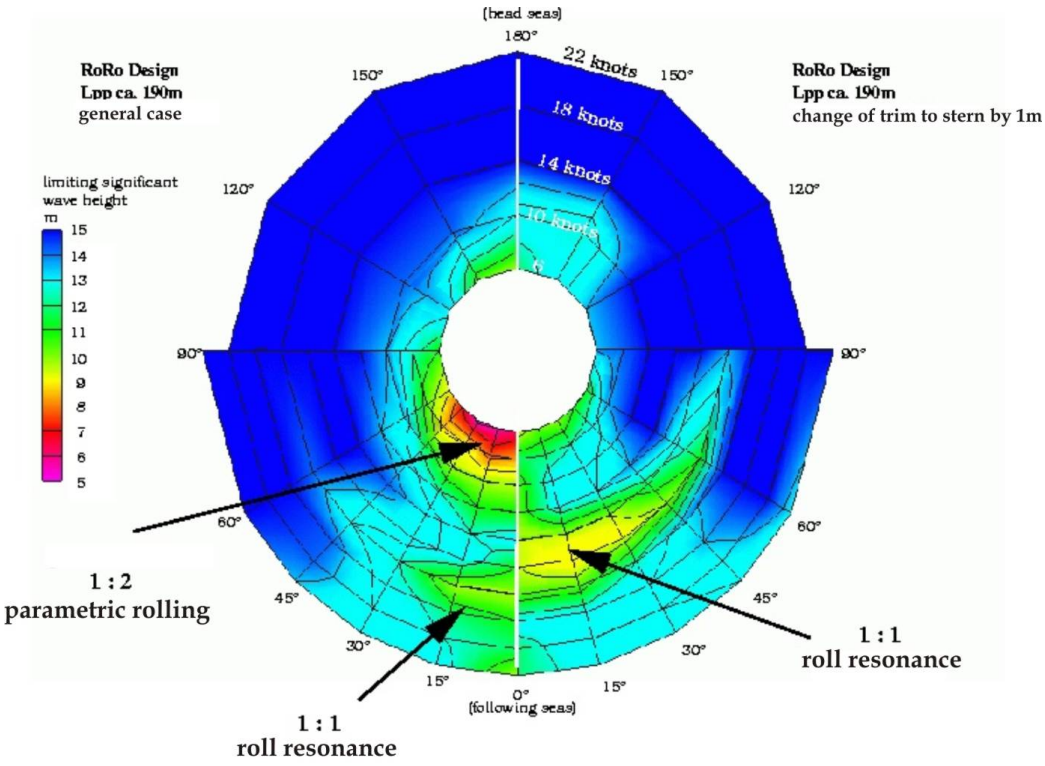

Figure 6.10: Polar plot with limiting wave heights for a RO-RO design – based on the numerical method *rolls* as validated by deterministic wave sequences and capsizing tests. The plot demonstrates how systematic variations in the numerical simulations can help building safer ships: Only a trim to 1 m astern reduces the capsizing risk significantly (right hand side).

One of the reasons of the booklet being inappropriate for real time decision support in dangerous situations is the difficulty to visually identify the basic characteristics of the seaway such as significant wave height and peak period from on board. Particularly, the peak period is the basic information needed to identify dangerous combinations of ship speed and encounter angle with respect to any roll resonance problems.

For determination of the seaway characteristics the sea-clutter data from a standard X-band marine radar can be used. E. g. the Wave Monitoring System WAMOS II was developed to calculate the directional wave spectrum and the related sea state parameters in real time from radar images. Also single wave detection is possible. This system can also be used as a basis for the development of decision support systems. Fig. 6.12 shows a sea surface elevation map corresponding to such a radar image (Cramer et al. (2004b)).

Concluding, deterministic wave sequences serve as a reliable tool to investigate dangerous seakeeping scenarios and to validate numerical simulations related to ship safety by direct comparison of time series. By the consequent application of validated simulation tools, the seakeeping performance of ship designs can be improved significantly and also reliable assistance for ship operation can be handed over to the crew. Within the time frame of several years, it might be also possible to increase the acceptance of numerical assessment of ship safety by authorities if the tools are validated by new sophisticated approaches as the given one. Thus, regulations with regard to a reasonable application of numerical motion simulations could be introduced. A first attempt towards this is documented by Germany (2004) where computer controlled capsizing tests for the validation of numerical motion simulations are proposed to the IMO. Another interesting question is, if the validation examples given above could also be applied to full scale cases where ships are equipped with motion registration systems and a wave monitoring tool in order to ensure that the mechanisms revealed by experimental and numerical model tests are also confirmed by full scale data.

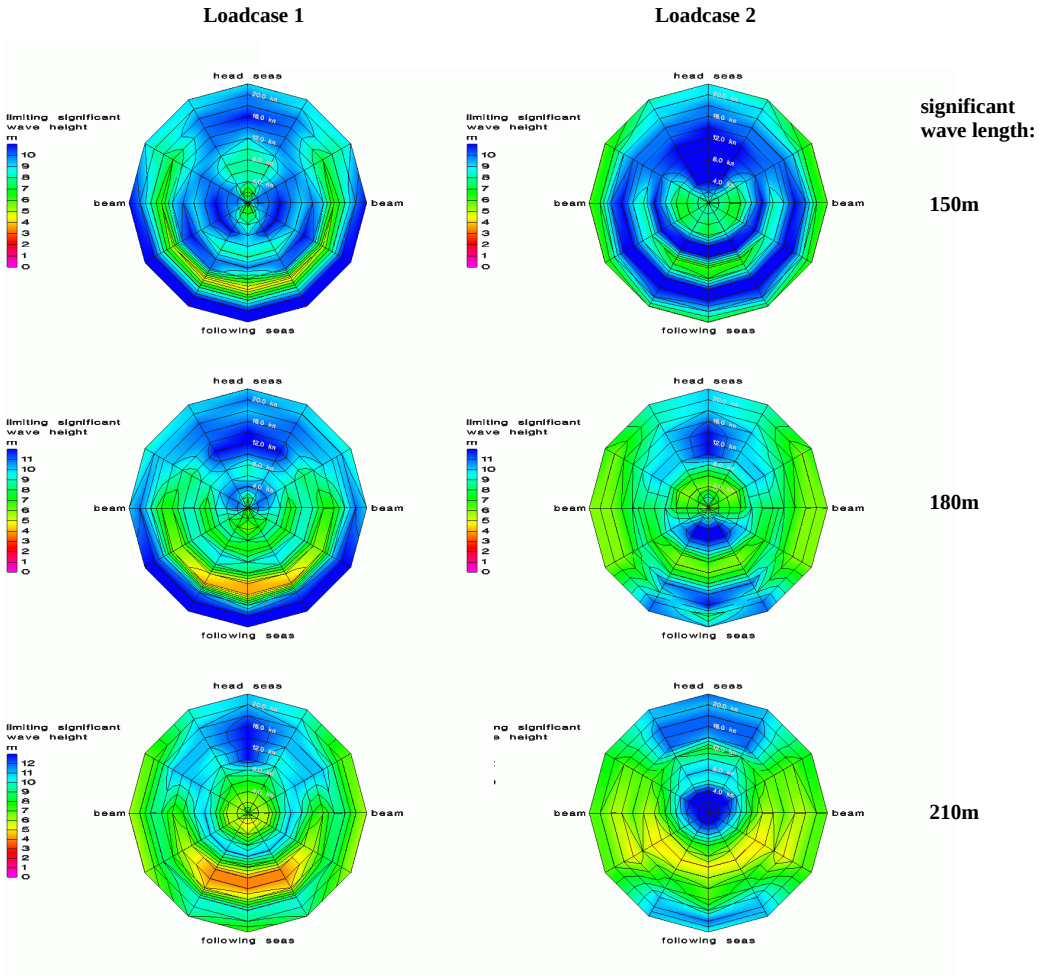

Figure 6.11: Polar plots illustrating the danger of sliding of unlashed cars for two different load cases in different significant wave lengths.

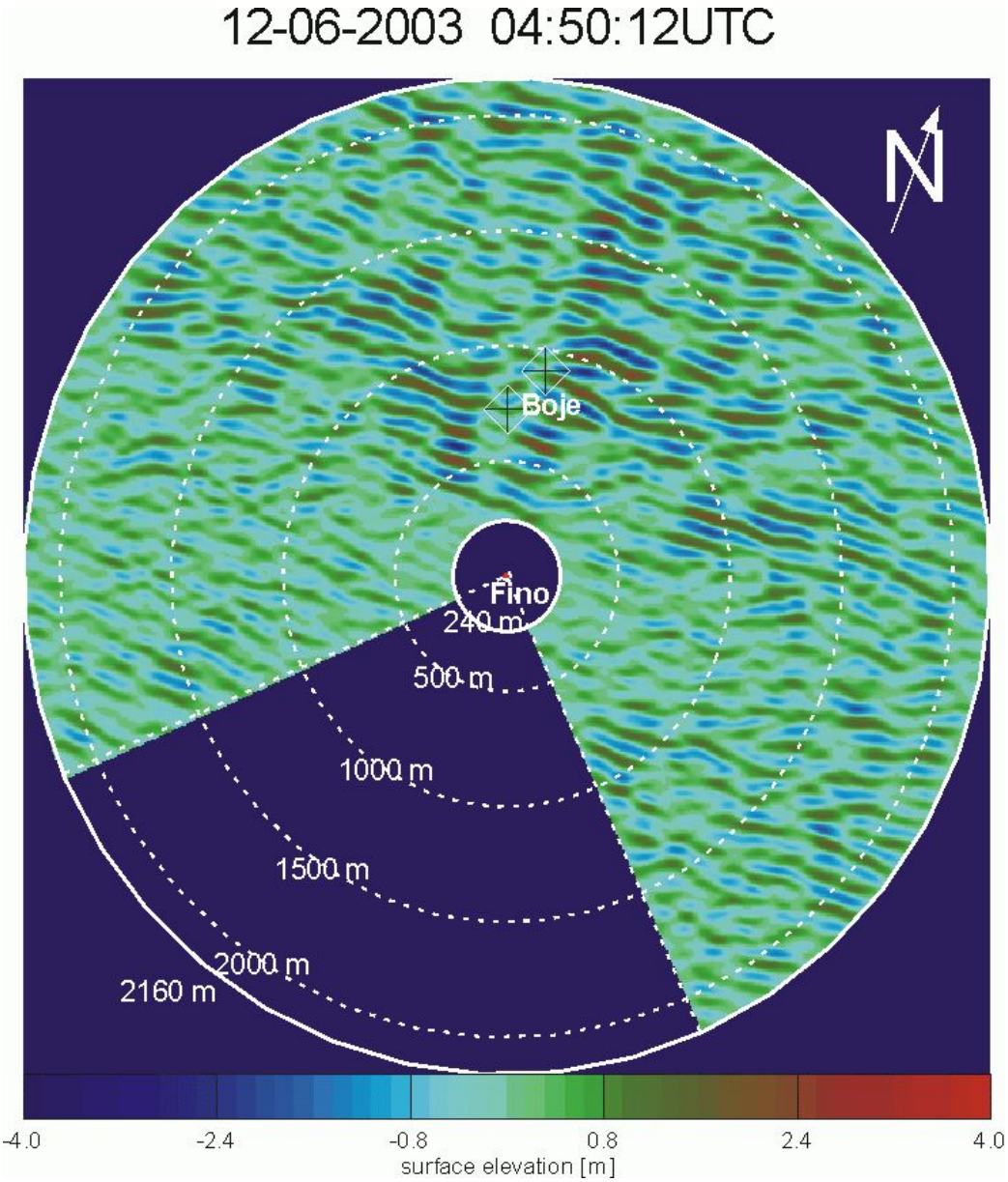

Figure 6.12: Sea surface elevation map corresponding to a radar image from WaMoS II, registered on December 6, 2003, 4:50 UTC, at the FINO platform in the North Sea. The scale indicates the surface elevation. This sea surface elevation map evaluated by the WaMoS II system gives statistical parameters of the sea state the ship sails in and also allows for single wave detection (Cramer et al. (2004b)).

Chapter 7

Conclusions and Perspectives

In this work, a *modified non-linear theory* for modelling wave propagation is presented. The hybrid model combines linear wave theory with Stokes Third Order wave theory to consider non-linear wave characteristics such as an increase of wave celerity and crest-trough asymmetry with wave steepness. The new approach is fast and precise and applicable in day-to-day use for experimental investigations. The method can be adapted easily for new requirements as the implementation of different wave theories as well as empirical terms is possible.

Compared to numerical wave tanks the method is capable of upstream transformation of wave trains and is therefore ideally suited for generating wave board control signals. The potential of the reproducible procedure is demonstrated by generating different kinds of tailored deterministic wave sequences both at Technical University Berlin and Hamburg Ship Model Basin. The following wave sequences are generated in the model basin and applied to the investigation of non-linear wave-structure interaction:

- Transient wave packets
- Sea states with deterministically embedded steep wave sequences
- Regular waves with a superimposed *Three Sisters* wave
- Observed wave records (*New Year Wave*)

For investigating a specific structure at a certain tank position, wave trains are designed individually, e. g. dedicated regular waves can precede an extremely high wave or wave group. By stretching or compressing the wave

sequence the associated period and slope can be tuned accordingly. Also phase relations between the existing wave and the resulting structure motions can be selected and varied deterministically. Any test can be repeated identically if a specific effect is analyzed. Observed wave registrations, like the extremely high and steep *New Year Wave* sequence can be generated in a wave tank at a selected model scale. Thus, the character and genesis of extreme events are analyzed in space and time. Also, the seakeeping behaviour of any structure can be evaluated in such extreme environments to learn how dangerous a selected wave event might be in terms of the investigated structure.

Deterministic wave sequences are applied to model tests for investigating the wave-ship interaction at extreme sea conditions. Even complicated interactions of wave group and structure are easy to analyze: The transformation to arbitrary - stationary or moving - positions or models allows a precise relation of cause and effect. With this technique wave scenarios can be analyzed from the point of view of a sailing ship. As an exact and reproducible encounter of ship and wave in the model basin is realized, mechanisms of large rolling and capsizing can be examined deterministically. Both extreme and resonance phenomena possibly leading to ship accidents are investigated:

- Parametric roll
- Loss of stability at the wave crest
- Impact excitation in combination with the above

Based on these developments methodologies for the quantitative assessment of capsizing risk are validated which then provide a basis for the improvement of current intact stability criteria. In conclusion, ships are designed with improved seakeeping characteristics and an increased safety with respect to the danger of extreme roll angles and capsizing.

In addition, applications of the presented non-linear wave calculation procedure are addressed, such as the validation of different numerical wave tanks and the experimental investigation of seakeeping characteristics of offshore structures. Recapitulating, the *modified non-linear theory* is a powerful tool to face the complex tasks related to the experimental investigation of extreme structure behaviour such as large rolling, capsizing, and rogue wave impacts.

Further developments of the technique with deterministic wave sequences might focus on the investigation of complex wave-wave interactions. Analytical or empirical terms from other wave theories could be implemented to allow a more general application of the *modified non-linear theory*.

The non-linear wave transformation techniques may be applied to full scale investigations where the measured motions of a RO-RO vessel are related to wave registrations from ship radar and compared to model test results as well as numerical simulations. For the tracking of single wave trains in radar images the knowledge of non-linear wave propagation is indispensable. Also for the validation of simulations of seakeeping loads, the described methods are applicable.

Future applications comprise a detailed validation of numerical motion simulation tools by the demonstrated procedure with deterministic wave sequences which is able to provide time series from model tests for the numerical simulation and vice versa. Developments might focus on a more reliable and consequent use of numerical safety assessment which requires precise methods for experimental investigations. Results from such investigations might result in onboard decision support systems as well as improved safety criteria as released by the IMO.

Focusing on seakeeping safety is justified by a rough ocean environment – whilst rogue waves are not frequent they are by no means rare, and ships should be prepared to survive the worst weather extremes.

Nomenclature

A	[m^2]	surface
A	[ms]	Fourier spectrum of wave elevation
B	[-]	spectral parameter
B	[m]	breadth of ship
C_0	[-]	Biésel transfer function
C_B	[-]	block coefficient, $C_B = \forall/(L_{pp}BT)$
C_{ij}	[-]	non-linear phase as function of time step i and frequency step j
F	[(ms,ms)]	Fourier transform
$\hat{F}$	[(ms,ms)]	Fourier transform
$F_{1,2,3}$	[-]	coefficients in Stokes Third Order particle displacements
GM	[m]	metacentric height
H	[m]	wave height
H_{hydrl}	$[\frac{V}{\circ}]$	hydraulic-electrical transfer function
H_{max}	[m]	maximum wave height
H_s	[m]	significant wave height
I	[m]	wave information
L	[m]	wave length
L'	[m]	wave length
L_0	[m]	wave length in deep water according to Airy theory
L_{pp}	[m]	length of ship between perpendiculars
N	[-]	number of multiplications in computational calculations
S	[m]	free surface
S	[m^2s]	energy density spectrum
T	[m]	draught
T	[s]	wave period
$T(t)$	[m/s]	function describing wave board oscillation

T_0	[s]	mean zero-upcrossing period
T_e	[s]	period of encounter
T_{meas}	[s]	measured time interval
T_r	[s]	time of signal fade-in and fade-out
T_{sim}	[s]	simulation interval
T_P	[s]	peak period
T_R	[s]	period of roll resonance
U	[V]	voltage signal
U_R	[-]	Ursell parameter, $U_R = \frac{HL^2}{d^3} = \frac{8\pi^2\zeta_a}{k^2d^3}$
V	[m^3]	volume of fluid
a	[m]	wave amplitude, representative amplitude of wave group, wave envelope
$\bar{a}$	[m]	wave board stroke
b	[m]	elevation of hinge of wave maker above bottom
c	[m/s]	wave celerity (phase velocity)
c_0	[m/s]	wave celerity (phase velocity) in deep water
c_I	[m/s]	wave celerity
c_{add}	[m/s]	additional wave celerity
c_{gr}	[m/s]	wave group velocity
c_{ij}	[m/s]	non-linear wave celerity as function of time step i and frequency step j, $c_{ij} = \frac{\omega_j}{k_{ij}}$
c_{lin}	[m/s]	wave celerity (linear wave theory)
d	[m]	water depth
f_r	[-]	windowing function
g	[m/s^2]	acceleration due to gravity, $g = 9.81\ \frac{m}{s^2}$
$h(z)$	[-]	function describing type of wave maker
i	[-]	(time) index
j	[-]	(frequency) index
k	[1/m]	wave number, $k = \frac{2\pi}{L}$
k_0	[1/m]	wave number in deep water, $k = \frac{2\pi}{L_0}$, real solution of dispersion relation
k_{ij}	[1/m]	non-linear wave number as function of time step i and frequency step j
k_s	[1/m]	representative wave number of wave group, $k_s = \frac{(\omega_{beg}+\omega_{end})^2}{4g}$
l	[-]	(space) index
l	[m]	parameter to distinguish between flap and piston type wave maker
m	[-]	index
m	[kg]	mass

n	[-]	(maximum) index
$\vec{n}$	[-]	unit normal vector
p	[Pa]	pressure
p_0	[Pa]	constant or atmospheric pressure
p_{dyn}	[Pa]	dynamic pressure
s_1	[m]	surge
t	[s]	time
$\triangle t$	[s]	time step
t_0	[s]	particular instance
t_e	[s]	instance of encounter of wave and ship
t_{end}	[s]	instance of end of simulation
t_{meas}	[s]	time coordinate in registration
t_{shift}	[s]	time shift
t_{sim}	[s]	time coordinate in simulation
u	[m/s]	horizontal (particle) velocity, current
$\dot{u}$	[m/s^2]	horizontal particle acceleration
v	[m/s], [kn]	velocity of ship
$\vec{v}$	[(m/s, m/s)^T]	vector of fluid velocity, $\vec{v} = (u, w)^T$
v_M	[m/s]	velocity of ship model or wave probe
v_{rel}	[m/s]	relative speed
w	[m/s]	vertical (particle) velocity
$\dot{w}$	[m/s^2]	vertical particle acceleration
x	[m]	horizontal space coordinate
x'	[m]	horizontal position of water particle in its mean position
$\triangle x$	[m]	horizontal distance, spatial step
$(\triangle x)_l$	[m]	non-equidistant spatial steps
x_0	[m]	horizontal (initial) position, ship coordinate
x_c	[m]	concentration point, position of maximum wave elevation
x_e	[m]	position of encounter of wave and ship
x_{meas}	[m]	measured horizontal ship position
x_{sim}	[m]	simulated horizontal ship position
x_{target}	[m]	target position of deterministic wave sequence
y	[m]	space coordinate
y_0	[m]	ship coordinate
z	[m]	vertical space coordinate, heave motion
z_0	[m]	ship coordinate
$\Lambda_{1,2}$	[-]	function defining Biésel transfer function
Φ	[m/s^2]	velocity potential
Φ_I	[m/s^2]	initial velocity potential

Ω	$[(\mathrm{m},\mathrm{m})^T]$	fluid domain
α	[-]	spectral parameter
α	[°]	flap angle of wave maker
α_{mf}	[°]	angle of main flap of double flap wave maker
α_{mf+uf}	[°]	angle of total flap length of double flap wave maker
α_{uf}	[°]	angle of upper flap of double flap wave maker
γ	[-]	peak enhancement factor
δ	[°]	rudder angle
ε	[-]	wave steepness, $\varepsilon = \zeta_a k$
ζ	[m]	free surface (or wave) elevation
ζ_0	[m]	wave information or initial wave train
ζ_H	[m]	Hilbert transformed linear wave elevation
ζ_I	[m]	initial wave elevation
ζ_a	[m]	wave amplitude
ζ_c	[m]	wave crest elevation
ζ_k	[m]	Creamer transform
ζ_l	[m]	instantaneous wave elevation at x_l
ζ_{max}	[m]	maximum wave elevation
ζ_{tr}	[m]	wave trough elevation
η	[m]	vertical displacement of water particle
θ	[-]	phase function $\theta = kx - \omega t$
θ'	[-]	phase function $\theta' = kx' - \omega t$
ϑ	[°]	pitch motion
λ	[m]	wave length
λ	[-]	scale
λ_0	[m]	particular wave length
λ_{max}	[m]	maximum wave length
μ	[°]	course angle where $\mu = 0$ means sea from astern
ξ	[m]	horizontal displacement of water particle
ρ	$[\mathrm{kg/m^3}]$	mass density
σ	[-]	spectral parameter
τ	[-]	splitting function of double flap wave maker
ϕ	$[\mathrm{m/s^2}]$	velocity potential
ϕ	[°]	rolling angle
φ	[-]	phase angle
φ	[°]	rolling angle
φ_0	[-]	initial phase spectrum
ω	[1/s]	circular wave frequency, $\omega = \frac{2\pi}{T}$
$\triangle\omega$	[1/s]	wave frequency step
ω_P	[1/s]	peak frequency

ω_R	[1/s]	frequency of roll resonance
ω_{beg}	[1/s]	lowest frequency of frequency band
ω_e	[1/s]	frequency of encounter
ω_{end}	[1/s]	highest frequency of frequency band
ω_{min}	[1/s]	minimum frequency
$\forall$	[m^3]	displacement

Bibliography

J. A. Battjes, T. J. Zitman, and L. H. Holthuijsen. A Renanalysis of the Spectra Observed in JONSWAP. *Journal of Physical Oceanography*, 17: 1288–1295, 1987.

T. B. Benjamin and J. E. Feir. The disintegration of wave trains on deep water. *Journal of Fluid Mechanics*, 27(3):417–430, 1967.

D. J. Benney. Non-linear gravity wave interactions. *Journal of Fluid Mechanics*, 14:577–584, 1962.

F. Biésel and F. Suquet. Les apparails générateurs de houle en laboratoire. *La Houille Blanche*, (2):147–165, 1951.

P. Blume and H. G. Hattendorff. Ergebnisse von systematischen Modellversuchen zur Kentersicherheit. *Jahrbuch der Schiffbautechnischen Gesellschaft*, pages 219–243, 1984.

F. Bonnefoy. Using a Nonlinear Spectral Model for Preparing Three-Dimensional Directional Wave Experiments. In *OMAE 2004 - 23rd International Conference on Offshore Mechanics and Arctic Engineering*, Vancouver, Canada, 2004.

B. Buchner. *Green Water on Ship-type Offshore Structures*. PhD thesis, Technische Universiteit Delft (ISBN: 90-4646-883-X), 2002.

B. Buchner and A. Voogts. Wave impacts due to steep fronted waves. In *Rogue Waves 2004*, Brest, France, 2004.

S. K. Chakrabarti and A. R. Libby. Further verification of Gaussian wave packets. *Applied Ocean Research*, 10(2), 1988.

J. R. Chaplin. On Frequency-Focusing Unidirectional Waves. *International Journal of Offshore and Polar Engineering*, 6(2):131–137, 1996.

D. Clamond and J. Grue. On an Efficient Numerical Model for Freak Wave Simulations. In *ISOPE 2001 - 11th International Offshore and Polar Engineering Conference*, Stavanger, Norway, 2001. ISBN 1-880653-54-0.

G. F. Clauss and J. Bergmann. Gaussian wave packets — a new approach to seakeeping tests of ocean structures. *Applied Ocean Research*, 8(4), 1986.

G. F. Clauss, L. Birk, and W. L. Kühnlein. Design by numerical optimization and innovative model testing. In *International Conference in Ocean Engineering (ICOE '96)*, pages 643–652, Madras, India, 1996.

G. F. Clauss, J. Hennig, H. Cramer, and K.-E. Brink. Validation of Numerical Motion Simulations by Direct Comparison with Time Series from Ship Model Tests in Deterministic Wave Sequences. In *OMAE 2005 - 24th International Conference on Offshore Mechanics and Arctic Engineering*, Halkidiki, Greece, 2005. OMAE2005-67123.

G. F. Clauss, J. Hennig, H. Cramer, and S. Krüger. Development of Safer Ships by Deterministic Analysis of Extreme Roll Motions in Harsh Seas. In *OMAE 2003 - 22nd International Conference on Offshore Mechanics and Arctic Engineering*, Cancun, Mexico, 2003a. OMAE2003-317174.

G. F. Clauss, J. Hennig, and C. E. Schmittner. Modelling Extreme Wave Sequences for the Hydrodynamic Analysis of Ships and Offshore Structures. In *PRADS 2004 - 9th International Symposium on Practical Design of Ships and Other Floating Structures*, Lübeck-Travemünde, Germany, 2004a.

G. F. Clauss, J. Hennig, C. E. Schmittner, and W. L. Kühnlein. Non-linear Calculation of Tailored Wave Trains for the Experimental Investigation of Extreme Structure Behaviour. In *OMAE 2004 - 23rd International Conference on Offshore Mechanics and Arctic Engineering*, Vancouver, Canada, 2004b. OMAE2004-51195.

G. F. Clauss and W. L. Kühnlein. Transient wave packets – an efficient technique for seakeeping tests of self-propelled models in oblique waves. In *3rd International Conference on Fast Sea Transportation*, pages 1193–1204, Vol. 2, Lübeck-Travemünde, Germany, 1995.

G. F. Clauss and W. L. Kühnlein. A new tool for seakeeping tests – nonlinear transient wave packets. In *Proceedings of the 8^{th} Int. Conference on the Behaviour of Offshore Structures (BOSS)*, pages 269–285, Delft, The Netherlands, 1997a.

G. F. Clauss and W. L. Kühnlein. Simulation of design storm wave conditions with tailored wave groups. In *Proceedings of the 7th International Offshore and Polar Engineering Conference (ISOPE)*, pages 228–237, Honolulu, Hawaii, USA, 1997b.

G. F. Clauss, E. Lehmann, and C. Östergaard. *Meerestechnische Konstruktionen*. ISBN 3-540-18964-5. Springer Verlag, Berlin, 1988.

G. F. Clauss, E. Lehmann, and C. Östergaard. *Offshore Structures*, volume 1: Conceptual Design and Hydrodynamics. Springer Verlag London, 1992.

G. F. Clauss and T. Riekert. Stochastische Analyse meerestechnischer Konstruktionen. Skript zur Vorlesung am Institut für Schiffs- und Meerestechnik, TU Berlin, 1996.

G. F. Clauss, C. E. Schmittner, and J. Hennig. Simulation of Rogue Waves and their Impact on Marine Structures. In *MAXWAVE Final Meeting, 8-10, October*, Geneva, Switzerland, 2003b.

G. F. Clauss, C. E. Schmittner, J. Hennig, C. Guedes Soares, N. Fonseca, and R. Pascoal. Bending Moments of an FPSO in Rogue Waves. In *OMAE 2004 - 23rd International Conference on Offshore Mechanics and Arctic Engineering*, Vancouver, Canada, 2004c. OMAE2004-51504.

G. F. Clauss, C. E. Schmittner, and K. Stutz. Freak Wave Impact on Semisubmersibles - Time-domain Analysis of Motions and Forces. In *ISOPE 2003 - 13th International Offshore and Polar Engineering Conference*, Honolulu, USA, 2003c. ISOPE 2003-JSC-371.

G. F. Clauss and U. Steinhagen. Numerical simulation of nonlinear transient waves and its validation by laboratory data. In *Proceedings of 9th International Offshore and Polar Engineering Conference (ISOPE)*, volume III, pages 368–375, Brest, France, 1999.

G. F. Clauss and U. Steinhagen. Optimization of transient design waves in random sea. In *Proceedings of 10th International Offshore and Polar Engineering Conference (ISOPE)*, volume III, pages 229–236, Seattle, USA, 2000.

H. Cramer and S. Krüger. Numerical Capsizing Simulations and Consequences for Ship Design. In *STG Summermeeting*, Gdansk, Poland, 2001.

H. Cramer, S. Krüger, and C. Mains. Assessment of Intact Stability – Revision and Development of Stability Standards, Criteria and Approaches. In

7th International Workshop on Stability and Operational Safety of Ships, Shanghai, China, 2004a.

H. Cramer, K. Reichert, K. Hessner, J. Hennig, and G. F. Clauss. Seakeeping Simulations and Seaway Models and Parameters Supporting Ship Design and Operation. In *PRADS 2004 - 9th International Symposium on Practical Design of Ships and Other Floating Structures*, Lübeck-Travemünde, Germany, 2004b.

H. Cramer and J. Tellkamp. Towards safety as a performance criteria in ship design. In *RINA International Conference on Passenger Ship Safety*, London, UK, 2003.

G. D. Crapper. *Introduction to Water Waves*. Ellis Horwood Limited, 1984.

D. B. Creamer, F. Henyey, R. Schult, and J. Wright. Improved linear representation of ocean surface waves. *J. Fluid Mech.*, 205:135–161, 1989.

M. C. Davis and E. E. Zarnick. Testing ship models in transient waves. In *5th Symposium on Naval Hydrodynamics*, 1964.

J. O. de Kat and J. R. Paulling. Prediction of Extreme Motions and Capsizing of Ships and Offshore Marine Vehicles. In *OMAE 2001 - 20th Conference on Offshore Mechanics and Arctic Engineering*, Rio de Janeiro, 2001.

R. G. Dean. Evaluation and development of water wave theories for engineering application. Special Report 1, Coastal Engineering Research Center, 1974.

D. Faulkner. Rogue Waves – Defining their Characteristics for Marine Design. In *Rogue Waves 2000*, Brest, France, 2000.

D. Faulkner. Freak waves. *Navigation News*, pages 7–10, 2003.

D. Faulkner and W. H. Buckley. Critical survival conditions for ship design. In *RINA International Conference*, pages 1–41, Glasgow, Scotland, 1997.

F. Fontaine. On the Evolution of High Energy Wind Induced Ocean Waves. In *OMAE 2001 - 20th International Conference on Offshore Mechanics and Arctic Engineering*, Rio de Janeiro, Brazil, 2001. OMAE2001/S&R-2172.

G. Z. Forristal. Nonlinear Wave Calculations for Engineering Applications. In *OMAE 2001 - 20th International Conference on Offshore Mechanics and Arctic Engineering*, Rio de Janeiro, Brazil, 2001. OMAE2001/S& R-2107.

W. N. France, M. Levadou, T. W. Treakle, J. R. Paulling, K. Michel, and C. Moore. An Investigation of Head-Sea Parametric Rolling and its Influence on Container Lashing Systems. In *SNAME Annual Meeting*, 2001.

Germany. REVIEW OF THE INTACT STABILITY CODE – Safety against capsizing in heavy seas. IMO, 2004.

F. J. Gerstner. Theorie der Wellen. In *Abhandlung der Königlichen Böhmischen Gesellschaft der Wissenschaften*, 1802.

R. Grevemeyer, R. Herber, and H. H. Essen. Microseismological evidence for a changing wave climate in the northeast Atlantic ocean. *Nature*, pages 349–352, 2000.

J. Grue. On four highly nonlinear phenomena in wave theory and marine hydrodynamics. *Applied Ocean Research*, 24:261–274, 2002.

C. Guedes Soares, Z. Cherneva, and E. M. Antão. Characteristics of Abnormal Waves in North Sea Storm Sea States. *Applied Ocean Research*, 2004a.

C. Guedes Soares, N. Fonseca, R. Pascoal, G. F. Clauss, C. E. Schmittner, and J. Hennig. Analysis of wave induced loads on a FPSO due to abnormal waves. In *OMAE Specialty Conference on Integrity of Floating Production, Storage & Offloading (FPSO) Systems*, Houston, USA, 2004b. OMAE-FPSO'04-0073.

K. Hasselmann, T. P. Barnett, E. Bouws, H. Carlson, D. E. Cartwright, K. Enke, J. A. Ewing, H. Gienapp, D. E. Hasselmann, P. Kruseman, A. Meerburg, P. Müller, D. J. Olbers, K. Richter, and W. Sell. *Measurements of Wind-Wave Growth and Swell Decay during the Joint North Sea Wave Project (JONSWAP)*. Ergänzungsheft zur Deutschen Hydrographischen Zeitschrift A8(12), Deutsches Hydrographisches Institut, Hamburg, 1973.

S. Haver. Some Evidences of the Existence of Socalled Freak Waves. In *Rogue Waves 2000*, Brest, France, 2000.

S. Haver and O. J. Anderson. Freak Waves: Rare Realization of a Typical Population or Typical Realization of a Rare Population? In *Proceedings of the 10th International Offshore and Polar Engineering Conference (ISOPE)*, pages 123–130, Seattle, USA, 2000.

N. Hogben. BMT Global Wave Statistics and Other Data. In *Design and Operation for Abnormal Conditions II*, London, UK, 2001. The Royal Institution of Naval Architects.

R. T. Hudspeth. Wave Force Predictions from Nonlinear Random Sea Simulations. In *Offshore Technology Conference*, volume I, pages 471–485, Dallas, Texas, USA, 1975. OTC 2193.

M. Huseby and J. Grue. An experimental investigation of higher harmonic wave forces on a vertical cylinder. *J. Fluid Mech.*, 414:75–103, 2000.

IMO. Code on Intact Stability for all types of ships covered by IMO instruments. Resolution A.749(18) as amended by resolution MSC.75(69), International Maritime Organization, 2002.

ITTC. Report of the Committee on Waves. In *Final Report and Recommendations to the 23rd International Towing Tank Conference*, pages 505–551, 2002.

T. Kano and T. Nishida. Sur les ondes de surface de l'eau avec une justification mathématique des équations des ondes en eau peu profonde. *J. Math. Kyoto Univ.*, 19(2):335–370, 1979.

B. Kinsman. *Wind Waves*. Prentice Hall Inc., Englewood Cliffs, New York, 1965.

S. P. Kjeldsen. Determination of severe wave conditions for ocean systems in a 3-dimensional irregular seaway. In *Contribution to the VIII Congress of the Pan-American Institute of Naval Engineering*, pages 1–35, 1983.

S. P. Kjeldsen. A sudden disaster – in extreme waves. In *Rogue Waves 2000*, Brest, France, 2000.

S. P. Kjeldsen. A sudden disaster – in extreme waves. In *Design and Operation for Abnormal Conditions*, RINA, London, UK, 2001.

P. Kröger. *Simulation der Rollbewegungen von Schiffen im Seegang*. PhD thesis, Universität Hamburg, 1987.

S. Krüger. Dynamic Stability of Ro-Ro Ships in Waves. In *Conference on Design and Safety of Ro-Ro Passenger Ships*, Copenhagen, Denmark, 2002.

W. Kühnlein. Seegangsversuchstechnik mit transienter Systemanregung. *Dissertation*, Technische Universität Berlin (D 83), 1997.

W. L. Kühnlein and K.-E. Brink. Model Tests for the Validation of Extreme Roll Motion Predictions. In *OMAE 2002 - Proceedings of 21st Conference on Offshore Mechanics and Arctic Engineering*, Oslo, Norway, 2002. OMAE2002-28269.

W. L. Kühnlein, G. F. Clauss, and J. Hennig. Tailor Made Freak Waves Within Irregular Seas. In *OMAE 2002 - 21st Conference on Offshore Mechanics and Arctic Engineering*, Oslo, 2002. OMAE2002-28524.

T. Levi-Civita. Détermination rigoureuse des ondes permanentes d'ampleur finie. *Mathematische Annalen*, 93:264–314, 1925.

M. S. Longuet-Higgins. The effect of non-linearities on statistical distributions in the theory of sea waves. *Journal of Fluid Mechanics*, 17:459–480, 1963.

E. P. D. Mansard and E. R. Funke. A new approach to transient wave generation. In *Proceedings of Coastal Engineering*, 1982.

K. McTaggart and J. O. de Kat. Capsize risk of intact frigates in irregular seas. In *SNAME transactions*, volume 108, pages 147–177, 2000.

N. Mori, T. Yasuda, and S. Nakayama. Statistical Properties of Freak Waves Observed in the Sea of Japan. In *Proceedings of the 10th Interational Offshore and Polar Engineering Conference (ISOPE)*, volume 3, pages 109–122, Seattle, USA, 2000.

T. Nishida. Equations of Fluid Dynamics – Free Surface Problems. *Communications on Pure and Applied Mathematics*, 39:S221–S238, 1986.

M. Olagnon. Representativity of Some Standard Spectral Models for Waves. In *ISOPE 2001 - 11th International Offshore and Polar Engineering Conference*, Stavanger, Norway, 2001. ISBN 1-880653-54-0.

A. S. Olsen, C. Schrøter, and J. J. Jensen. Encountered Wave Height Distributions for Ships in the North Atlantic. In *PRADS 2004 - 9th International Symposium on Practical Design of Ships and Other Floating Structures*, Lübeck-Travemünde, Germany, 2004.

F. Petey. Abschlussbericht zur Erweiterung des Vorhabens Leckstabilität im Seegang. Technical report, Institut für Schiffbau der Universität Hamburg, 1988.

W. J. Pierson and L. Moskowitz. A proposed spectral form for fully developed wind seas based on the similarity of S. A. Kitagorodskii. *Journal of Geophysical Research*, 96(2), 1964.

H. A. Schäffer. Second-order wavemaker theory for irregular waves. *Ocean Engineering*, 23(1):47–88, 1996.

M. Schulz. "Ich spürte den Atem Gottes". Der Spiegel, 2001. No. 51/2001.

J. Sharma and R. G. Dean. Second-order directional seas and associated wave forces. In *Offshore Technology Conference*, volume IV, pages 2505–2514, Houston, Texas, USA, 1979. OTC 3645.

L. Skjelbreia. Gravity Waves — Stokes' Third Order Approximation. *California Research Corporation*, 1959.

R. J. Sobey. Irregular waves and their generation. In *Advanced Short Course, Lecture notes*, Braunschweig, 2002.

H. Söding. Ermittlung der Kentergefahr aus Bewegungssimulationen. *Schiffstechnik*, 34, 1987a.

H. Söding. Simulation der Bewegungen intakter und lecker Schiffe. 23. Fortbildungskurs, 1987b.

U. Steinhagen. Synthesizing nonlinear transient gravity waves in random seas. *Dissertation*, Technische Universität Berlin (D 83), 2001.

S. Takezawa and T. Hirayama. Advanced experimental techniques for testing ship models in transient water waves. Part II: The controlled transient water waves for using in ship motion tests. In R. Bishop, A. Parkinson, and W. Price, editors, *Proceedings of the 11th Symposium on Naval Hydrodynamics: Unsteady Hydrodynamics of Marine Vehicles*, pages 37–54, 1976.

P. H. Taylor and C. O. G. Clifford. Focussed wave groups II: Global nonlinearity and resonant wave-wave interactions. In *Offshore Mechanics and Arctic Engineering (OMAE)*, St. Johns, Newfoundland, Canada, 1999. OMAE99/S&R-6462.

P. H. Taylor, C. O. G. Clifford, and J. Sauvee. Focussed wave groups I: Local structure, kinematics, and the Creamer transform. In *Offshore Mechanics and Arctic Engineering (OMAE)*, St. Johns, Newfoundland, Canada, 1999. OMAE99/S&R-6461.

A. Toffoli, J. M. Lefevre, J. Monbaliu, H. Savina, and E. Bitner-Gregersen. Freak Waves: Clues for Prediction in Ship Accidents? In *13th International Offshore and Polar Engineering Conference (ISOPE)*, pages 23–29, Honolulu, Hawaii, USA, 2003. ISBN 1-880653-60-5 (Set), ISSN 1098-6189 (Set).

P. S. Tromans, A. R. Anaturk, and P. Hagemeijer. A new model for the kinematics of large ocean waves - application as a design wave. In *Proceedings of the First International Offshore and Polar Engineering Conference (ISOPE)*, pages 64–71, Edinburgh, United Kingdom, 1991.

E. Truckenbrodt. *Fluidmechanik*, volume 1,2. Springer-Verlag Berlin, Heidelberg, 1968.

F. Ursell, R. G. Dean, and Y. S. Yu. Forced small-amplitude water waves: a comparison of theory and experiment. *J. Fluid Mech.*, 1959.

G. Walz. *Lexikon der Mathematik*. Spektrum, Akademischer Verlag, Heidelberg, 2001.

J. V. Wehausen and E. V. Laitone. *Surface Waves. Encyclopedia of Physics*, volume IX, pp. 446-778 of *Fluid Dynamics III*. Springer Verlag Berlin, 1960. Edited by S. Flügge.

J.-H. Westhuis. *The Numerical Simulation of Nonlinear Waves in a Hydrodynamic Model Test Basin*. PhD thesis, Universiteit Twente, Enschede, and MARIN, Wageningen (ISBN: 90-365-1575-0), 2001.

J. Wienke, U. Sparboom, and H. Oumeraci. Large Scale Experiments with Slender Cylinders in Breaking Waves. In *ISOPE 2001 - 11th International Offshore and Polar Engineering Conference*, Stavanger, Norway, 2001. ISBN 1-880653-54-0.

J. Wolfram, B. Linfoot, and P. Stansell. Long- and short-term extreme wave statistics in the North Sea: 1994-1998. In *Rogue Waves 2000*, pages 363–372, Brest, France, 2000.

S. Woltering. Eine Lagrangesche Betrachtungsweise des Seegangs. In *Mitteilungen des Franzius-Instituts für Wasserbau und Küsteningenieurwesen der Universität Hannover*, volume 77, pages 1–212, 1996. ISSN 0340-0077.

Y. Xing, I. Hadzic, S. Muzaferija, and M. Peric. CFD simulation of flow-induced floating-body motions. In *Proceedings of the 16th International Workshop on Water Waves and Floating Bodies*, Hiroshima, Japan, 2001a.

Y. Xing, I. Hadzic, and M. Peric. Predictions of floating-body motions in viscous flow. Technical report, NUTTS – Numerical Towing Tank Symposium, Hamburg, 2001b.

J. Zhang, J. Yang, J. Wen, I. Prislin, and K. Hong. Deterministic wave model for short-crested ocean waves. *Applied Ocean Research*, 21:167–206, 1999.

Index